MULTIBODY SIMULATION OF HELICOPTER ROTOR WITH STRUCTURAL FLEXIBILITY

A THESIS SUBMITTED TO
THE GRADUATE SCHOOL OF NATURAL AND APPLIED SCIENCES
OF
MIDDLE EAST TECHNICAL UNIVERSITY

BY

BALİ İHSAN ÖZTURAN

IN PARTIAL FULFILLMENT OF THE REQUIREMENTS
FOR
THE DEGREE OF MASTER OF SCIENCE
IN
AEROSPACE ENGINEERING

SEPTEMBER 2019

Approval of the thesis:

MULTIBODY SIMULATION OF HELICOPTER ROTOR WITH STRUCTURAL FLEXIBILITY

submitted by **BALİ İHSAN ÖZTURAN** in partial fulfillment of the requirements for the degree of **Master of Science in Aerospace Engineering Department, Middle East Technical University** by,

Prof. Dr. Halil Kalıpçılar
Dean, Graduate School of **Natural and Applied Sciences** ________________

Prof. Dr. İsmail Hakkı Tuncer
Head of Department, **Aerospace Engineering** ________________

Prof. Dr. Altan Kayran
Supervisor, **Aerospace Engineering, METU** ________________

Examining Committee Members:

Assoc. Prof. Dr. Ercan Gürses
Aerospace Engineering, METU ________________

Prof. Dr. Altan Kayran
Aerospace Engineering, METU ________________

Prof. Dr. Hüseyin Nafiz Alemdaroğlu
School of Civil Aviation, Atılım University ________________

Prof. Dr. Ozan Tekinalp
Aerospace Engineering, METU ________________

Assoc. Prof. Dr. İlkay Yavrucuk
Aerospace Engineering, METU ________________

Date: 09.09.2019

I hereby declare that all information in this document has been obtained and presented in accordance with academic rules and ethical conduct. I also declare that, as required by these rules and conduct, I have fully cited and referenced all material and results that are not original to this work.

Name, Surname: Bali İhsan Özturan

Signature:

ABSTRACT

MULTIBODY SIMULATION OF HELICOPTER ROTOR WITH STRUCTURAL FLEXIBILITY

Özturan, Bali İhsan
Master of Science, Aerospace Engineering
Supervisor: Prof. Dr. Altan Kayran

September 2019, 144 pages

Most of the multibody simulation tools used for modeling helicopter rotor use beam models of the blade and the rigid rotor hub. Stress recovery in the blade and in the hub are then performed by means of cross-sectional analysis tools or finite element analysis tools. In this study, multibody model of a helicopter main rotor is established using three dimensional flexible models of the blade and the rotor hub, and multibody simulations of the rotor are performed for the hover and the forward flight load cases. The scope of the multibody simulation consists of kinematic modeling of the rotor mechanism, flexible modeling of the hub and the blade, implementation of aerodynamic loads, trim calculations, and time response analysis with the objective of getting time history of dynamic stresses in the flexible parts. The flexible modeling of the rotor blade consists of the implementation of large deformation and centrifugal stiffening geometric nonlinearities.

Keywords: Helicopter Rotor, Multibody Simulation, Kinematics, Structure Dynamics, Geometric Nonlinearity

ÖZ

HELİKOPTER ROTORUNUN YAPISAL ESNEKLİK DAHİL EDİLEREK ÇOK GÖVDELİ SİMÜLASYONU

Özturan, Bali İhsan
Yüksek Lisans, Havacılık ve Uzay Mühendisliği
Tez Danışmanı: Prof. Dr. Altan Kayran

Eylül 2019, 144 sayfa

Helikopter rotorunu modellemek için kullanılan çoklu simülasyon araçlarının çoğu, pallerin kiriş modelini ve esnek olmayan rotor göbeğini kullanır. Pal ve göbek içindeki gerilme geri kazanımı daha sonra enine kesitsel veya sonlu elemanlar analiz araçları vasıtasıyla gerçekleştirilir. Bu çalışmada, bir helikopter ana rotorunun çok gövdeli modeli, palin ve rotor göbeğinin üç boyutlu esnek modelleri kullanılarak oluşturulmuştur. Askı ve ileri uçuş durumları için rotorun çok gövdeli simülasyonları gerçekleştirilmiştir. Çok gövdeli simülasyonun kapsamı, rotor mekanizmasının kinematik modellemesi, göbek ve palin esnek modellemesi, aerodinamik yüklerin uygulanması, dengeleme hesaplamaları ve esnek parçalarda dinamik gerilmelerin zaman geçmişini almak amacıyla zaman yanıtı analizinden oluşur. Rotor palinin esnek modellenmesinde, büyük deformasyon ve santrifüj sertleştirici geometrik doğrusal olmayan etkiler dahil edilmiştir.

Anahtar Kelimeler: Helikopter Rotoru, Çok Gövdeli Simülasyon, Kinematik, Yapı Dinamiği, Geometrik Doğrusal Olmayanlık

to my family

ACKNOWLEDGEMENTS

First of all, I would like to express my very profound gratitude to my parents for their support and trusting me all my life. This accomplishment would not have been possible without them.

I would like to express my deepest gratitude to my supervisor Prof. Dr. Altan Kayran for his guidance, advice, criticism, insight and encouragements throughout this work.

I would like to thank my colleagues at Turkish Aerospace for their support and understanding.

Finally, very special thanks to my love Betül for her understanding, endless support and love through the duration of this study.

TABLE OF CONTENTS

LIST OF TABLES

TABLES

LIST OF FIGURES

FIGURES

CHAPTER 1

INTRODUCTION

1.1. Background

In the design of the multibody mechanical systems, numerical simulations are powerful tools for understanding the kinematic and the dynamic behavior of the mechanical system. Numerical simulations provide better understanding of how single components work and give chance to test whether the designed mechanism is capable of producing the desired motion or not before the manufacturing phase. For the complex multidisciplinary system that consists of several different subcomponents, numerical simulation becomes the fundamental tool in order to study how the loads are distributed within the moving parts because their capability and accuracy have been considerably improved. By using these modern multibody dynamic tools, complex mechanisms that consist of joints, sensors, motions, actuators can be built by using the direct imports of the arbitrary shaped computer aided design (CAD) solid models. In addition to this, deformable parts can also be imported to the multibody system for more accurate results and further structural analysis.

Helicopter rotor is a complex multidisciplinary mechanical system which combines different disciplines such as aerodynamics, structural dynamics, multibody dynamics, aero elastics, flight dynamics, control theory, and numerical analysis. Moreover, it consists of several substructures and structural properties of the substructures have significant coupling effect with all of the disciplines. Besides, several modifications are usually done in the preliminary design stage of the helicopter rotor and physical testing of these modifications usually require long time and high costs. Therefore, analytical tools that combine all of the related disciplines provide significant advantage before the manufacturing stage to improve the designs. Multibody simulation of such a complex mechanism provides opportunity for testing and exploring various conditions before the manufacturing phase or setting up a physical test model. It allows the setting up of the complex multibody mechanical system in the computer environment and design modifications of the mechanical system involving mechanisms can be implemented easily. Following the design modifications, multibody simulations let the engineers to decide on the suitability of the kinematics of the mechanical system as well as the integrity of the mechanical components.

A helicopter’s rotor system is the critical part of the helicopter because it allows the vehicle to fly and control the vehicle by means of rotary wings. The rotor system mainly consists of rotor blades, a hub, and a mast. The mast is a hollow cylinder and it is used for transferring engine power as torque to rotate the rotor blade system by connecting the lower end to the transmission and the upper end to the rotor hub through series of special linkages. The rotor hub provides attachment points to the rotor blades and they are attached to the rotor hub by using different methods. Blade attachment methods are used for categorizing helicopter rotor head types in the literature. The main rotor systems are classified in three basic types as rigid, semi rigid, and fully articulated. In addition to these three basic rotor systems, hingeless rotor system type, which uses an engineered combination of these three types, also exists. In Figure 1.1, some typical helicopter rotor head types are shown.

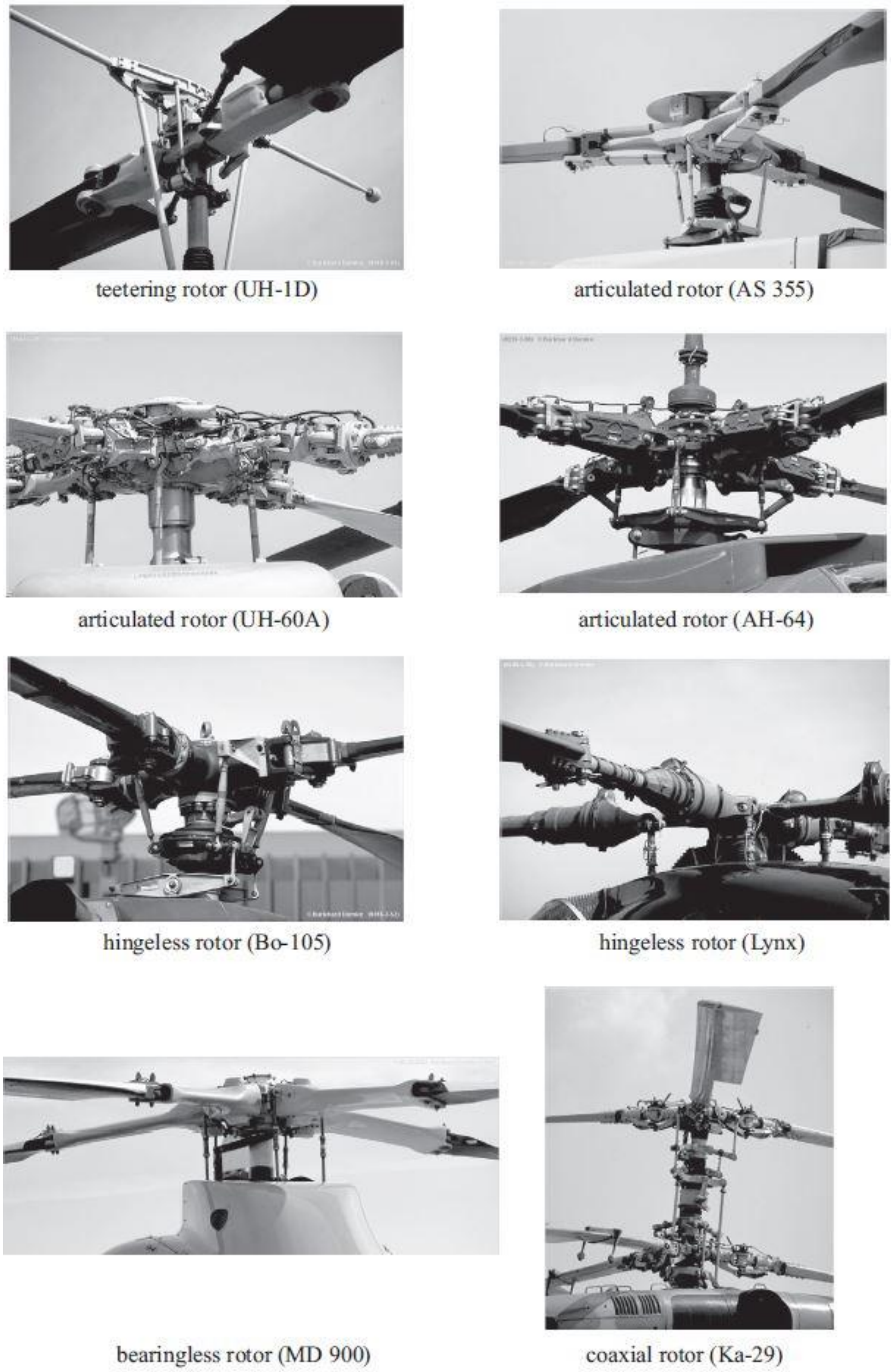

Figure 1.1 Main rotor types [1]

These rotor heads are categorizing based on the existence of hinges between the blade and the rotor hub which provide the rotational motion to the blades. The rotor blade loads change faster compared to the fixed wing aircraft because of the rotational motion of the rotor blades. This situation yields unbalanced aerodynamic and inertial loads among the rotor blades and excessive moment at the blade roots. As a result of this, rotor blades tend to rotate relative to the rotor hub individually. In order to eliminate the rolling moment from unbalanced aerodynamic and inertial loads and reduce the bending stresses at the blade root, hinge system has been developed to attach the rotor blades to the rotor hub. Usage of the hinge system allows the blades to lead/lag (backward and forward motion), flap (up and down motion), and pitch (rotation around feathering axis to change the lift). A sample application of the hinges and their motions are demonstrated in Figure 1.2. The lead/lag is forward and backward motion of the blade due to the coriolis forces from rotation of the hub, the flap is upward and downward motion of the blade due to the lift dissymmetry among the blades, and feathering is the pitching motion of the blades to control the production of the lift.

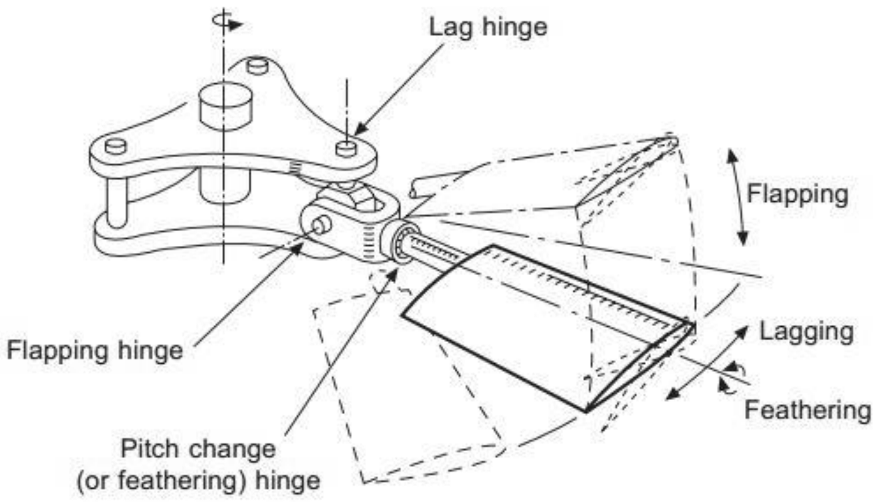

Figure 1.2 Hinge System and Blade Angles [2]

In the rigid rotor system, only the feathering hinge exists and other motions are accommodated by the blade bending. In the semi rigid rotor system, both feathering and flapping hinges exist, and in the articulated rotor system, feathering, flapping, and leading/lagging hinges all exist. The bearingless rotor system behaves like fully articulated rotor head but it has no mechanical hinges. In this system, the blades are mounted to the rotor hub by using specially designed elastomeric bearings, consisting of combination bonded elastomer and metallic material.

1.2. Literature Review

In the literature, several studies have been established to model and analyze helicopter rotor mechanism. In this section, some examples of the helicopter rotor modeling are given from the literature.

Bauchau, Bottasso, and Nikishkov [3] studied the multibody dynamic modeling approach for a rotorcraft system. In this study, structural and joint element library is described, equation of motion integration algorithms are discussed, dynamic, static, trim, and stability analyses procedures are explained. Moreover, selected rotorcraft applications are presented. In this respect, the stability analysis of an articulated helicopter rotor with control linkages and a mast mounted sight, shown in Figure 1.3, is introduced. In this study, multibody model of the rotor includes blades, control linkages, mast mounted sight, elastic shaft, scissors, and the swash plate. The shaft and the blade are modeled by using beam elements to represent their flexibility whereas other parts are modeled as rigid body since their flexibility can be neglected and all of the rotor parts are connected to each other by using a series of joints. The aerodynamic loads applied on the blades are based on the dynamics inflow model.

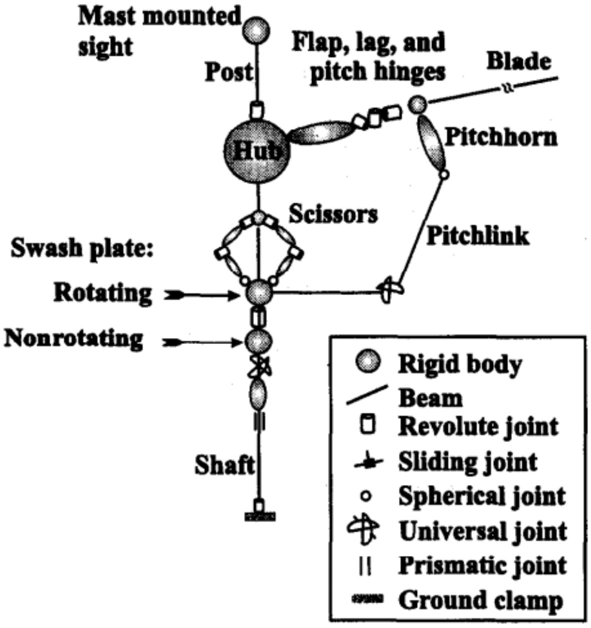

Figure 1.3 Articulated rotor with control linkages and a mast mounted sight [3]

Johnson [4] developed CAMRAD II, which is a comprehensive helicopter and rotorcraft analysis tool. CAMRAD II is utilized for the calculation of performance, stability, conceptual design, and loads by including aerodynamics, multibody dynamics, and nonlinear finite elements. Figure 1.4 illustrates the model of a helicopter with articulated rotor modeled in CAMRAD II.

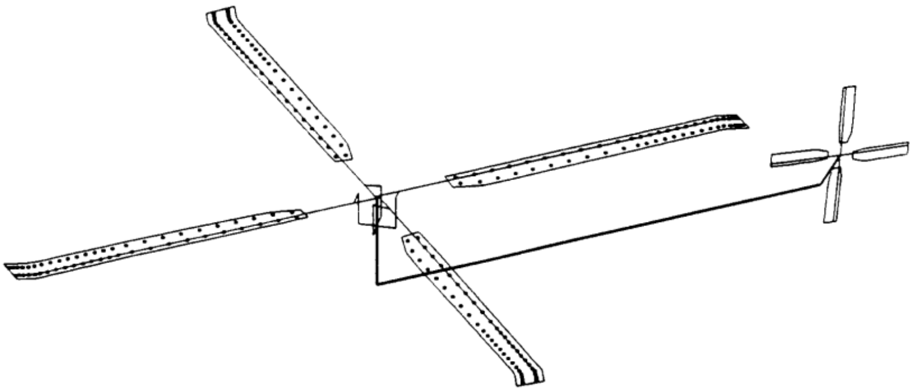

Figure 1.4 CAMRAD II model of a helicopter with articulated rotor [4]

Sun, Tan, and Wang [5] developed a multi-body analytic model (Figure 1.5) to predict servo loads, pitch link loads, and rotor control system loads. In the developed multi-body rotor model, rigid rotor hub and pitch horn are used, the blades are modeled by using flexible beam elements and the pitch links and lag dampers are represented as linear spring-damper force elements. For the application of the aerodynamic loads, lifting line method is utilized.

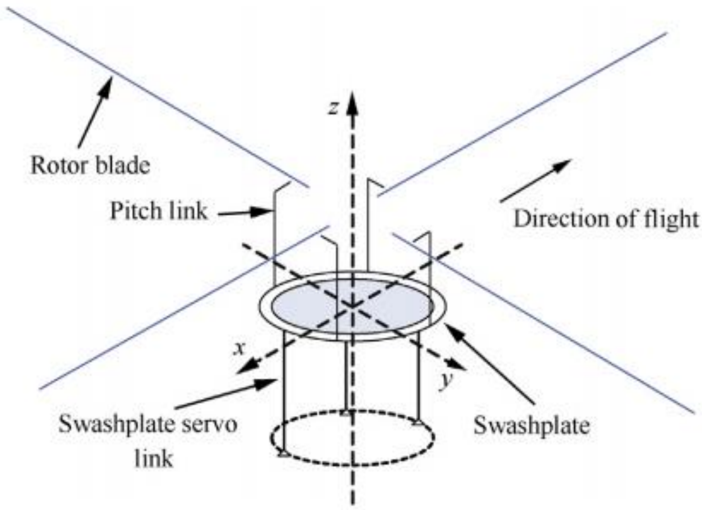

Figure 1.5 Representation of the rotor swashplate system [5]

Park and Jung [6] studied the helicopter rotor aeromechanics in descending forward flight by using a nonlinear flexible multibody dynamic analysis code, DYMORE, which has rigid bodies, rigid and elastic joints and elastic bodies by means of beams, plates, and shells. In this DYMORE model, helicopter rotor model is composed of a rigid hub and a total of four nonlinear elastic blades as ten cubic beam elements for each blade, which is illustrated in Figure 1.6.

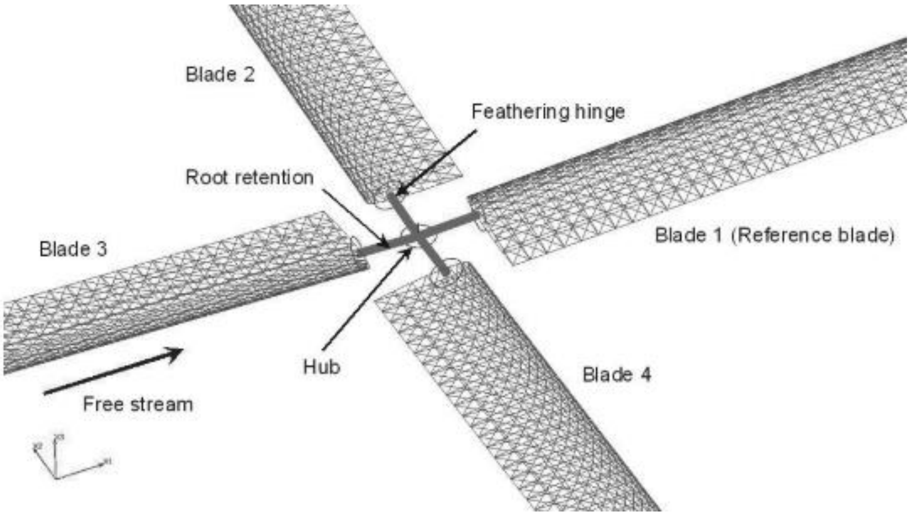

Figure 1.6 DYMORE modeling for four bladed helicopter rotor [6]

Monteggia and Alessandro [7] studied the calculation of the loads acting on a non-rotating rotor blade in the presence of gust on the ground by using the ADAMS software. In order to model the flexible blade, beam element and concentrated mass element are used in NASTRAN for obtaining its structural mass, damping and stiffness properties. For the implementation of the aerodynamic model, 2D strip theory has been used. In this work, the blade flexibility, application of gust, the impact of the blade on the flap limiter, the recovering of the internal loads is studied by using ADAMS.

Bianchi and Agusta [8] have performed the dynamic simulation of a partially flexible tail rotor model of an Agusta helicopter in order to investigate capabilities of ADAMS as a complex mechanical system simulation tool. For this purpose, the study has been focused on evaluating the load sharing, kinematic analysis, and implementation and the effects of flexibility of rotor components. Modeled tail rotor consists of fully rigid bodies for understanding and evaluating the kinematic behavior of the multibody model. Subsequently, some components are replaced by flexible ones in order investigate flexibility effects. At the end, aerodynamic and inertial loads are applied to the partially flexible multibody ADAMS model. Loads have been evaluated by using aero elastic code CAMRAD/JA and applied to the blades as concentrated forces and moments.

Persson, Weinerfelt and Saab Aeronautics [9] presented simulation of the Saab Skeldar V200 helicopter model with coupled aero and structural dynamics for the computation of the unsteady loads by using MSC/ADAMS. The simulation model consists of structural dynamics, aerodynamics and control system to form a multi physics-based simulation framework. Rotor blade and helicopter frame are modeled as deformable body whereas other rotor parts are modeled rigid, and this model is presented in Figure 1.7. For the calculation of the aerodynamic loads, lifting line theory has been used and application of the control system has been done by the PID-regulation. Finally, simulation results and flight test results are compared and it is commented that the simulation gives satisfactory model characteristics.

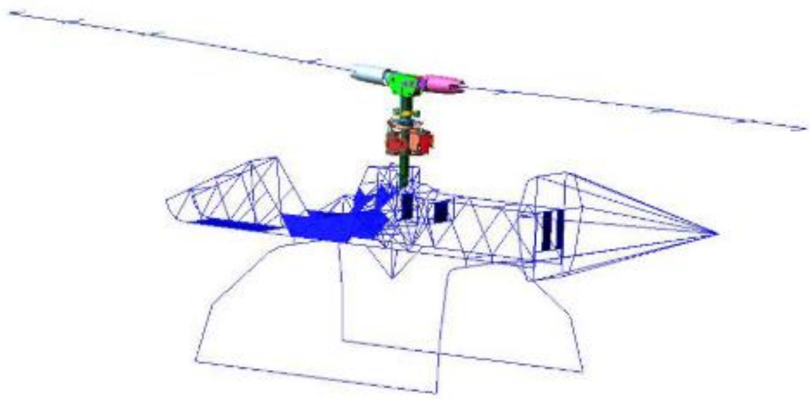

Figure 1.7 Helicopter simulation model of the Saab Skeldar V200 [9]

Vittorio, Francesco, and Marco [10] modeled the main rotor of the AGUSTA A109c helicopter by using ADAMS for the dynamic and aerodynamic analyses. The purpose of this study is about the feasibility analysis of the ADAMS software capabilities for the helicopter main rotor dynamics with blade flexibility, unsteady aerodynamic loading, and active control for stability. In addition to this, design optimization is performed by modifying the existing design to improve the performance and quality of the helicopter by means of decreasing vibration level. The model consists of mechanical modeling of the control system and the rotor hub, deformable model of the blades, aerodynamic model, stability and trimming.

Abhishek [11] developed an inverse flight dynamics simulation tool for helicopters in order to estimate blade loads under unsteady flight maneuvers. Inverse flight dynamic simulation means estimation of control angles for an unsteady maneuver to use as input for the calculation of blade loads. In the steady flight, estimation of the control angles are done by trimming the helicopter to maintain the equilibrium condition. However, for unsteady maneuvers, calculations of control inputs are done by using the desired position of the helicopter with the integration based approach. In this study, pull-up maneuver is used as unsteady flight maneuver and estimated control angles are used in University of Maryland Advanced Rotorcraft Code as input to predict blade loads. Calculations are done by using a simplified helicopter dynamic model with rigid blades and quasi-steady aerodynamics. Results are compared against the flight-test data for a UH-60A Black Hawk helicopter and the control angles show correct trend of variation.

A full scale four bladed UH-60 rotor system was tested in the NASA Wind Tunnel and modeled analytically by Shinoda [12] in order to discuss and compare hover and forward flight performance results of the helicopter rotor for improving future rotor design and analysis. The test system of the rotor consists of the hub, spindles, blades, and swash plate. The analytical model of the UH-60A rotor has been prepared as an isolated rotor by using comprehensive rotorcraft analysis code CAMRAD II. In the analytical rotor model, blades are modeled as flexible blade by using nonlinear beam finite elements and aerodynamic loads are represented by using the second-order lifting line theory. As a result of this study, it is seen that CAMRAD II results match well with the wind tunnel test results for hover case. On the other hand, for forward flight case, it is concluded that CAMRAD II shows good agreement with wind test results but some improvements are needed.

1.3. Objective

The main objective of this study is to perform multibody simulations of the helicopter rotor system with flexible modeling of the helicopter blade and the rotor hub and integration of the user defined simple load cases and aerodynamic load calculations into the multibody simulation tool MSC ADAMS [13]. MSC ADAMS is a Multibody Dynamic software and it is widely used in the literature for building models of mechanical systems and solving equations of motion for kinematic, quasi-static, static, and dynamic events with the application of loads and motions that can be defined by using expressions, functions, and subroutines. It is also capable of implementation of flexible bodies by coupling it with the finite element analysis software MSC NASTRAN [14] and allows stress history output data for further calculations and evaluations to improve the component design.

Most of the multibody modeling and simulation tools for modeling helicopter rotors use beam models of the blade and the rigid rotor components. Stress recovery procedure in the blade and the rotor parts are then performed by means of cross-sectional analysis tools or finite element analysis tools which use the load information obtained in the multibody simulation of the rotor. In the present study, 3D finite element models of the blades and the hub have been implemented into ADAMS in order to achieve more realistic simulation of the helicopter rotor and obtain time dependent stress history result for the investigation of the effect of design modification on the stress history in the rotor hub and in the critical section of the blade. Since the rotor blades have significant effect in the dynamics of a rotor system, more detailed approach needs to be used for implementation of the blade flexibility. For this purpose, large deformation and stiffening nonlinear effects are also taken into account during the modeling of the flexible rotor blades because of the presence of the centrifugal force due to the rotation of the rotor and the long and slender structural form of the helicopter blade.

The implementation of the rotating blade aerodynamic forces and moments is another important parameter in the simulation of the helicopter rotor mechanism because the torque, thrust, and other forces and moments on the rotor are produced from the blade aerodynamic loads. Therefore, accurate computation of aerodynamic loads is essential for the realistic simulation of the helicopter rotor. In addition to this, a simple and computationally effective but still accurate aerodynamic model needs to be implemented in modeling the rotor system. For this reason, in the present study, the lifting line theory is used for calculation of the aerodynamic forces and moments and formulation of the lifting line theory is implemented into the ADAMS model for the calculation of these loads instantaneously in the ADAMS model. Hence, different flight scenarios can be simulated easily in the generated ADAMS model without a need for an external aerodynamic loads calculation tool. In this study, it is not intended to integrate a detailed rotary wing aerodynamic solver to the established rotor system since this requires substantial amount of work and this is considered as future work of this study.

As a course of its nature, the helicopter is an unstable flying vehicle and maintaining a stable flight condition is needed therefore, a trimming procedure has been applied to the multibody simulation model in order to obtain more realistic simulation results. In the trim state, all forces and moment vectors need to be in balance for desired flight condition. This state can be accomplished by optimizing the main rotor blades pitch angle settings individually to obtain balanced moments and forces.

With the established rotor model generated in MSC ADAMS, one can study the effect of design changes on the hub loads which are very critical in the design of the helicopter rotor. For instance, rotor blade pitch, flap, and lag angle variations are important parameters in the design stage of the helicopter rotor since it consists of several moving parts and these parts need to be designed by considering required rotor blade angles motion limits. Moreover, excessive rotor blade motions cause to increase in rotor hub loads which can be investigated easily by using established rotor model. In addition to this, effects of blade control linkages attachment point locations on the hub loads and the blade angles can be investigated. Present study aims to generate a rotor system model consisting of a rather high-fidelity structural model based on 3D blade and hub FE models and a rather low fidelity aerodynamic model based on lifting line theory. In the future, the present work can be improved by incorporating a higher fidelity aerodynamic model based on dynamic inflow theory.

CHAPTER 2

MULTIBODY MODELING OF THE HELICOPTER ROTOR SYSTEM

2.1. Helicopter Rotor Components

A fully articulated main rotor head assembly mainly made up of a rotor hub, dampers, rotor blades, pitch control levers, pitch links, and a swash plate. The major elements of the main rotor assembly are listed in Table 2.1.

Table 2.1 *Rotor Parts*

Rotor Components
Main Rotor Hub
Main Rotor Blades
Swash Plate Assembly
Pitch Horn
Pitch Link
Damper

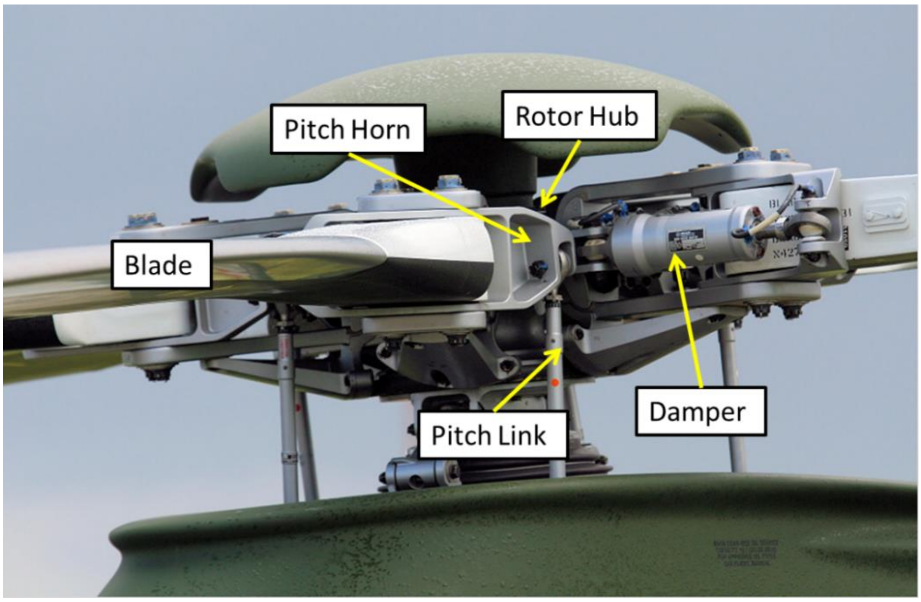

Figure 2.1 Rotor assembly [15]

As demonstrated in Figure 2.1, equally spaced rotor blades are mounted to the rotor hub. The rotor hub is mounted to the drive shaft to transfer the engine power. Main purpose of the rotor hub is to transfer the engine power to the rotor blades by providing attachment points for the blades. Rotor blades are controlled by adjusting pitch angles via the swash plate assembly. Connection of the rotor blades and swash plate are provided by the pitch link and the pitch horn assembly. Pitch horn, also known as pitch control lever or pitch control arm, provides connection interface to the blades for the pitch link, hub and the lead-lag damper attachments. Lead-lag dampers are connected between the hub and the blade to limit excessive lead-lag motions. Schematic representation of rotor mechanism is given in Figure 2.2.

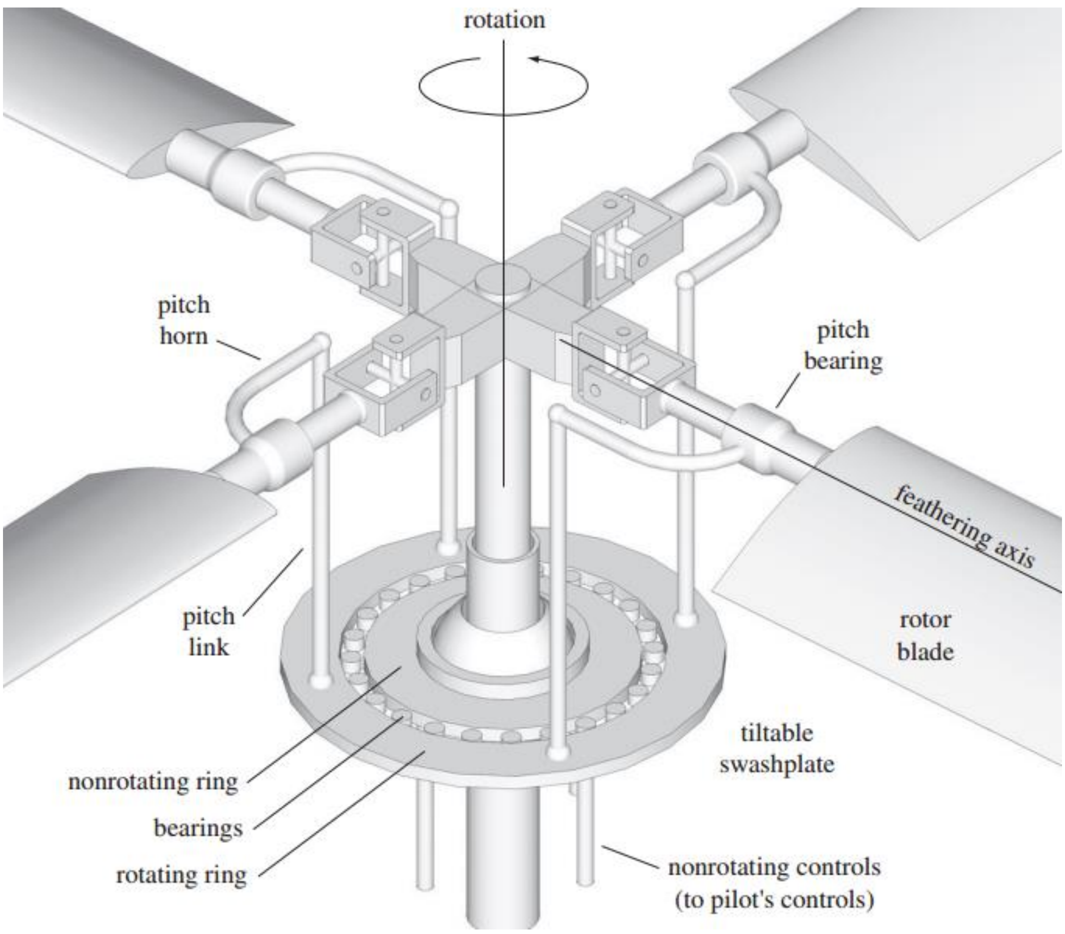

Figure 2.2 Schematic representation of the Rotor Assembly [1]

2.1.1. Main Rotor Hub

The rotor hub is the main load carrying component in the rotor system since it transfers mechanical power produced from the engine while provides connection for the rotor blades. Therefore, to handle these high loads, the rotor hub must be extremely strong. The hub is a single piece, forged, steel alloy unit and it is machined to provide the necessary attachments. In this study, rotor hub shape and dimensions are arbitrarily chosen in view of the existent helicopter main rotor hubs to simulate a real-like helicopter main rotor.

The outer section of the hub provides mounting of the blades and the dampers. The inner section of the hub provides attachment with the main rotor gearbox mast by spline type connection to provide mechanical power interference between the rotor system and the transmission.

2.1.2. Main Rotor Blade

The rotor blades are fundamental parts of the helicopter rotor system and they are subjected to various distributed external loading. Therefore, rotor blades play an essential role for dynamic characteristics of the rotor system and loading conditions of the other rotor parts.

The main rotor blades are usually made of composite material. Composite materials are highly efficient for the use in helicopter rotor blades because they have superior fatigue life and mass and stiffness distribution can be adjusted to increase the aeroelastic performance.

Typical main rotor blade structure is shown in Figure 2.3. The main structural components of the rotor blades are the spar, skin, and the honeycomb core. Spar is placed at the leading-edge section of the blade and it is the primary load carrying member in the blade assembly. Upper and lower skins are used to form the airfoil shape of the blade. Between the upper and lower skins honeycomb structure is used as the filler material.

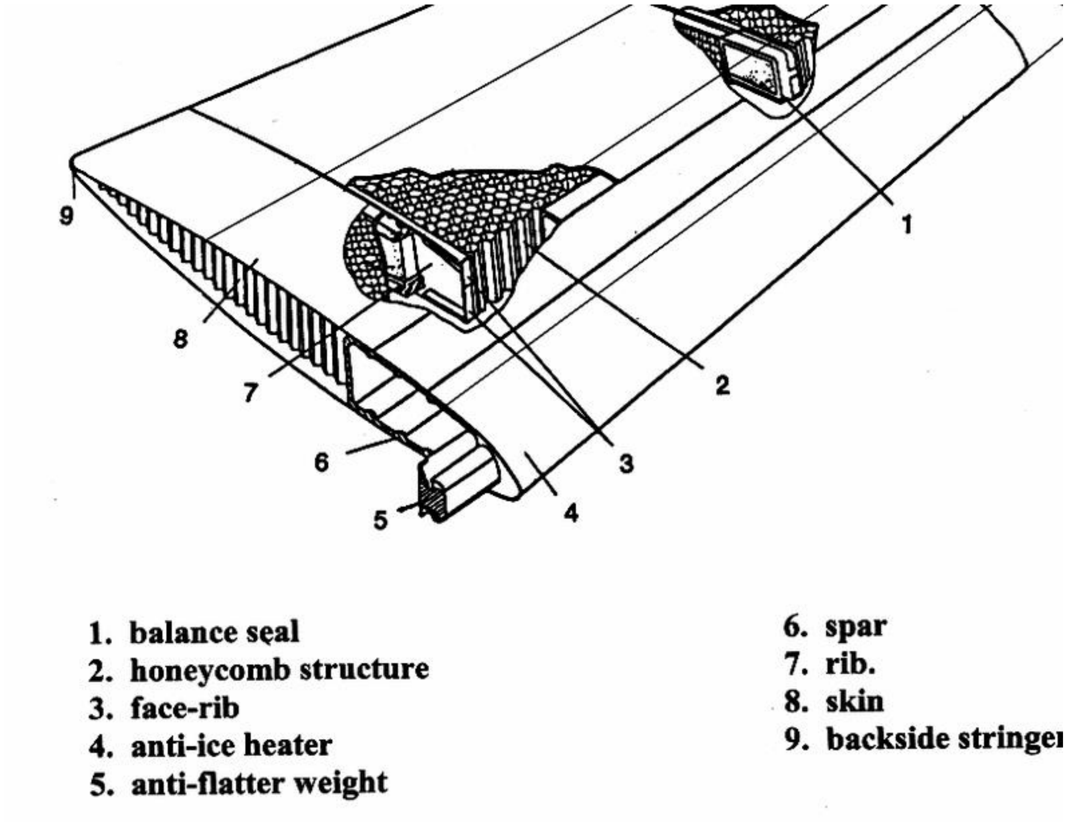

Figure 2.3 Typical helicopter blade structure [16]

2.1.3. Swash Plate Assembly

The swash plate assembly is used to transmit the pilot control inputs to the main rotor blades via linkages to control the pitch angles. The swashplate mechanism, shown in Figure 2.4, consists of two main parts; rotating swashplate and non-rotating (fixed) swash plate. The flight control actuators are connected to the fixed swashplate with the linkages and the fixed swashplate is mounted around the main rotor mast via spherical shaped uniball sleeve, which makes the swashplate to tilt around it in lateral and longitudinal directions and move vertically. The rotating swashplate rotates at same speed with the main rotor and it sits on the fixed swashplate by using a ball bearing located between them to allow relative rotation while the orientation and the vertical position of the rotating plate along the shaft axis is governed by the fixed swashplate. Finally, pitch links are connected to the rotating swash plate to control pitch angles of the rotor blades.

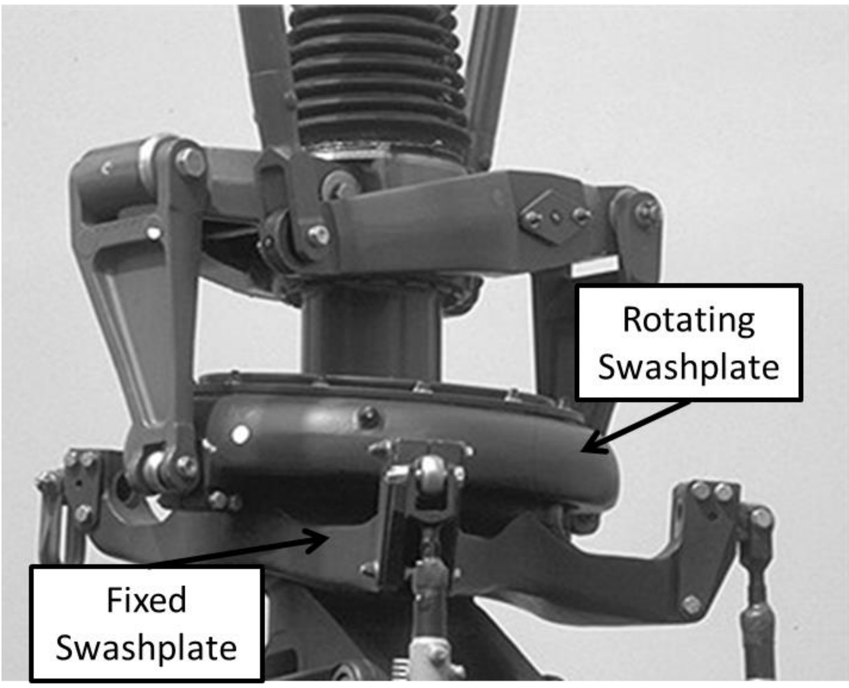

Figure 2.4 Swashplate Assembly [15]

2.1.4. Pitch control lever

Pitch control lever is the connection interface for the pitch link, damper, the blades, and the hub. It transfers the torsional loads on the blade to the flight control system and loads due to the change in the pitch angle to the blades.

2.1.5. Pitch link

Pitch link is used for the transfer pitch change commands to the rotor blades. One end of the pitch link is connected to the blade via the pitch control lever and the other end is connected to the rotating swash plate. Pitch link assembly consists of two spherical type rods ends at both sides and a pitch link rod.

2.1.6. Damper

Dampers are installed between the blades and the hub to damp out the lead and lag movement of the blades. In an articulated type rotor head, the rotor blades are free to move about the lag hinge. For this reason, the main rotor dampers are used in order to limit excessive lead lag motion of the rotor blades and to absorb shocks caused from inertial forces. At both ends of the lag dampers, spherical types of connections are used.

2.2. Kinematic Model

Helicopter rotor is a complex mechanical system that consists of several sub structure with several joints. Helicopter rotor parts are connected to each other with different types of joints with different ways. Therefore, kinematics modeling and analyzing of the rotor mechanism are important.

2.2.1. Kinematic Joint types

Joints are used to connect two parts by creating restriction on the relative motion, such as restricting one part to always rotate about a selected axis relative to the second part. In the kinematic model of the main rotor, combination of different joint types is used; fixed joint, revolute joint, prismatic joint, and spherical joint.

2.2.1.1. Fixed joint

Fixed joint (Figure 2.5) is used for locking two parts together so they cannot move with respect to each other and they act like single parts. In the main rotor kinematic model fixed joint is used between the blade and the pitch control lever; because these parts are locked together by using bolt connection.

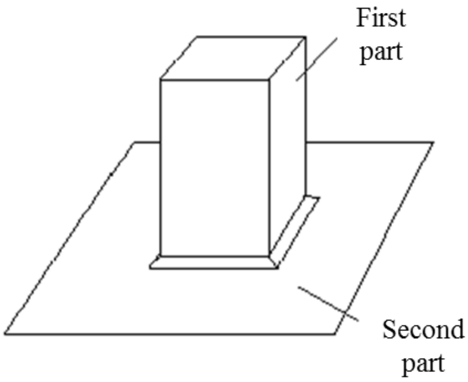

Figure 2.5 Fixed Joint [13]

2.2.1.2. Revolute joint

Revolute joint allows the rotation of one part relative to the second part about a selected axis and it is also known as the hinge joint, which is represented in Figure 2.6.

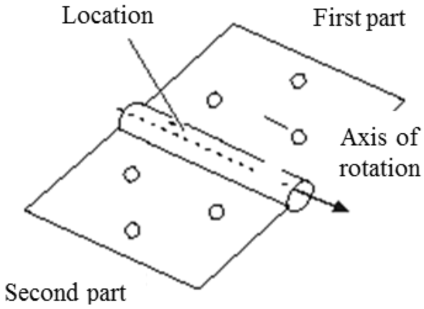

Figure 2.6 Revolute joint [13]

2.2.1.3. Prismatic Joint

Prismatic joint allows only translation of one part relative to the second part along a selected axis and it is also known as the translational joint, which represented in Figure 2.7.

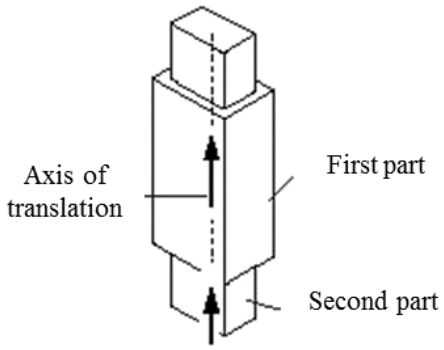

Figure 2.7 Prismatic Joint [13]

2.2.1.4. Spherical joint

Spherical joint allows the free rotation of one part relative to the second part about a selected point while restricting relative translational motions. Spherical joint is also known as the ball joint, which is represented in Figure 2.8.

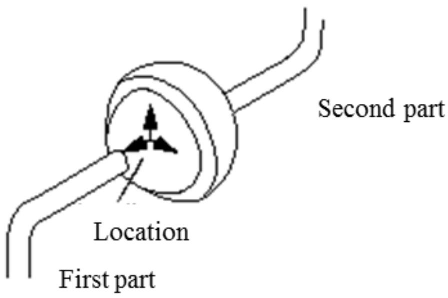

Figure 2.8 Spherical Joint [13]

2.2.2. Kinematic Modeling of the Helicopter Main Rotor

Kinematic model of a helicopter main rotor and joints locations of a blade are represented in Figure 2.9. This model is generated in MSC ADAMS. In the kinematic model, since the isolated main rotor model is simulated, hub is connected directly to the ground with a revolute joint (joint 1), which is used to give rotational motion to the system. Other parts are connected to the rotor hub by series of joints because the hub transmits the rotational motion to the other rotating parts of the rotor. Specifically, blades are connected to the hub by a spherical joint (joint 6) via the pitch control lever, also called as the pitch horn, in order to represent the fully articulated rotor configuration, which is demonstrated schematically in Figure 2.10.

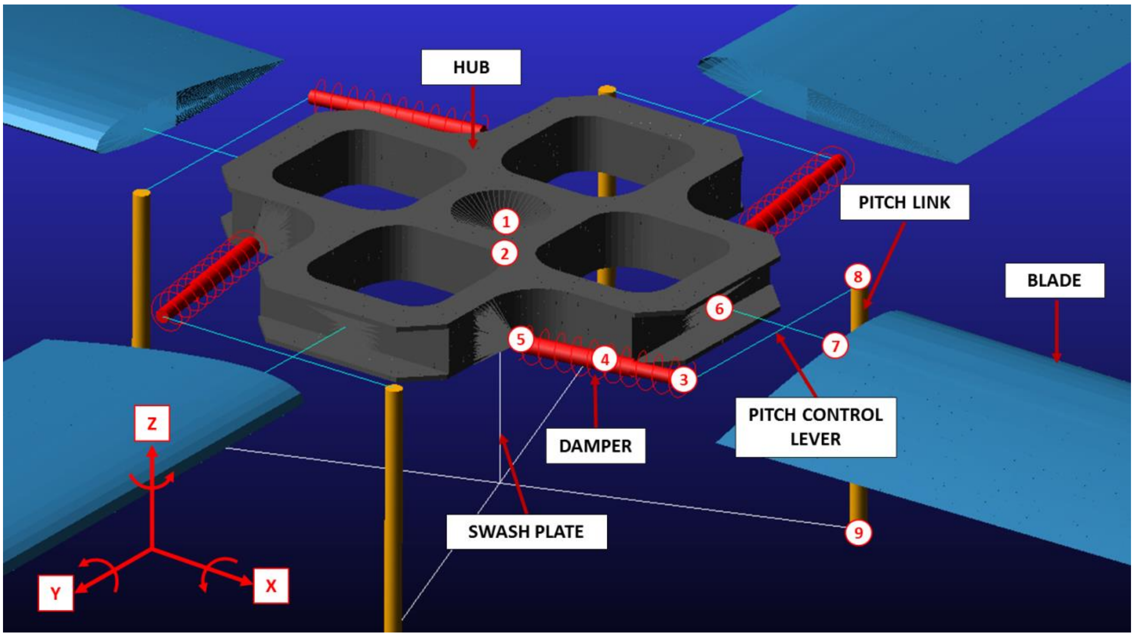

Figure 2.9 Main rotor kinematic model in MSC ADAMS

Blade and pitch control lever connection are done by the rigid joint (joint 7); because it transfers the control inputs to the blades directly. The pitch angle of each blade is controlled by the swashplate mechanism through the pitch link. One end of the pitch link is connected to the blade via pitch control lever by a spherical joint (joint 8), and the other end of the pitch link is connected to the swash plate via spherical joint (joint 9). The swashplate assembly is connected to the hub by prismatic joint (joint 2) since it is used for changing pitch links' positions to control the blade angles while rotating with the hub. The damper consists of two parts and they are connected to each other via the prismatic joint (joint 4). One end of the damper is connected to the hub (joint 5) and the other end is connected to the pitch control lever (joint 3) via the spherical joints. Table *2.2* summarizes the joint numbers, joint types and the connected parts. For other blades and rotor parts, connection methodology is identical.

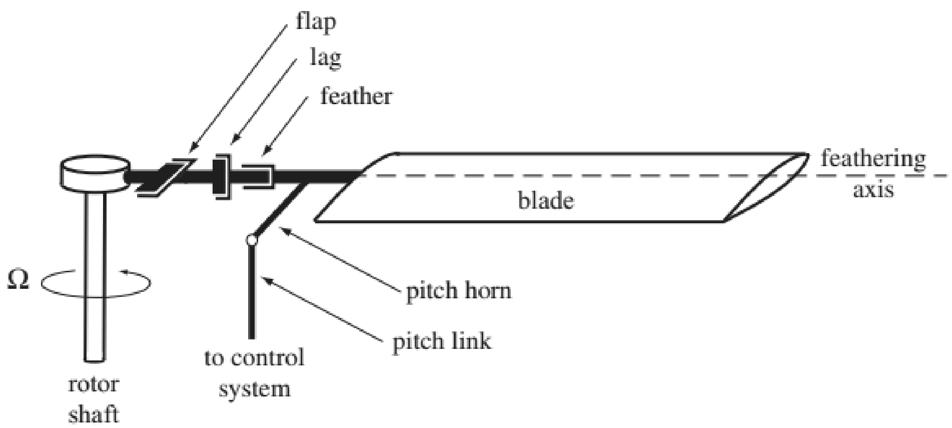

Figure 2.10 Schematic representation of an articulated rotor [1]

Table 2.2 *Joint used in Main Rotor Kinematic Model*

Joint Number	Joint Type	Parts Connected
1	Revolute	Hub - Ground
2	Prismatic	Hub - Swash Plate
3	Spherical	Damper - Pitch Control Lever
4	Prismatic	Damper (Hub Side) Damper (Pitch Control Lever Side)
5	Spherical	Hub - Damper
6	Spherical	Pitch Control Lever - Hub
7	Fixed	Blade - Pitch Control Lever
8	Spherical	Pitch Control Lever - Pitch Link
9	Spherical	Swash Plate - Pitch Link

In the design of the helicopter rotor, locations of the joints relative to the hub center are important parameters for the kinematics and dynamics of the system. In Figure 2.11 and Table *2.3*, locations of the joints for the rotor model used in the present study are given.

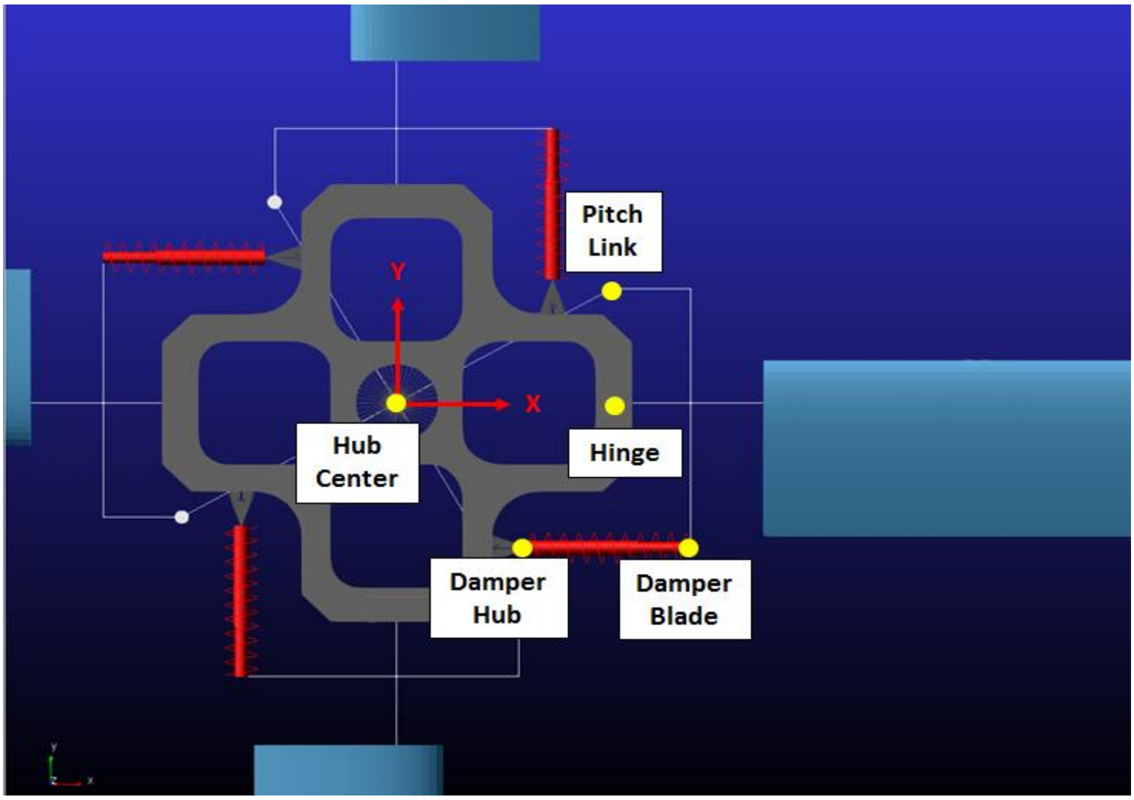

Figure 2.11 Kinematic model attachments

Table 2.3 *Attachment Locations*

Attachment Name	Location (mm)
Hub Center	(0, 0, 0)
Hinge	(439.5, 0, 0)
Pitch Link	(439.5 250 0)
Damper Hub	(270, -318, 0)
Damper Blade	(600, -318, 0)

2.3. Blade Structural Model

In the early design stage of the helicopter rotor blades, wooden and fabric materials were used for the construction of rotor blades like classic wing design. After improvement on aluminum and steel structures, metallic blades were started to be used in design. Use of metallic materials brought significant improvement to helicopter blade designs such as cheapness and manufacturing easiness. However, besides the advantages of steel blades, still some problems existed on the usage of metallic blades. The most critical problems were poor fatigue life and strength to weight ratio. Since the helicopter blades are subjected to extremely hard conditions due to the rotary motion under high rotational speed and maneuverable nature of helicopters, high fatigue resistance and low weight becomes more important for rotor blade designs.

In order to overcome restrictions of the metallic materials, composite materials have been started to be used in modern helicopter blade designs. Composite materials also enable to adjust stiffness and inertial properties of the blades by changing the fiber angle direction and layer thickness. Demonstration of a typical composite layup can be seen in Figure 2.12. Fiberglass and carbon fiber composite materials are commonly used for manufacturing rotor blade components.

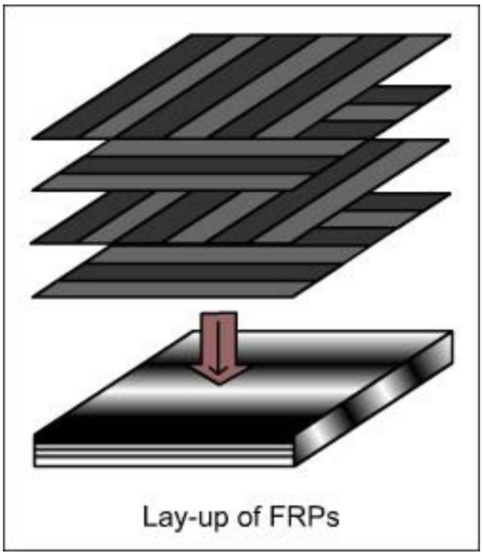

Figure 2.12 Composite Layup [17]

Helicopter rotor blades consist of several substructures; outer skin, inner-outer wrap, spar, honeycomb, erosion shield, heater mat, etc. A typical cross-sectional view of a helicopter blade is given in Figure 2.13.

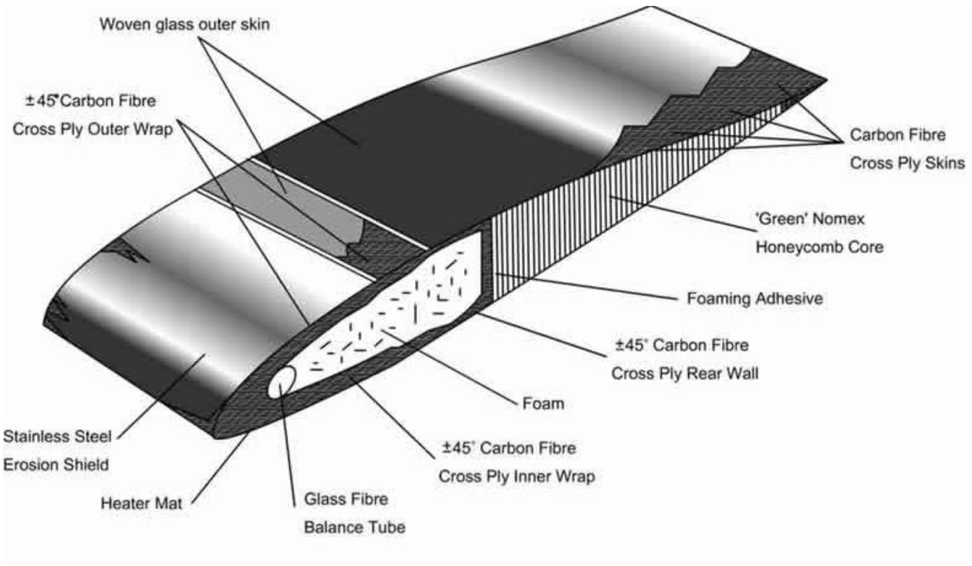

Figure 2.13 Cross-Sectional View of a Composite Blade [17]

The airfoil type selection is also important design parameter for helicopter blade design since helicopter blade needs to have high Lift/Drag ratio while providing the required structural properties. Therefore, most of the helicopter rotor blades have symmetrical airfoils to prevent high internal forces. Figure 2.14 shows typical airfoil types used in helicopter blade designs.

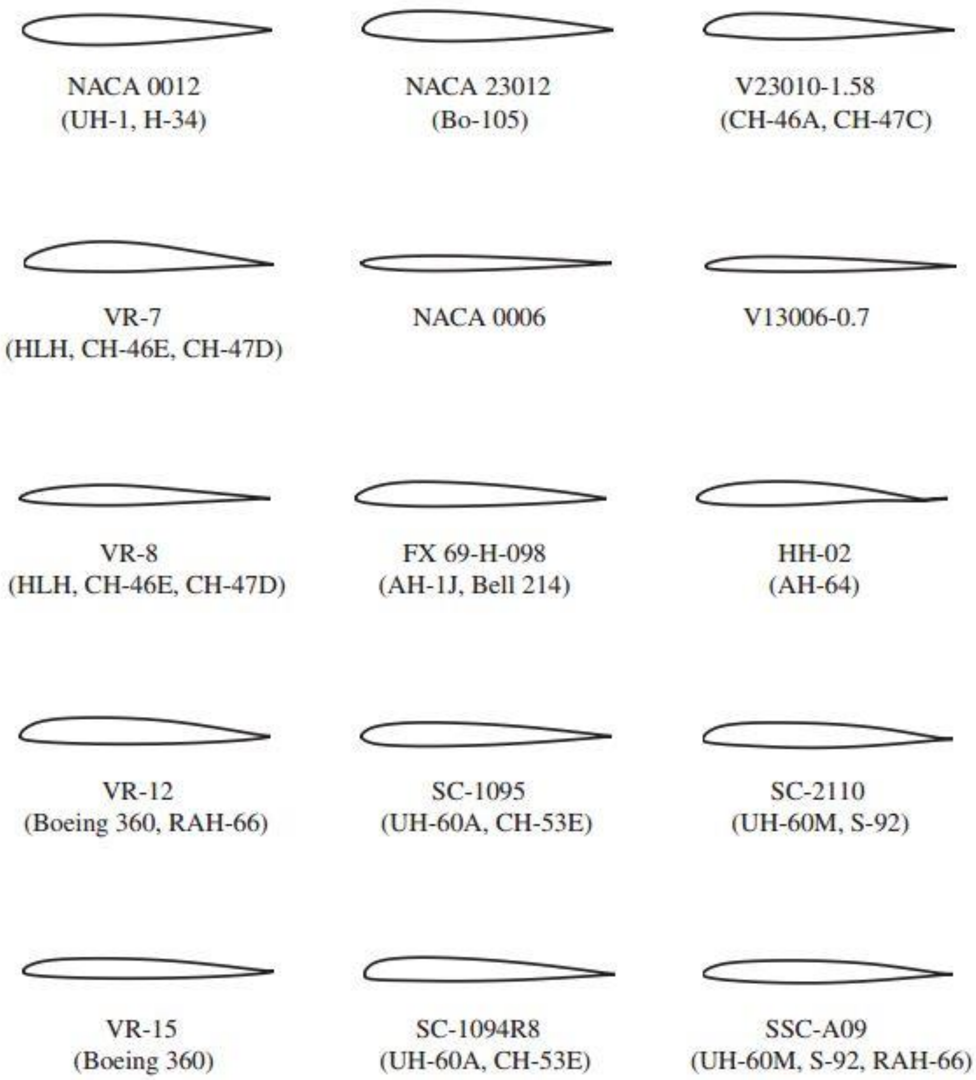

Figure 2.14 Typical Airfoil Types used in Helicopter Designs [1]

In this study, NACA 0012 symmetric airfoil profile has been chosen and, for the structural modeling of the rotor blade; skin, spar and honeycomb substructures have been modeled as the main load carrying members. Blade has been modeled as a composite part with fiberglass skin, fiberglass spar, and Nomex Honeycomb core. Span length of the blade is about 4m with constant 0.375m chord length. Blade dimensions are arbitrarily chosen in view of the existent helicopter rotor blades to simulate a real-like helicopter main rotor. Blade dimensions are presented in Figure 2.15.

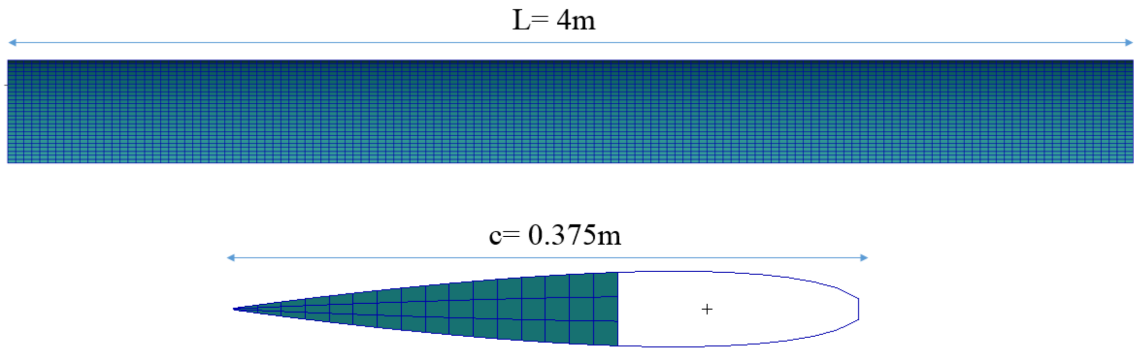

Figure 2.15 Blade Dimensions

2.3.1. Finite Element Model and Implementation of Flexibility

In the rotor model, blade and hub are modeled as flexible parts by using MSC Patran [18] and MSC Nastran. Computer aided design (CAD) files of the parts are imported to Patran for meshing and generation of the connection points. Following the preparation of the finite element models of the hub and the blade for analysis in Patran, modal analysis approach is used for modal stress recovery by using solution sequence 103 of Nastran. After performing the modal analysis in Nastran, model neutral file (mnf) generated by Nastran is exported to MSC ADAMS. In addition to the solution sequence 103, for the implementation of blade geometric nonlinearity, solution sequence 106 is also used by using restart analysis method. Details of the implementation of geometric nonlinearity are discussed in the related section discussing geometric nonlinearity.

2.3.1.1. Finite Element Model of the Rotor Blade

For the finite element model of the rotor blade, combination of 2D shell elements and 3D solid elements are used. The rotor blade model consists of 6480 six sided solid elements with 8 grid points (CHEXA) and 7965 isoparametric quadrilateral elements (CQUAD4) and total 11980 nodes. For the simplicity, spar, skin, and honeycomb components are modeled in FE, as shown in Figure 2.16; because they are the main load carrying members of the blades. D-shaped spar is the main stiffness contributor for the blade structure. Skin is important for chord-wise stiffness, and honeycomb provides structural integrity by supporting the skin.

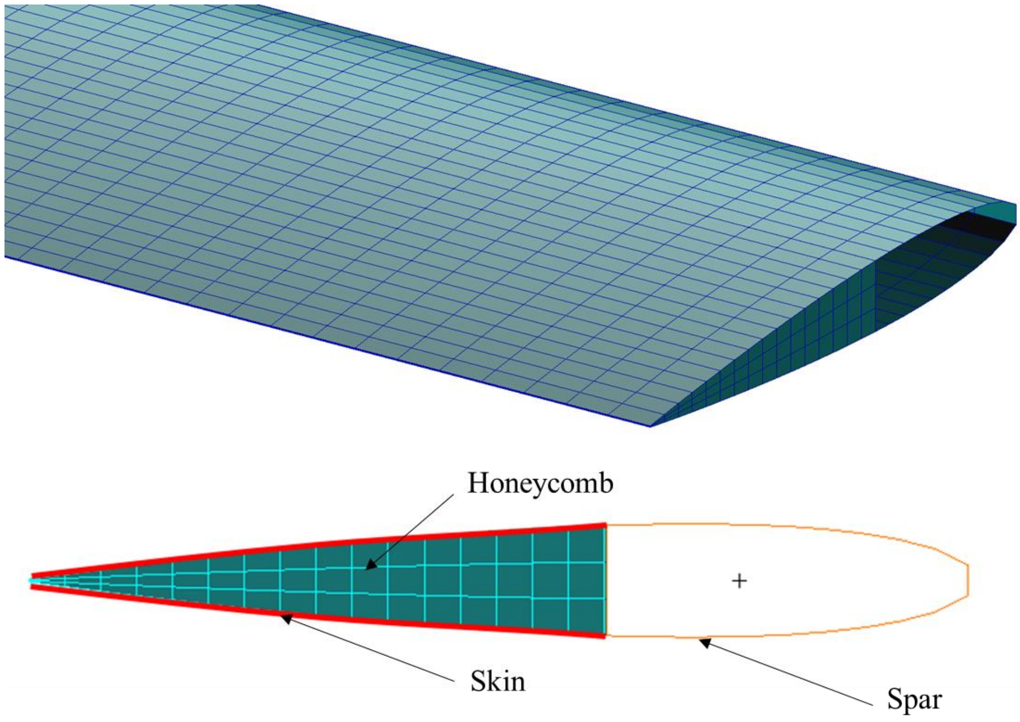

Figure 2.16 Blade FE Model

Since the rotor blade is formed from composite material, material modeling is another important parameter in Patran. For the spar and skin S-Glass/Epoxy Composite material is selected and the mechanical properties are given in Table 2.4. The spar is modeled as 2D orthotropic material with 3mm thickness. The skin is modeled as a laminated composite with 45°/90°/45° material orientation, reference system is given in Figure 2.17 and in Table *2.5* laminated composite material properties are given. The honeycomb is modeled as a 3D orthotropic material and the mechanical properties are given in Table *2.6*.

Table 2.4 *Mechanical properties of the S-Glass/Epoxy Material*

Elastic Modulus, E_{11} (MPa)	50000
Elastic Modulus, E_{22} (MPa)	12000
Poisson Ratio, υ	0.30
Shear Modulus, E_{12} (MPa)	5000
Shear Modulus, E_{23} (MPa)	6000
Shear Modulus, E_{13} (MPa)	5000
Density (kg/mm^3)	1.85e-06

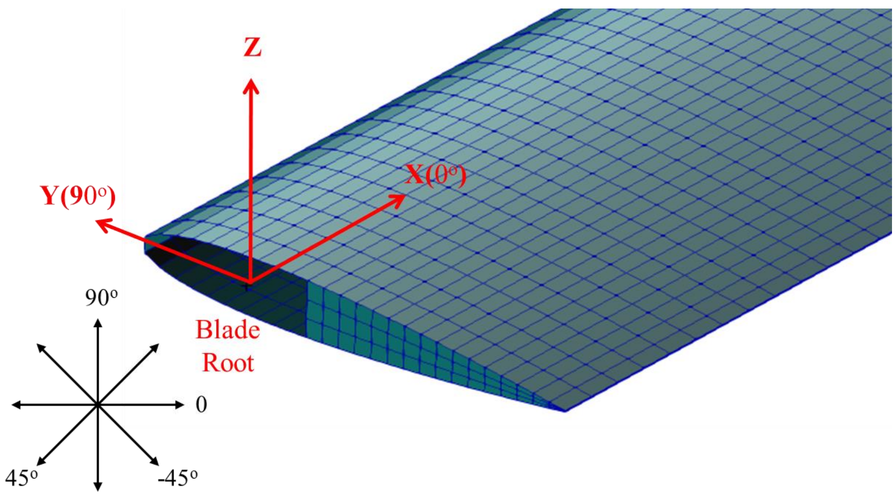

Figure 2.17 Reference system for composite material orientation

Table 2.5 *Laminated Composite Material of the Skin*

Material Name	**Thickness**	**Orientation**
Glass	0.23 mm	45^o
Glass	0.23 mm	90^o
Glass	0.23 mm	45^o

Table 2.6 *Mechanical properties of the Honeycomb Core*

Elastic Modulus, E_{11} (MPa)	0.10
Elastic Modulus, E_{22} (MPa)	0.10
Elastic Modulus, E_{33} (MPa)	140
Poisson Ratio, υ_{12}	0.001
Poisson Ratio, υ_{23}	0.001
Poisson Ratio, υ_{13}	0.001
Shear Modulus, E_{12} (MPa)	0.01
Shear Modulus, E_{23} (MPa)	30
Shear Modulus, E_{13} (MPa)	50
Density (kg/mm^3)	4.80e-08

For the load application and attachment point, Rigid Body Element (RBE) feature of the Patran is used. RBEs are multi point constraint (MPC) elements and they are used to connect one node to several nodes. Different types of RBEs exist with different features and the most common types are RBE2 and RBE3. RBE2 (Figure 2.18a) is rigid connection with independent DOF at one node, and dependent DOF at arbitrary number of nodes. In RBE2, there is no relative motion between dependent nodes so it adds extra stiffness to the structure. On the other hand, in RBE3 (Figure 2.18b), reference node is a dependent node and motion at a dependent node is the weighted average of the motions of a set of independent nodes. Forces/moments applied at a reference node are distributed to the independent nodes according to their weighting factor in the RBE3. Therefore, RBE3 allows warping and 3D effects and does not add stiffness to the structure.

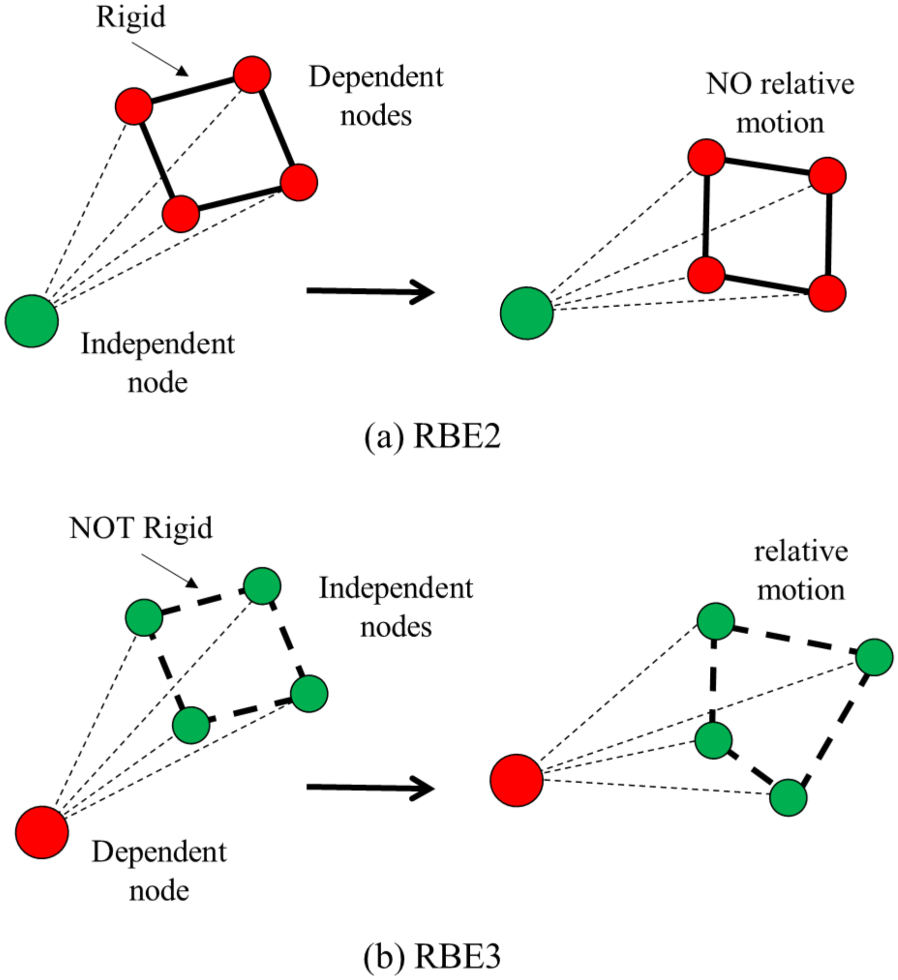

Figure 2.18 Multi Point Constraints: RBE2 and RBE3

Since the loads are applied to the blade in MSC ADAMS during the simulation as a concentrated force, ten different load application nodes, shown in Figure 2.19, are created at the aerodynamic center of the blade and these nodes are connected to the blade by using the RBE3 coupling method. In the RBE3 implementation on the rotor blade, load application point is selected as dependent node and it is connected to related nodes at the outer surface of the blade for each section, given in Figure 2.20.

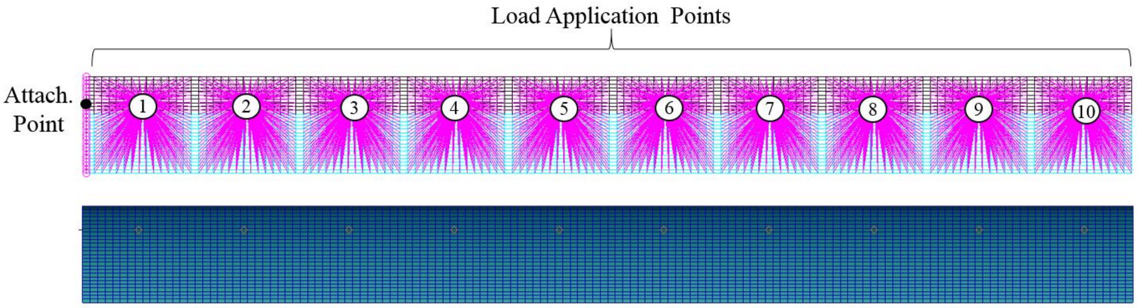

Figure 2.19 Blade Load Application Points

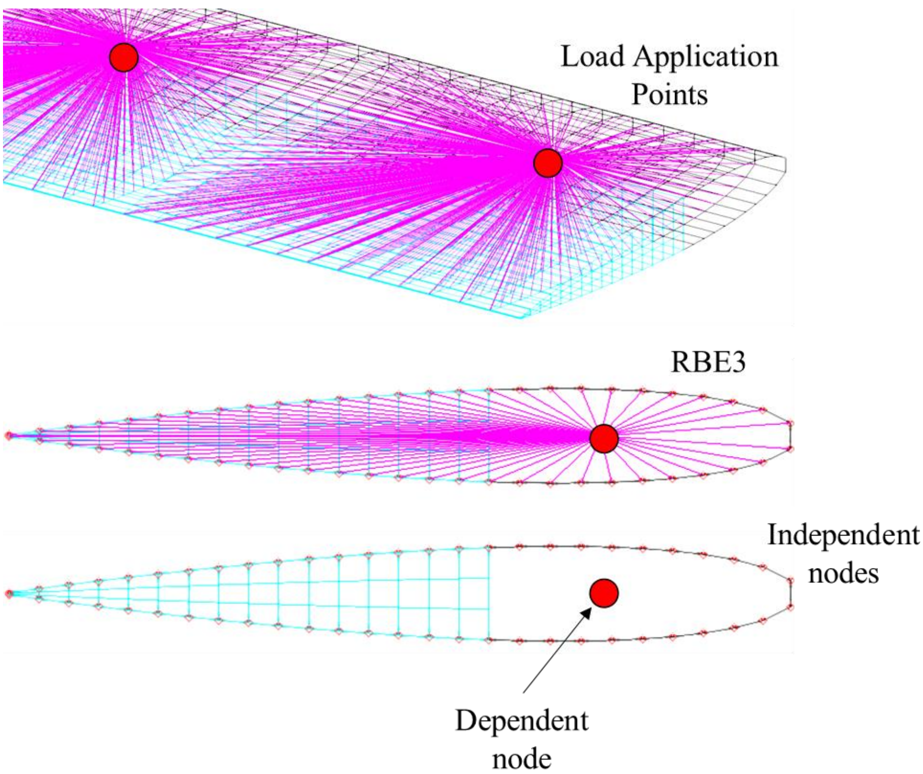

Figure 2.20 Load application points and RBE3 implementation

For the joint connection point, one node is created and connected to the blade with the RBE2 coupling method. Figure 2.21 shows the RBE2 implementation of the attachment point such that the attachment node is selected as the independent node and it is connected to all the nodes at the root section of the blade.

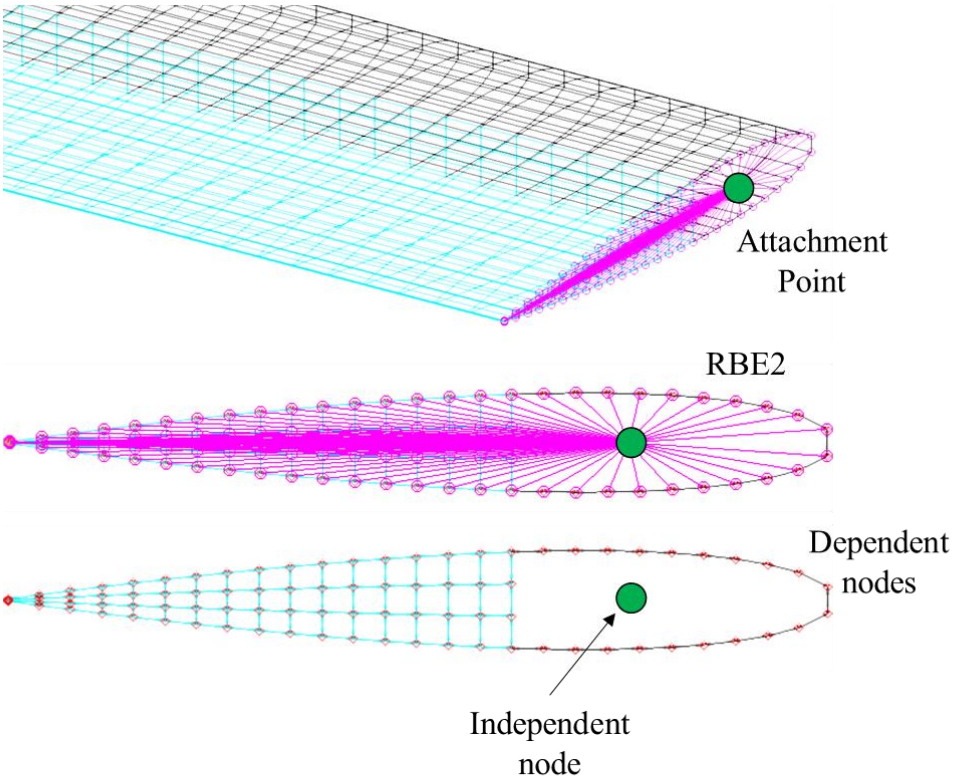

Figure 2.21 Blade Attachment Point and RBE2 implementation

For the boundary condition, cantilever boundary condition is applied to the rotor blade by fixing at the attachment point; because one end of the blade is free and the other end is attached to the rotor hub.

For the determination of the proper mesh size for the rotor blade FE model, mesh convergence study is utilized. For this purpose, FE models of the rotor blade are prepared using different elements sizes. The rotor blades are supported at one end while a transverse force is applied at their free end and their tip deflections and von Mises stress results are compared. The results are given in Figure 22 - Figure 24 and summarized. The results show that the 14445-elements rotor blade FE model is suitable for efficiency and accuracy for ADAMS multibody simulation rotor model.

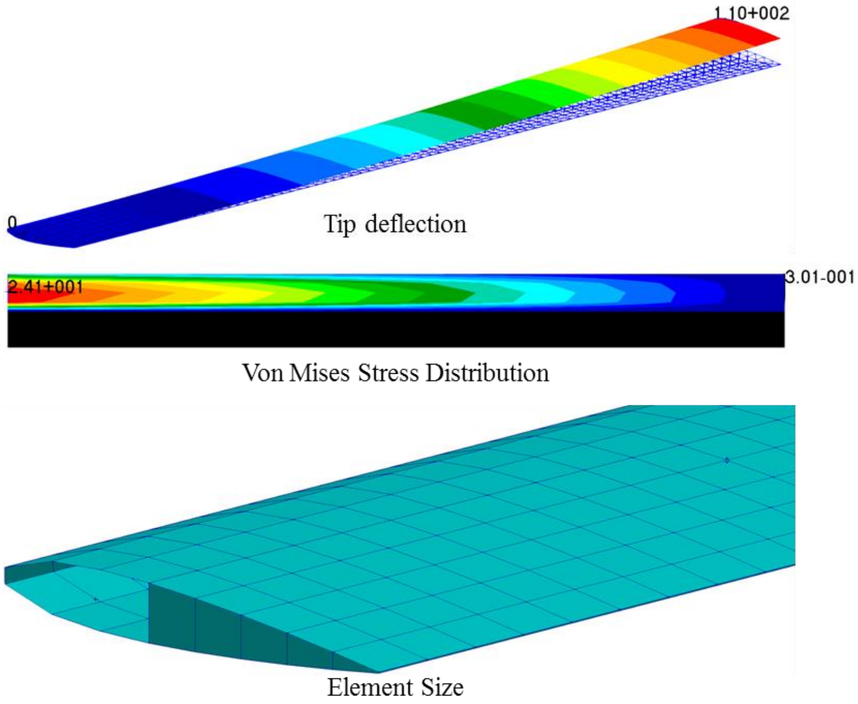

Figure 22 The rotor blade FE model with total 1949 elements

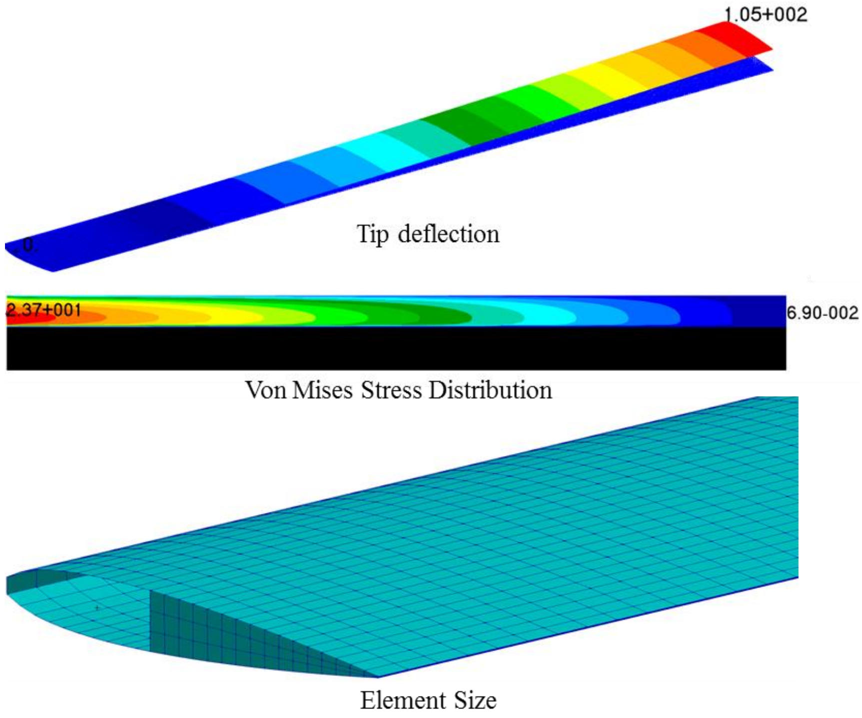

Figure 30 The rotor blade FE model with total 14445 elements

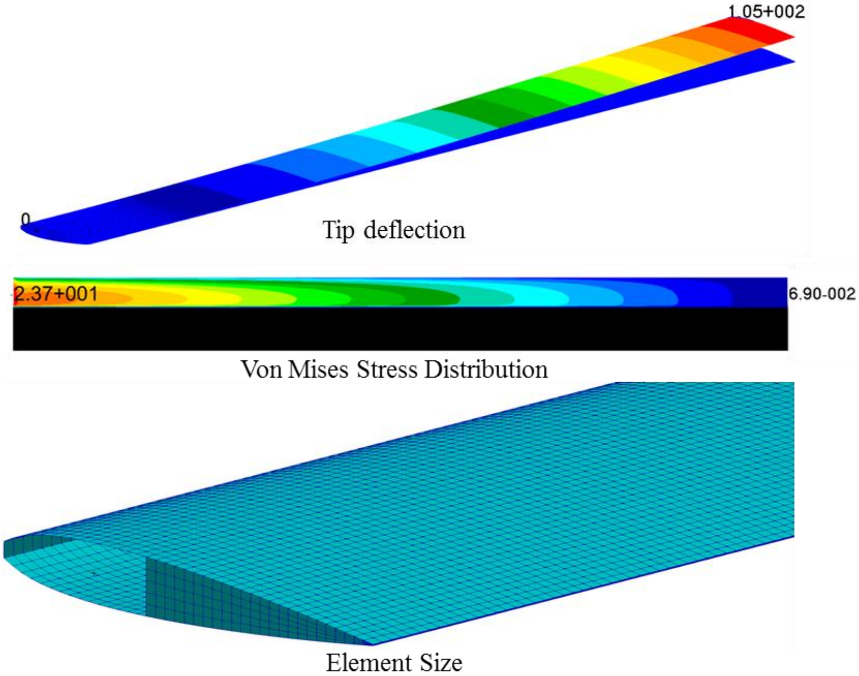

Figure 24 The rotor blade FE model with total 84765 elements

2.3.1.2. Finite Element Model of the Rotor Hub

For the FE modeling of the rotor hub, 3D solid element is used. The rotor hub model consists of 14487 six sided solid elements with 8 grid points (CHEXA) and 20589 nodes. The Figure 2.32 shows the FE model of the rotor hub.

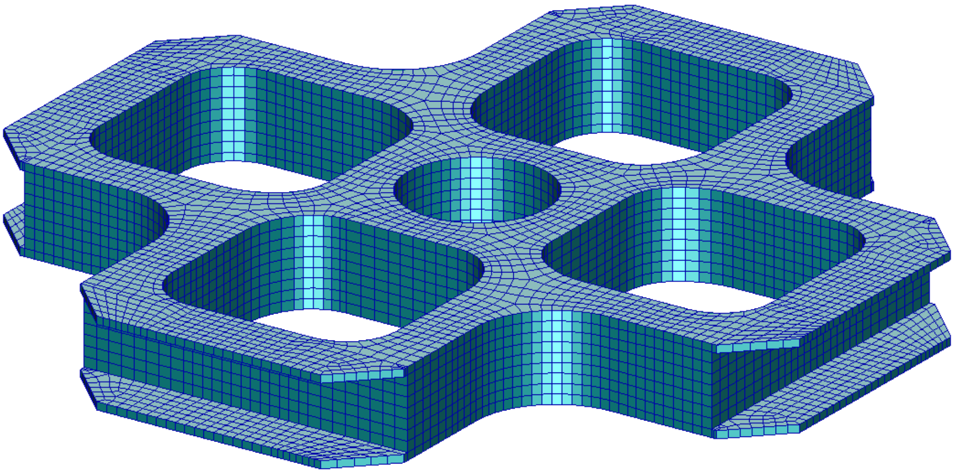

Figure 2.32 Rotor hub FE model

Since the rotor hub is made of metallic material, it is modeled by using isotropic material in Patran. For the material of the hub, 6000 Series Aluminum Alloy is chosen and mechanical properties are given in Table *2.7*.

Table 2.7 *Mechanical properties of Steel used in the Rotor Hub [19]*

Elastic Modulus (MPa)	68900
Poisson Ratio	0.33
Shear Modulus (MPa)	26000
Density (kg/mm^3)	2.7E-006

In order to connect the rotor parts to the hub, attachment locations need to be specified as a node and these nodes are joined to the FE parts by using the RBE 2 MPC method. As shown in Figure 2.33, attachment nodes are chosen as independent node (reference node) and they are connected to the hub structure at the related nodes. In the hub model, nine connection points are created for the blades, dampers, and the ground connection, and all of these are shown in Figure 2.34. Attachment points 1, 3, 5, and 7 are used for the damper connections; 2, 4, 6, and 8 are used for the blade connections and 9 is used for the hub-ground connection.

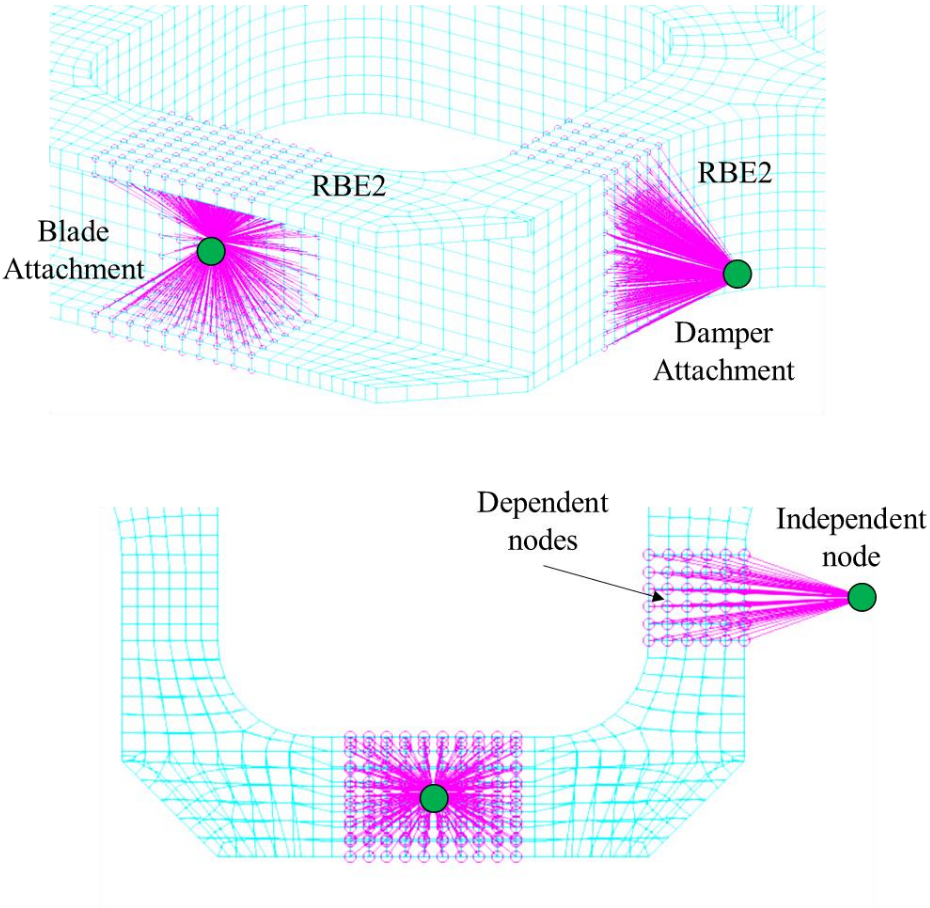

Figure 2.33 Damper and blade attachments on the rotor hub

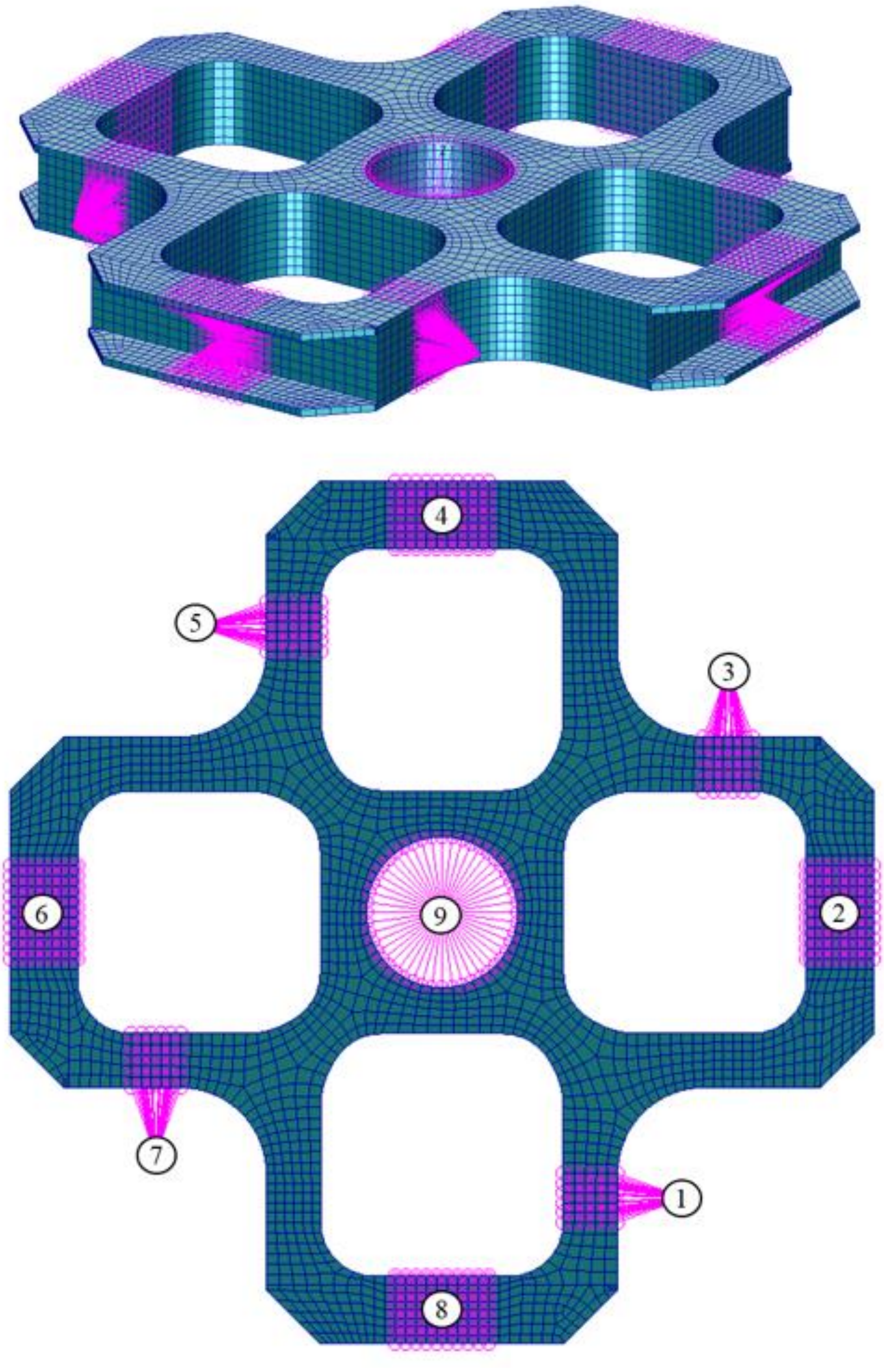

Figure 2.34 Rotor hub connection points

Since the hub is attached to the ground at connection point 9, required boundary condition is applied at that node. In the simulation of the rotor model, the hub is rotated around z-direction, shown in Figure 2.35, and it has zero displacement in all directions and zero rotation around x and y direction, so the same boundary condition is applied when the flexible hub is prepared.

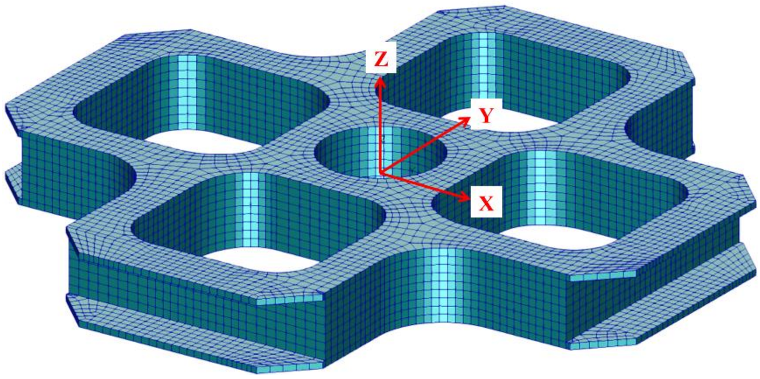

Figure 2.35 Rotor hub coordinate system

Following the preparation of the finite element models of the hub and the blade for analysis in Patran, modal analysis approach is used for modal stress recovery by using the solution sequence 103 of Nastran. After performing the modal analysis in Nastran, model neutral file (mnf) generated by Nastran is exported to MSC ADAMS. In the following section, methodology of the flexible part implementation is described.

2.3.1.3. Implementation of the flexibility

After preparing the finite element models in Patran, the MSC.Nastran/ADAMS [20] integration is used for generating the MSC.ADAMS Modal Neutral File (MNF). MNF is required for the ADAMS/Flex solver, and it can be directly imported to the MSC.ADAMS. The MNF is a binary file that contains large amount of data about the flexible body.

In a modal neutral file following information are stored:

- Mode shapes
- Nodal mass and inertia
- Location of nodes
- Generalized mass and stiffness for the mode shapes

In general, for the preparation of the MNF file to create a flexible body, modal superposition principle is utilized. In the modal superposition method, the linear deformations of the nodes are approximated as a linear combination of a smaller number of mode shape vectors, as shown in following relation:

$$\boldsymbol{u} = \sum_{\boldsymbol{i}=\boldsymbol{1}}^{\boldsymbol{M}} \boldsymbol{\phi}_{\boldsymbol{i}} \boldsymbol{q}_{\boldsymbol{i}} \tag{1}$$

where u is the linear deformation vector, M is the mode shape number, ϕ is the mode shape vector and q is the scale factor (amplitude). By using this principle, complex shapes can be built as a linear combination of simple shapes, as demonstrated in Figure 2.36.

Figure 2.36 Modal superposition principle [20]

Based on this methodology, when the flexible body is prepared, active mode shapes need to be selected carefully to capture the blade deformation of interest. In this study, for the main rotor blade and the main rotor hub flexibility, utilized mode shapes are presented in the Figure 2.37 and Figure 2.38, respectively. For higher order modes, local effects were observed and they had to be deactivated considering the calculation accuracy and efficiency.

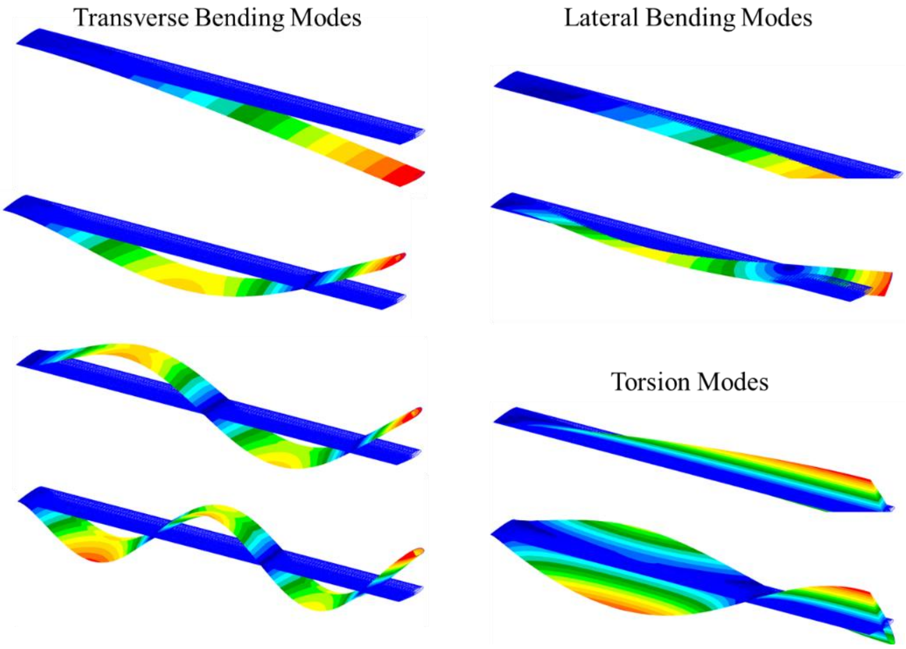

Figure 2.37 Active mode shapes of the flexible main rotor blade

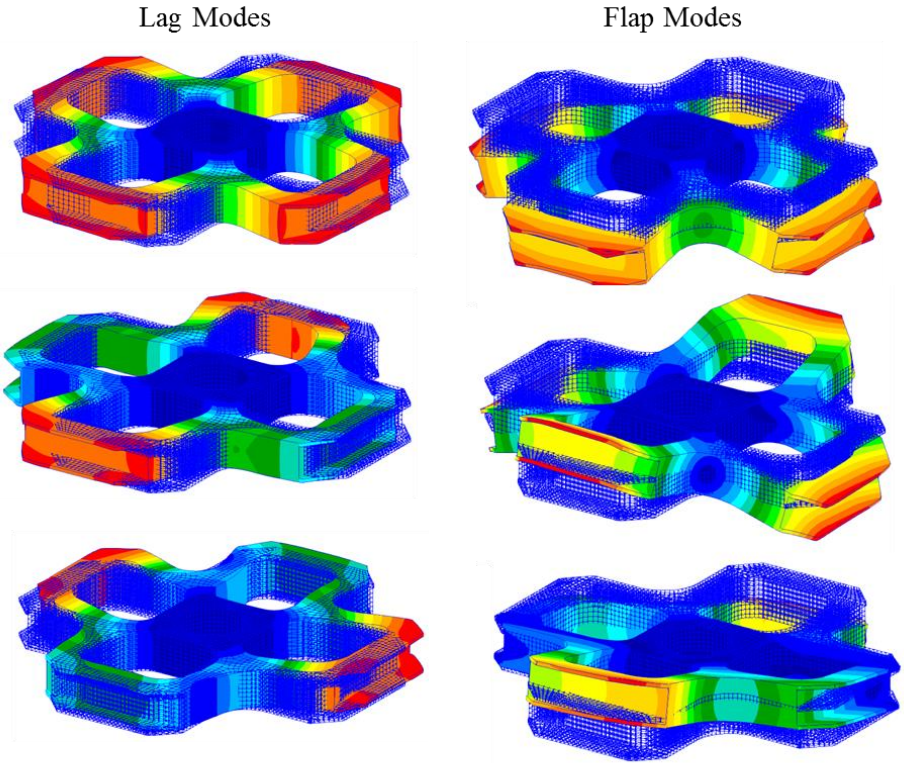

Figure 2.38 Active mode shapes of the flexible main rotor hub

2.4. Blade Loads

In the simulation of a helicopter rotor, accurate prediction of the blade loads is crucial. A rotating helicopter blade produces three types of forces namely, inertial, centrifugal, and aerodynamic forces. Figure 2.39 illustrates the loads acting on a blade section.

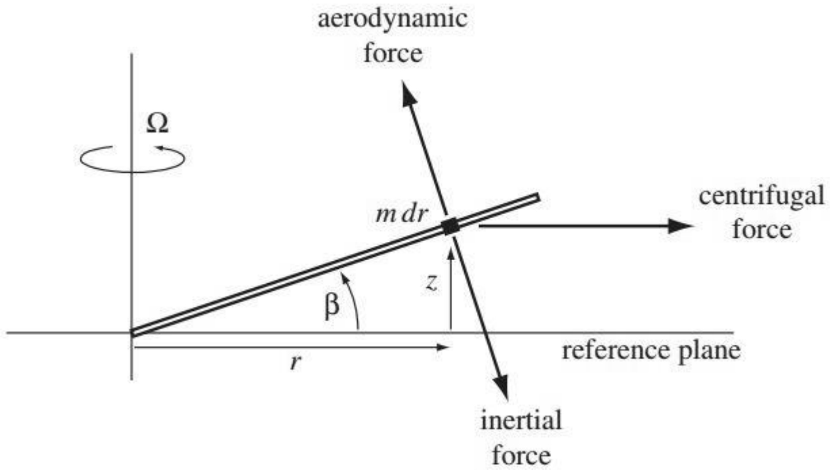

Figure 2.39 Blade Loads [1]

- Centrifugal force ($m\Omega^2 r$): due to the rotational velocity of the rotor blades around the hub center.
- Inertial forces: due to the blade motions (lag, flap) relative to the hub.
- Aerdynamic forces: produced by the rotor blades.

2.4.1. Inertia and Centrifugal Loads

The helicopter rotors are subjected to a series of motions in order to control the direction of the helicopter in the flight. Hence, rotor parts are subjected to significant inertia loads. Inertia and centrifugal loads of the rotor mainly come from blade motion and rotation of the helicopter rotor.

In the ADAMS rotor model, rotor is rotated at the hub center at a specified rotational velocity and blade control inputs are given via the swash plate and pitch links as collective input and inertia loads are calculated by ADAMS automatically.

2.4.2. Aerodynamic load

The rotating blade aerodynamic loads analysis and implementation is another major parameter for the accurate representation of the helicopter rotor simulation. In this study, since simple and efficient but still accurate aerodynamic load calculation methodology is needed, lifting line theory is used, [1], [2], [21]. In order to prevent unnecessary complexity for calculation of aerodynamic forces, simplest possible case is considered based on the following assumptions:

- constant chord
- no pitch flap coupling
- no lead-lag motion effect on blade velocity
- rigid flapping
- rigid pitch control
- no reverse flow, tip loss, and root cutout, inflow effect

For these conditions, formulation of the lifting line theory is implemented into the ADAMS model for direct calculation of aerodynamic loads without a need for external calculations.

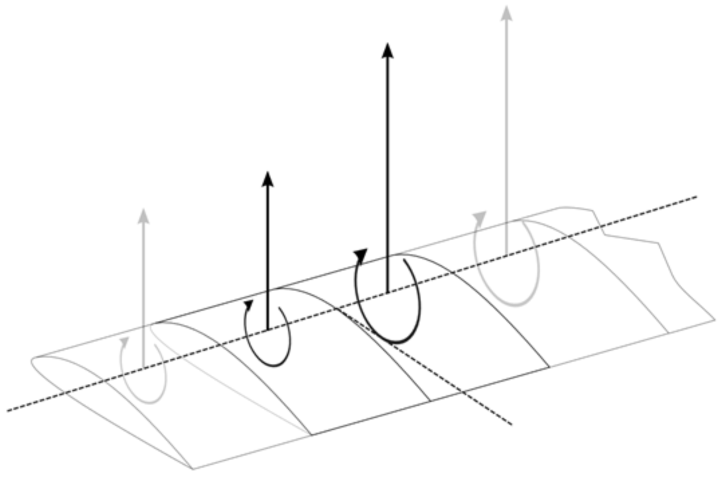

Figure 2.40 Lifting Line Theory

For the implementation of the lifting line theory, the three-dimensional rotor blades are discretized into several smaller segments, as demonstrated in Figure 2.40. For each blade segment, aerodynamic load calculations are performed by using the related two-dimensional blade section properties and variables which are shown in Figure 2.41.

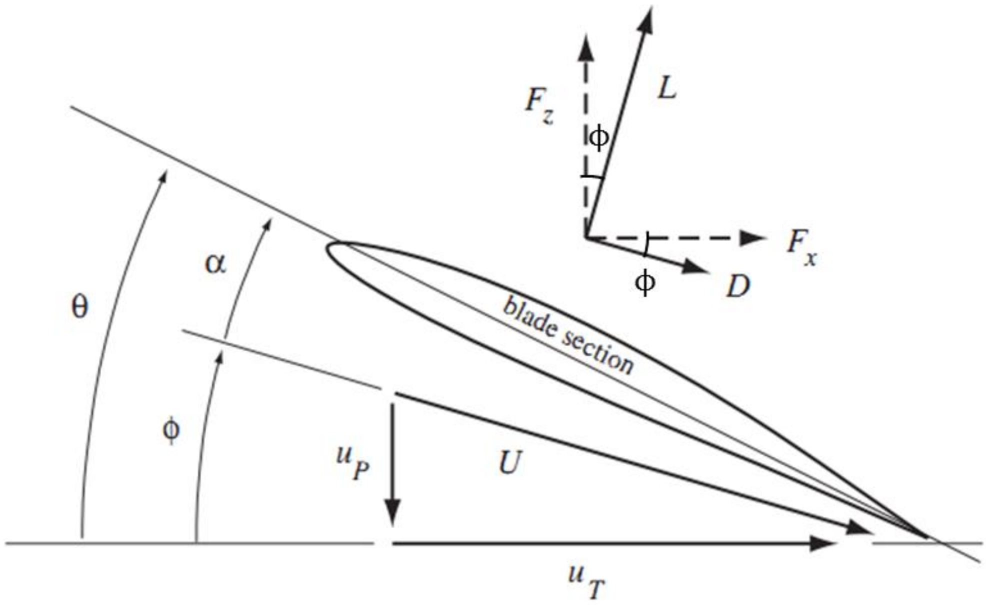

Figure 2.41 Blade Section Velocity and Force Variables [1]

In Figure 2.41;

$\boldsymbol{\theta}$: Blade section pitch angle, directly related to collective and cyclic pitch control.

$\boldsymbol{\phi}$: Inflow angle, which is related to the blade flap motion.

$\boldsymbol{\alpha}$: Section angle of attack.

$\boldsymbol{u_P}$: Perpendicular component of the relative air velocity (relative to the disk plane)

$\boldsymbol{u_T}$: Tangential component of the relative air velocity (relative to the disk plane)

$\boldsymbol{U}$: Resultant air velocity

$\boldsymbol{L}$: Lift force

$\boldsymbol{D}$: Drag force

For the calculation aerodynamic loads, angle of attack and resultant air velocity need to be determined. As it shown in Figure 2.42, perpendicular component of air velocity can be calculated if blade flap angle (β), flap angular velocity ($\dot{\beta}$), and advance ratio, shown in Figure 2.43, are known. On the other hand, tangential component of the free stream velocity (u_T) depends on the rotational velocity of the rotor and the free stream velocity.

$$u_P = \dot{\beta}\, r + \beta\, \mu\, \cos\psi \qquad (2)$$

$$U = \sqrt{u_T^2 + u_P^2} \qquad (3)$$

$$\phi = \tan^{-1}\frac{u_P}{u_T} \qquad (4)$$

$$\alpha = \theta - \phi \qquad (5)$$

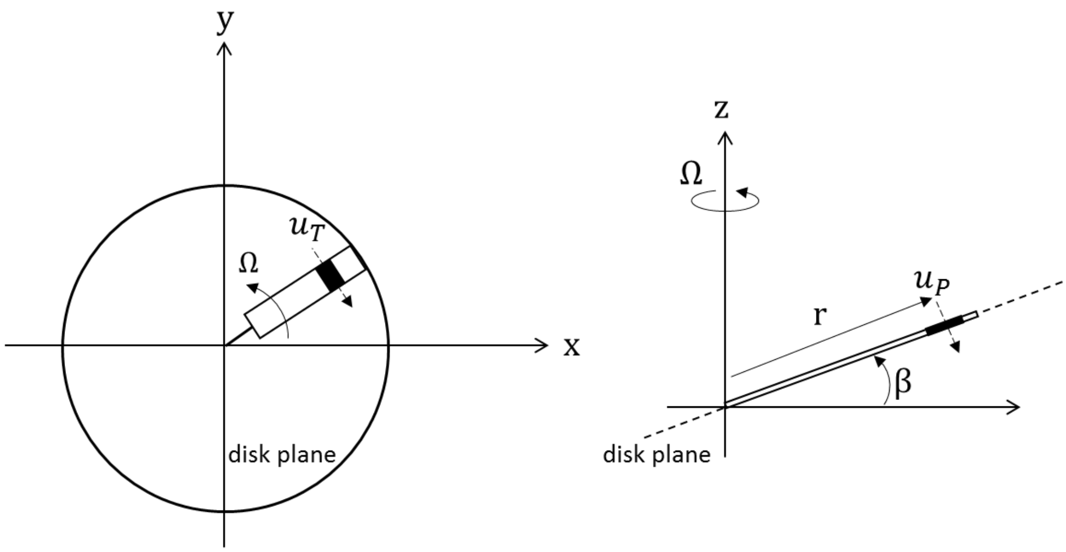

Figure 2.42 Tangential and perpendicular component of the relative air velocity

In Figure 2.43;

Rotor advance ratio: $$\mu = \frac{V \cos i}{\Omega R} \tag{6}$$

The advance ratio is the ratio of the forward velocity to the rotor tip speed.

where, V is the helicopter velocity with respect to the air, i is the disk plane incidence angle, R is the rotor radius, measured from center of rotation to blade tip, Ω is the rotational velocity of the rotor.

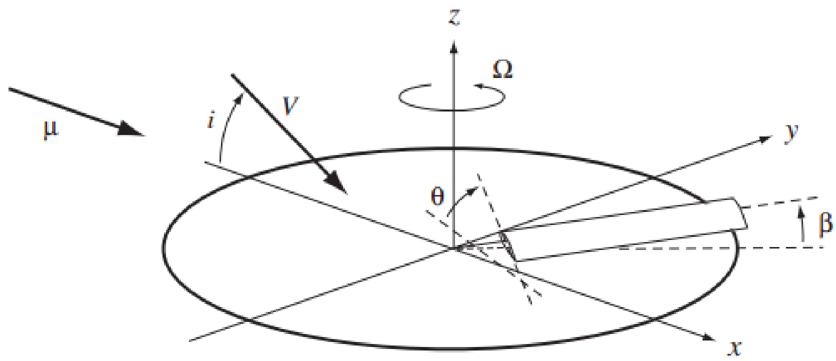

Figure 2.43 Rotor velocity and blade motion

For the determination of $\dot{\beta}$, θ and u_T ADAMS simulation model can be used. In the ADAMS model, joint motions can be measured and used as a variable in the equations. Hence, $\dot{\beta}$ and θ can be measured directly from the related joints. Tangential component of the relative velocity u_T is obtained indirectly by using the measured data and entered environmental conditions into the ADAMS analysis model. It should be noted that for the rotating blade, tangential component of the resultant air velocity depends on the free stream velocity (V) and the rotational velocity (Ω) of the rotor. If no wind condition is assumed, free stream velocity is only due to the helicopter motion during the flight. For instance, for the hover condition and zero forward velocity, resultant air velocity depends only on the rotational velocity of the rotor. However, for the forward flight condition, as it is demonstrated in Figure 2.44, resultant air velocity varies depending on the azimuth angle of the blade due to the forward flight velocity component.

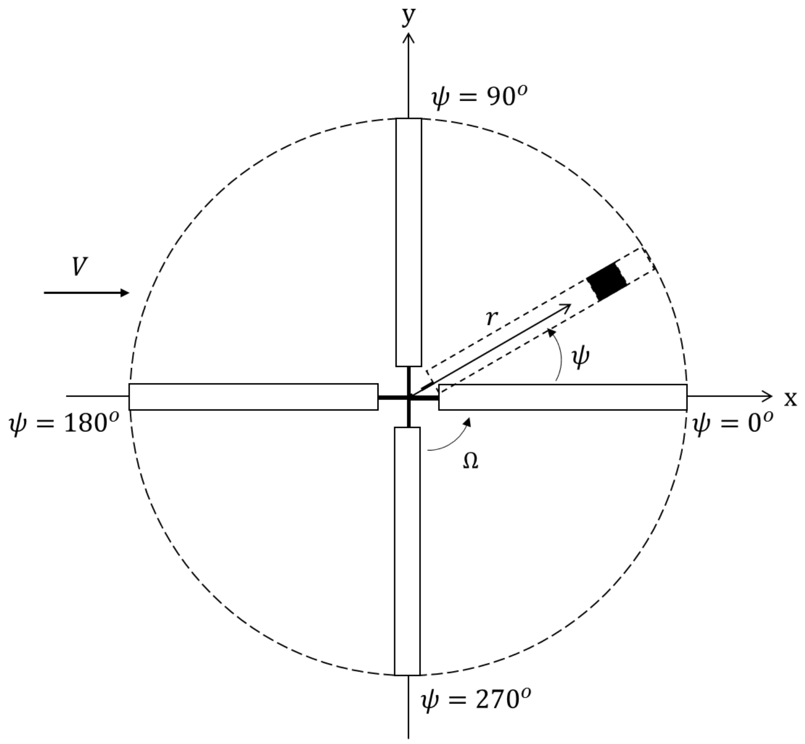

Figure 2.44 Resultant air velocity variation

Equation (7) gives the total tangential component of the relative velocity,

$$\boldsymbol{u_T = r + \mu \sin \psi} \tag{7}$$

where, r is the radial location on the blade, μ is the advance ratio, ψ is the azimuth angle of the blade.

In the ADAMS model, aerodynamic loads depend on the resultant air velocity (U) and the blade angle of attack (α), at each load calculation point in the blade. Since both resultant air velocity and angle of attack values are evaluated in ADAMS and used as input for the aerodynamic loads calculations, different flight scenarios can be analyzed easily. For the instantaneous calculation of the aerodynamic loads, aerodynamic coefficients (lift, drag, and moment coefficients) need to be known for each angle of attack value. For this purpose, these coefficients are implemented into the ADAMS model by using the curve fitting methodology. Aerodynamics coefficients used depend on α and Mach number, which are presented in Figure 2.45 - Figure 2.47 for the NACA0012 airfoil.

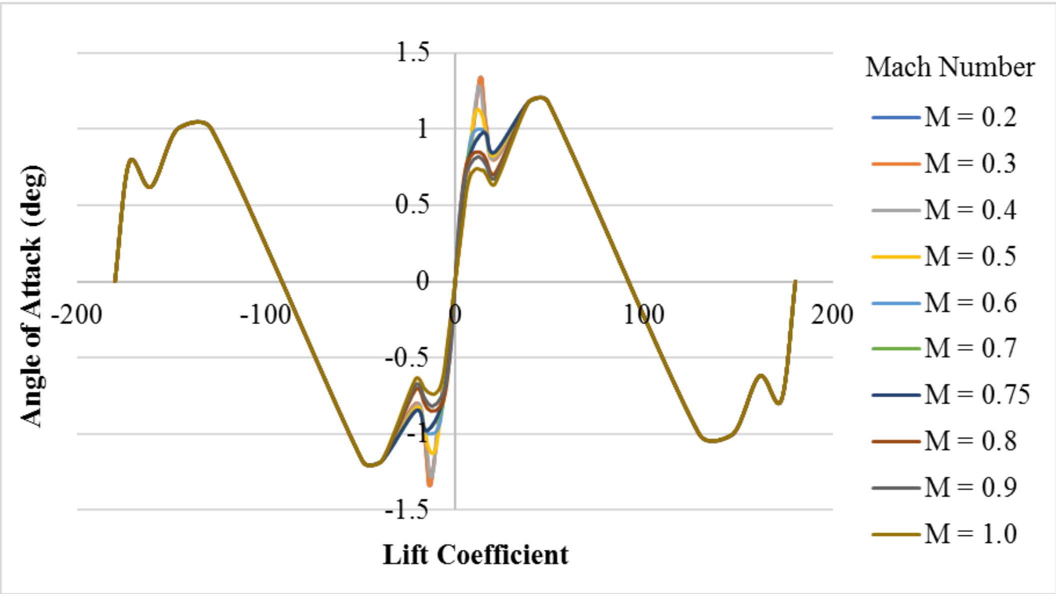

Figure 2.45 $\boldsymbol{c_l - \alpha}$ data for different Mach numbers for the NACA0012 airfoil [22]

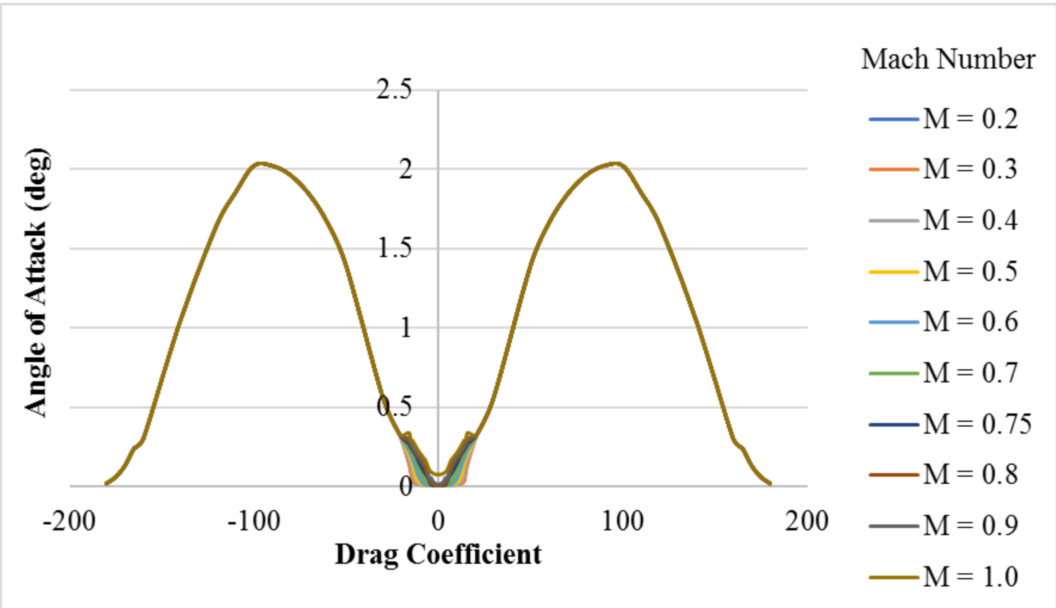

Figure 2.39 $\boldsymbol{c_d - \alpha}$ data for different Mach numbers for the NACA0012 airfoil [22]

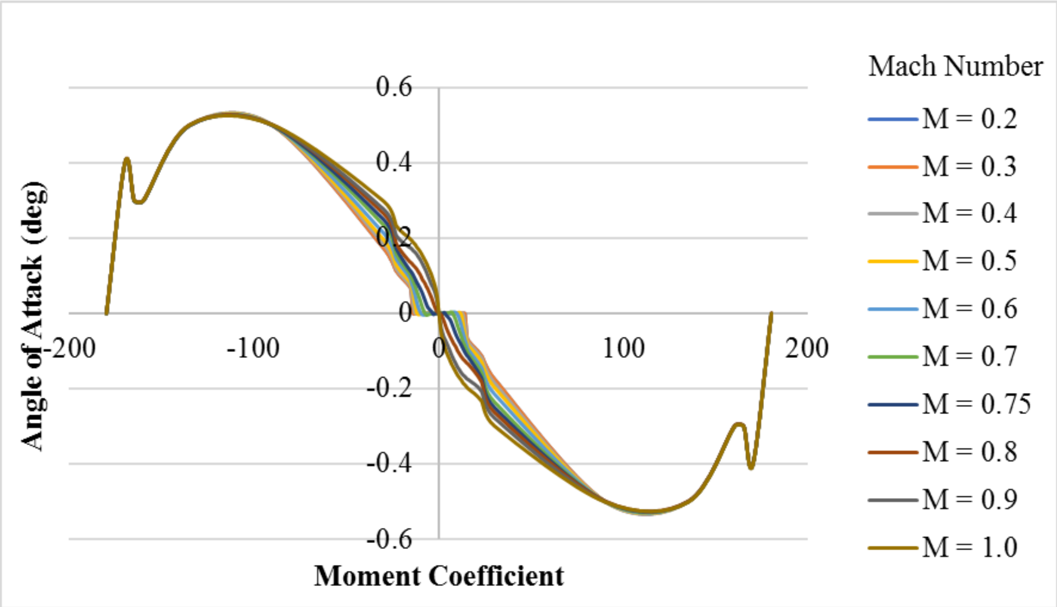

Figure 2.47 $\boldsymbol{c_m - \alpha}$ data for different Mach numbers for the NACA0012 airfoil [22]

In order to determine the aerodynamic loads for a rotor blade section, following relations are used:

Lift: $$L = \frac{1}{2}\,\rho\,U^2\,c\,c_l \qquad (8)$$

Drag: $$D = \frac{1}{2}\,\rho\,U^2\,c\,c_d \qquad (9)$$

Pitching Moment: $$M = \frac{1}{2}\,\rho\,U^2\,c^2\,c_m \qquad (10)$$

where,

c: chord length

c_l: lift coefficient

c_d: drag coefficient

c_m: moment coefficient

ρ: air density

2.5. Control System

During the flight, in order to control the helicopter, three main control types exist to be used by the pilot; the anti-torque pedals, the cyclic pitch control, and the collective pitch control. The anti-torque pedals are used for adjusting tail rotor blade pitch angles to control the thrust at the tail of the helicopter for the purpose of controlling the yaw motion. On the other hand, cyclic and collective pitch controls, as demonstrated in Figure 2.41, are related to the main rotor blade angle adjustment. The collective pitch control is used for changing pitch angles of all the main rotor blades by the same amount via a series of hinges. Since the helicopter main rotors are operated at fixed RPM, in order to adjust the lift force on the helicopter, angle of attacks of all the main rotor blades are increased or decreased to control the lift force produced by the blades by using the collective control. The cyclic pitch control allows the pilot to control the helicopter motion during the flight by changing pitch angles of the blades by different amount by tilting the swash plate to control the helicopter in longitudinal and lateral directions. Basically, collective pitch control is used for controlling the average blade force, and hence the main rotor thrust magnitude, whereas the cyclic pitch control is used for controlling the helicopter direction by changing main rotor thrust vector direction.

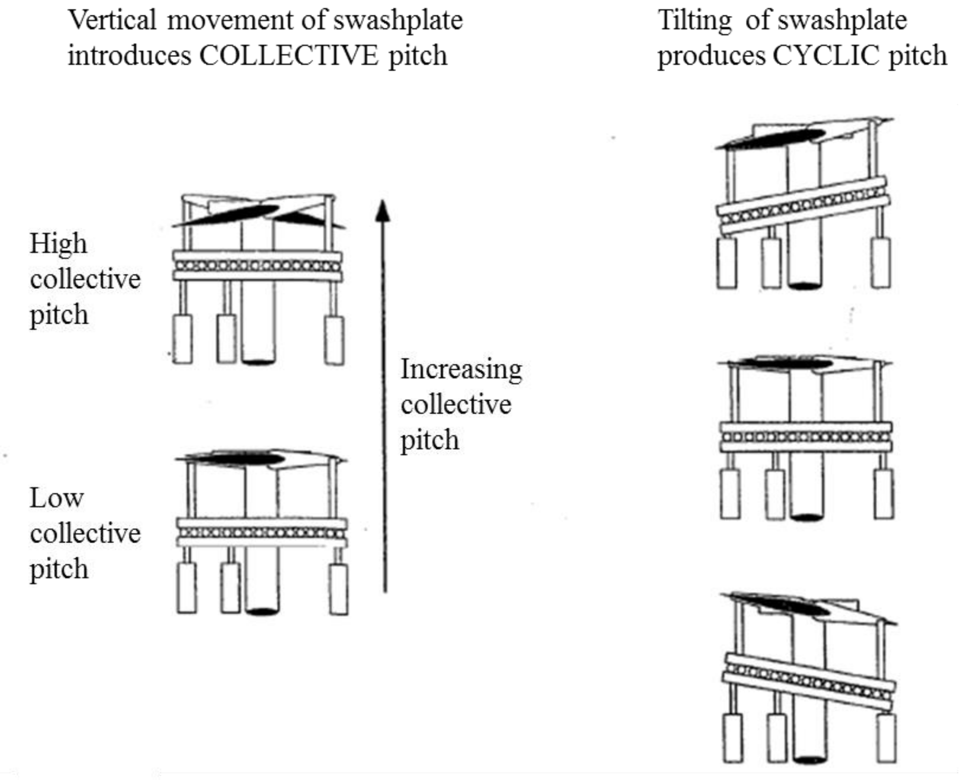

Figure 2.41 Collective and cyclic pitch control [21]

As demonstrated in Figure 2.42, since the blades are connected to the swash plate, all of the main rotor blades angles are kinematically related each other. In addition to this, the rotor is the main source of the force and moment generation through the blades and external loads are controlled by changing the blades's pitch angle, which is commanded from the helicopter control system. Controlling the blade pitch angle is a very effective method for controlling the rotor forces because the feathering moments on the blade are low, and lift force change due to the pitch action is large. The blades's pitch angle can be expressed as a function of the azimuth angle (ψ), collective (θ_0), lateral (θ_{1c}) and longitudinal (θ_{1s}) pitch control. Longitudinal cyclic control provides longitudinal control of the helicopter and lateral cyclic control provides lateral control of the helicopter. Blade's pitch angle is calculated by Equation (11) and Figure 2.42 shows the schematic of collective and lateral/longitudinal cyclic pitch angle.

$$\theta(\psi) = \theta_0 + \theta_{1c} * \cos\psi + \theta_{1s} * \sin\psi \quad (11)$$

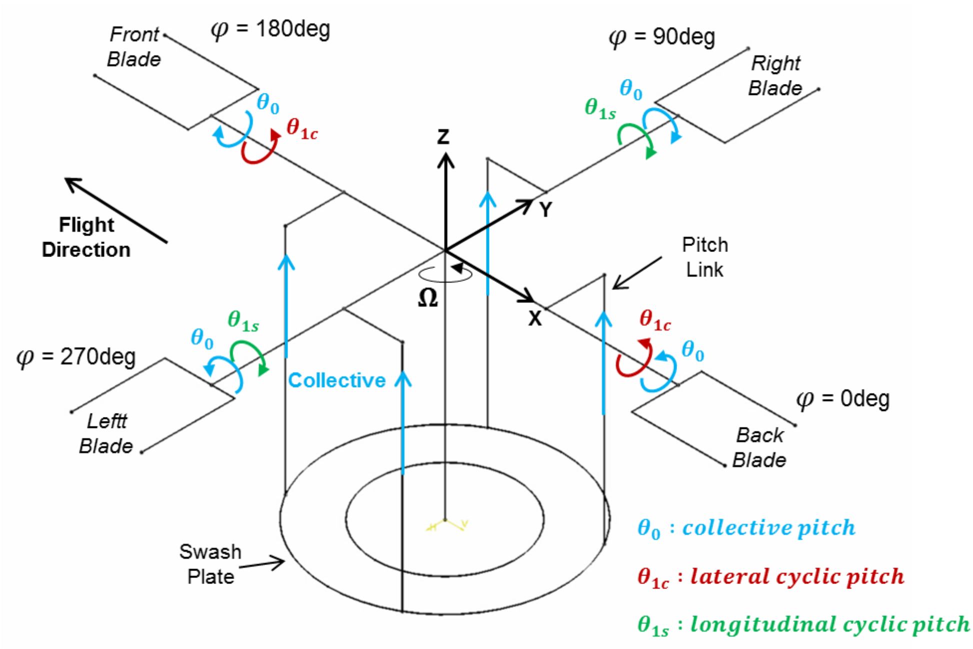

Figure 2.42 Schematic of collective and lateral/longitudinal cyclic pitch angle

For a four bladed helicopter rotor, pitch angles at the azimuth angles 0^o, 90^o, 180^o and 270^o are calculated by Equations (12) - (15).

$$\theta_{right} = \theta_0 + \theta_{1s} \tag{12}$$

$$\theta_{front} = \theta_0 - \theta_{1c} \tag{13}$$

$$\theta_{left} = \theta_0 - \theta_{1s} \tag{14}$$

$$\theta_{back} = \theta_0 + \theta_{1c} \tag{15}$$

Variations of the pitch angle of the main rotor blades cause the tip path plane to tilt, hence the thrust vector of the helicopter rotor. The tip path plane (TPP), demonstrated in Figure 2.43, is the plane that describes the circle created by the flight path of the tips of the main rotor blades and the thrust vector of the helicopter main rotor is always perpendicular to the tip path plane. Therefore, in order to control helicopter motion, tip path plane needs to be tilted to change the direction of the thrust vector for the desired flight direction. For this purpose, since there is no chance to tilt the helicopter rotor shaft, swash plate mechanism is used.

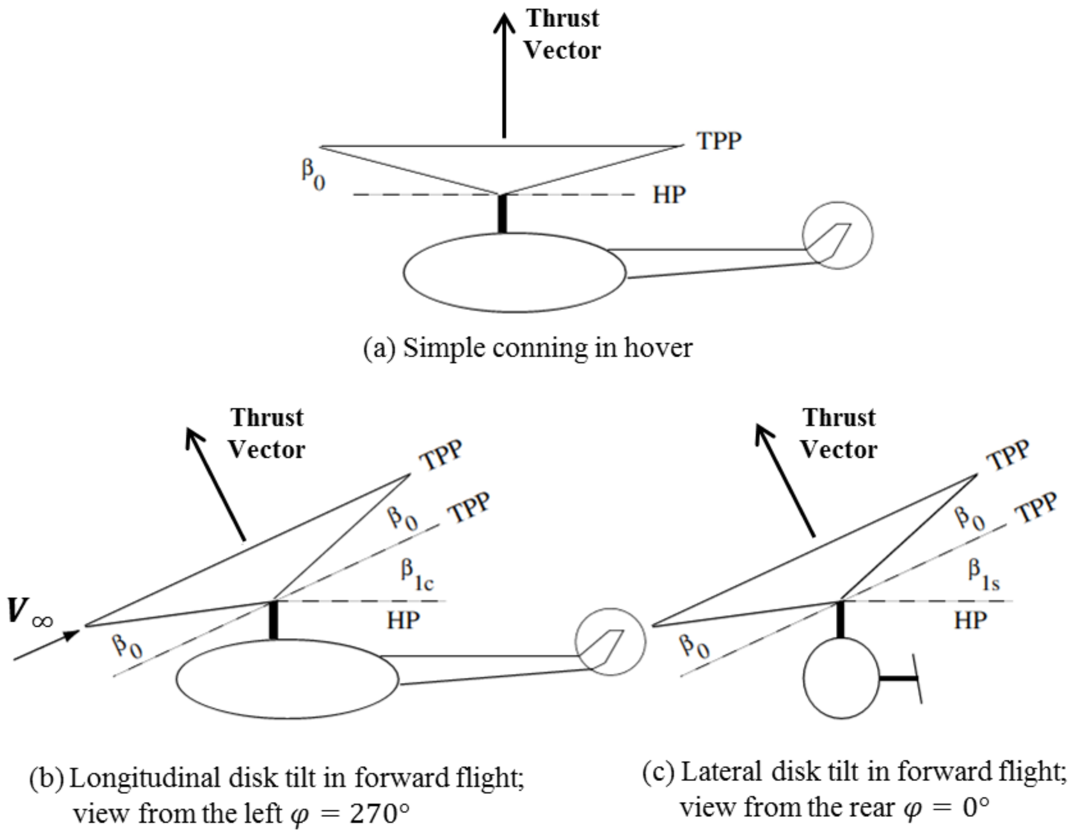

Figure 2.43 Tip path plane (TPP)

The swash plate mechanism transmits the cyclic and collective inputs from flight control actuators to the main rotor blades via linkages. The swashplate mechanism, shown in Figure 2.44, consists of two main parts; rotating swashplate and non-rotating (fixed) swash plate. The flight control actuators are connected to the fixed swashplate with the linkages and the fixed swashplate is mounted around main rotor mast via spherical shaped uni-ball sleeve, which allows the swashplate to tilt in lateral and longitudinal directions and move vertically. The rotating swashplate rotates at same speed with the main rotor and it sits on the fixed swashplate by using a ball bearing located between them to allow relative rotation while the orientation and the vertical position of the rotating plate along the shaft axis is governed by the fixed swashplate. Finally, the pitch links are connected to the rotating swash plate and pitch levers on each main rotor blade to control the pitch angles. As shown in Figure 2.42, collective pitch control input changes all of the main rotor blades pitch angles equally, whereas cyclic pitch control changes the blade pitch angles individually.

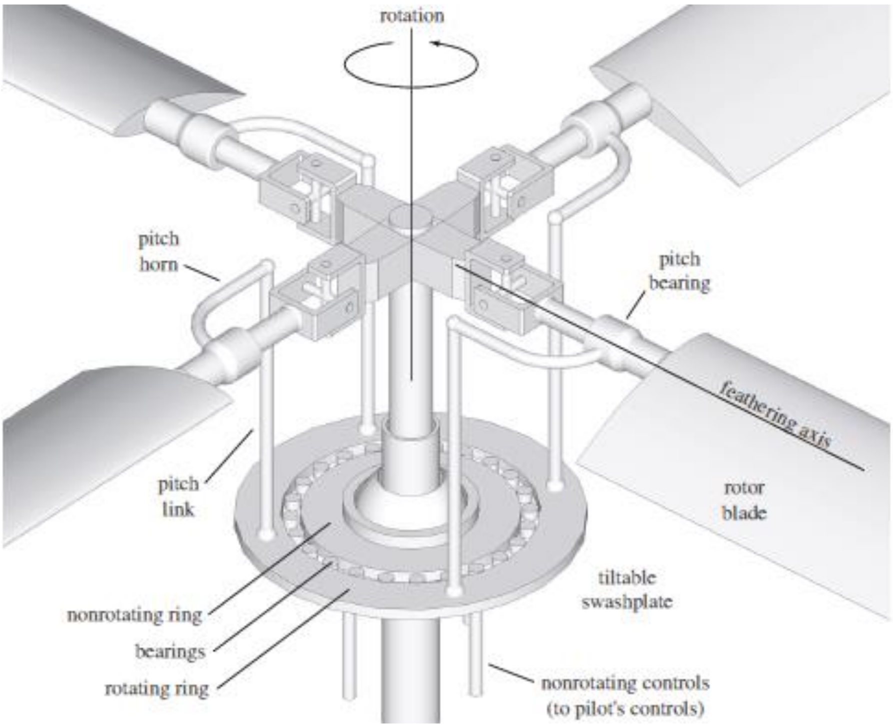

Figure 2.44 Swash plate mechanism [1]

2.6. Rotor Trim

In general, for the successful flight of any aircraft, the inertial, gravitational and aerodynamic forces and moments about the three mutually perpendicular axes have to be in balance. For this purpose, to maintain the specified flight condition in equilibrium, the aircraft needs to be trimmed to satisfy the force and the moment equilibrium by adjusting the control inputs to change the force and the moment produced. Trimming a helicopter is generally classified into two types; full aircraft trim and isolated rotor trim.

In full aircraft trim, the purpose is to make sure that the rotor forces and moments are equal and in opposite direction to those produced by the rest of the aircraft. Basically, the target is to achieve 3 force and 3 moment equilibriums. Therefore, it is necessary to have 6 control variables. In this case, the three main rotor controls angles; θ_0, θ_{1s}, and θ_{1c} , the tail rotor collective; aircraft yaw control, and the two aircraft attitude angles; the lateral tilt and the longitudinal tilt are control variables for calculating the equilibrium condition by using the six vehicle equilibrium equations.

For an isolated rotor trim, the three rotor control angles; collective pitch θ_0, lateral θ_{1c} and longitudinal cyclic pitch θ_{1s} are the control variables to satisfy the three specified targets; the rotor thrust T, the rotor roll moment M_x, and the rotor pitch moment M_y, given in Figure 2.45. Isolated rotor trim is widely used in the wind tunnel test. In this study, since the multibody model represents the isolated main rotor, this approach is used for trim calculations.

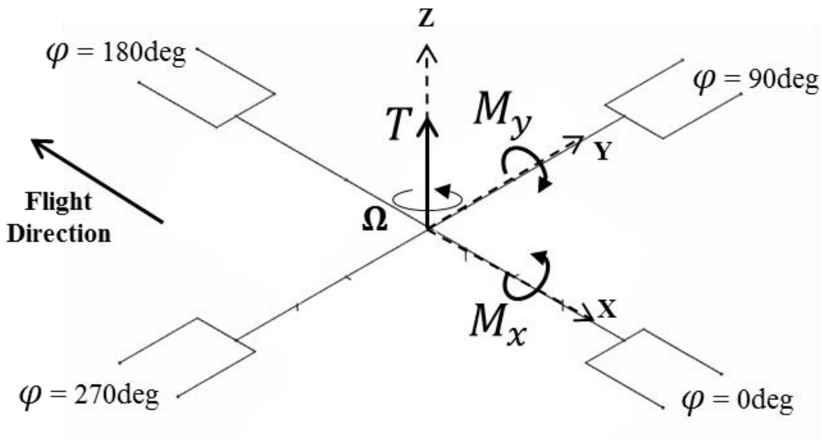

Figure 2.45 Trim targets of an isolated rotor

For trimming, rotor thrust (T^t), rotor hub roll moment (M_x^t) and rotor hub pitch moment (M_y^t) are trim the targets, and collective pitch trim (θ_0^t), lateral cyclic pitch trim (θ_{1c}^t), longitudinal cyclic pitch trim (θ_{1s}^t) are the unknowns. In order to evaluate $\theta_0^t, \theta_{1c}^t$ and θ_{1s}^t at the desired rotor thrust value, force and moment equilibrium equations are used. In order to determine the equilibrium equations, blade forces, which are shown in Figure 2.46 for a blade element, are calculated at the hub center. For this purpose, variations of the rotor thrust and the moments due to the change in the blade pitch angle θ have to be determined.

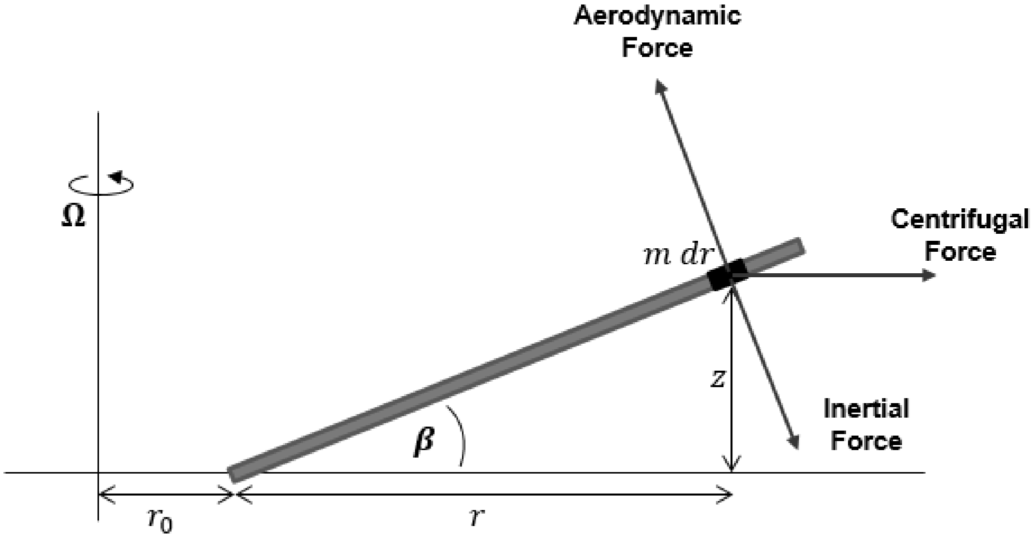

Figure 2.46 Blade Forces

In order to determine the rotor hub moments and the rotor thrust which are used in trim calculations, ADAMS multibody rotor model is utilized. In the ADAMS model, rotor is simulated to obtain the individual effect of a single blade on the rotor thrust, rotor hub roll moment and rotor hub pitch moment. For 'nth' blade, rotor thrust is denoted as T^{t,B_n}, rotor hub roll moment denoted as M_x^{t,B_n}, and rotor hub pitch moment is denoted as M_y^{t,B_n}. The other three blades are deactivated and only a single blade is considered to evaluate the effect of variations of the blade pitch angle on the rotor moments and the thrust. In this analysis, the helicopter main rotor forces are controlled by changing the blade pitch angles only. Therefore, for every 0.5^o pitch angle, which represents the sum of the collective pitch and the cyclic pitch angle, in the range of -10^o to +10^o, the rotor is allowed to undergo full revolution. For every 10^o azimuth angle increment the hub moments and the thrust variations are calculated for all possible conditions. At every pitch angle condition, full revolution analysis need to be done because the rotor blade forces change at different azimuth locations due to the resultant air velocity variations. As a result of this, for a single blade, rotor hub moments and rotor thrust values are obtained with respect to the blade pitch angle and the azimuth angle. Basically, for the rotor thrust, rotor hub roll moment and the rotor hub pitch moment, different datasets are obtained and these datasets depend on the pitch angle and the azimuth angle of a blade. In Figure 2.47, a sample dataset is given for rotor thrust variations, produced from a single blade.

Azimuth Angle

Pitch Angle

	0°	**10°**	**20°**	**30°**	**...**	**350°**
0°	59.46	59.46	59.47	59.45		59.46
0.5°	306.02	312.72	322.11	333.80		302.27
1°	550.18	563.58	582.35	605.75		542.73
⋮						⋮
10°	1669.81	1821.14	2144.09	2590.10	...	1739.85

Figure 2.47 Sample dataset for the nth blade, produced by using the ADAMS rotor model

This procedure is repeated for the rest of the blades to obtain their effects on the hub moments and the thrust individually for the non-rotated blade positions shown in Figure 2.48. Following the completion of the ADAMS analysis for each blade, hub moments and rotor thrust datasets are utilized in the DATA-FIT Matlab code in order to convert them into the equation form and then to use in trim calculations.

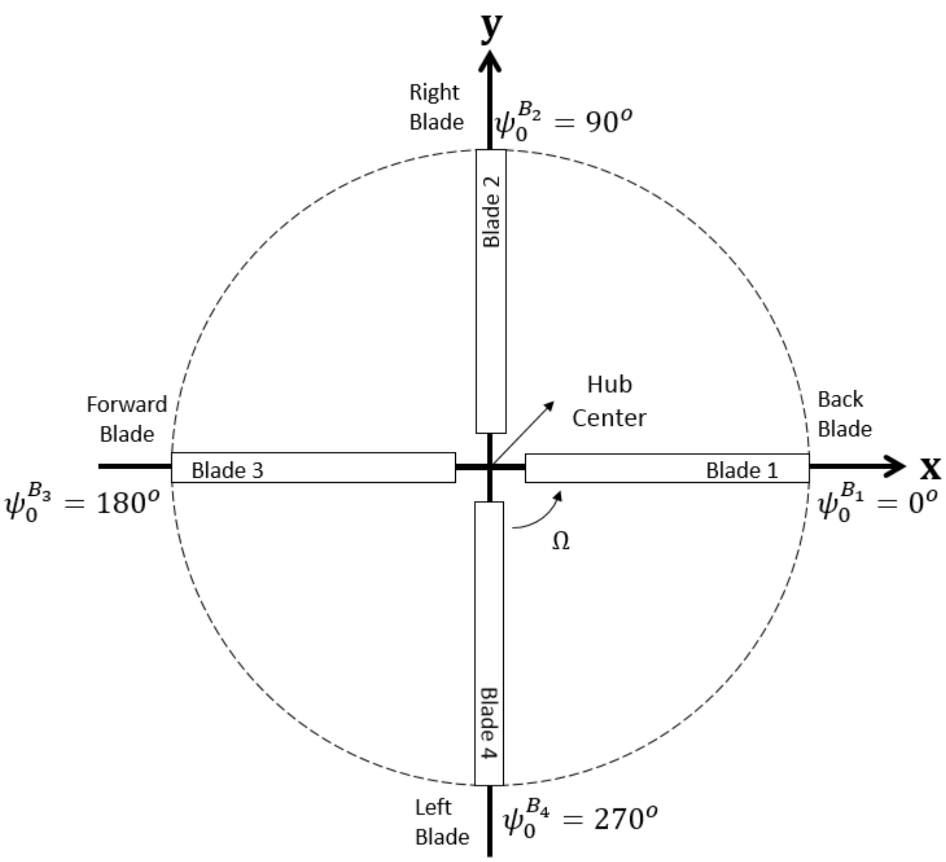

Figure 2.48 Blade positions

In the DATA-FIT Matlab code, by using the generated datasets in the curve fitting tool, for each blade polynomial fit functions are generated for the rotor thrust, rotor roll and pitch moments as a function of the pitch angle and the azimuth angle individually and they are described in Equations (16)-(18),

Thrust polynomial:	$T^{t,B_n}(\theta_{B_n}, \psi^{B_n})$	(16)
Roll moment polynomial:	$M_x^{t,B_n}(\theta_{B_n}, \psi^{B_n})$	(17)
Pitch moment polynomial:	$M_y^{t,B_n}(\theta_{B_n}, \psi^{B_n})$	(18)

where $n = 1, 2, 3, 4$ denotes the blade number.

Since total moments and thrust are trimmed by adjusting the blade pitch angles individually, summation of the fitted data is used as presented in Equations (19)-(21),

$$\begin{aligned} T^{t,TOT} &= T^{t,B_1}\left(\theta_{B_1},\psi^{B_1}\right) + T^{t,B_2}\left(\theta_{B_2},\psi^{B_2}\right) \\ &+ T^{t,B_3}\left(\theta_{B_3},\psi^{B_3}\right) + T^{t,B_4}(\theta_{B_4},\psi^{B_4}) \end{aligned} \tag{19}$$

$$\begin{aligned} M_x^{t,TOT} &= M_x^{t,B_1}\left(\theta_{B_1},\psi^{B_1}\right) + M_x^{t,B_2}\left(\theta_{B_2},\psi^{B_2}\right) \\ &+ M_x^{t,B_3}\left(\theta_{B_3},\psi^{B_3}\right) + M_x^{t,B_4}(\theta_{B_4},\psi^{B_4}) \end{aligned} \tag{20}$$

$$\begin{aligned} M_y^{t,TOT} &= M_y^{t,B_1}\left(\theta_{B_1},\psi^{B_1}\right) + M_y^{t,B_2}\left(\theta_{B_2},\psi^{B_2}\right) \\ &+ M_y^{t,B_3}\left(\theta_{B_3},\psi^{B_3}\right) + M_y^{t,B_4}(\theta_{B_4},\psi^{B_4}) \end{aligned} \tag{21}$$

where

θ_{B_1}, θ_{B_2}, θ_{B_3} and θ_{B_4} are back, right, front, and left blade pitch angle respectively, as it is presented in Figure 2.48. By using Equation (11), blade angles are calculated from Equations (22)-(25).

$$\theta_{B_1} = \theta_0^t + \theta_{1c}^t * \cos\psi^{B_1} + \theta_{1s}^t * \sin\psi^{B_1} \tag{22}$$

$$\theta_{B_2} = \theta_0^t + \theta_{1c}^t * \cos\psi^{B_2} + \theta_{1s}^t * \sin\psi^{B_2} \tag{23}$$

$$\theta_{B_3} = \theta_0^t + \theta_{1c}^t * \cos\psi^{B_3} + \theta_{1s}^t * \sin\psi^{B_3} \tag{24}$$

$$\theta_{B_4} = \theta_0^t + \theta_{1c}^t * \cos\psi^{B_4} + \theta_{1s}^t * \sin\psi^{B_4} \tag{25}$$

Since the initial positions of blades are known (Figure 2.48) and they remain constant with respect to each other, at any given time, azimuth location of the nth blade can be obtained by using following relation,

$$\psi^{B_n} = \psi_0^{B_n} + \Omega * t \tag{26}$$

where t is the simulation time and it is constant at every simulation step, Ω is the rotational velocity and it is also constant value. Then, azimuth locations of each blade in radians are calculated from Equations (27) - (30).

$$\psi^{B_1} = \Omega * t \qquad (27)$$

$$\psi^{B_2} = \frac{\pi}{2} + \Omega * t \qquad (28)$$

$$\psi^{B_3} = \pi + \Omega * t \qquad (29)$$

$$\psi^{B_4} = \frac{3\pi}{2} + \Omega * t \qquad (30)$$

Hence, the hub roll and pitch moments and thrust equations include only three unknowns which are the collective and cyclic pitch angles; $\theta_0^t, \theta_{1c}^t, \theta_{1s}^t$.

For the trim calculations of the main rotor, at each time step, hub moments and thrust equations are used in one force and two moment equilibrium equations. Then, three set of nonlinear equations in terms of three unknowns are obtained as given by Equations (31)-(33).

$$T^{t,TOT}(\theta_0^t, \theta_{1c}^t, \theta_{1s}^t) = thrust \qquad (31)$$

$$M_x^{t,TOT}(\theta_0^t, \theta_{1c}^t, \theta_{1s}^t) = 0 \qquad (32)$$

$$M_y^{t,TOT}(\theta_0^t, \theta_{1c}^t, \theta_{1s}^t) = 0 \qquad (33)$$

In order to solve the nonlinear trim equations, iterative based Newton-Raphson method is used. After the control trim angles are obtained for each time step by using the developed TRIM-FIT Matlab Code, the mean of the trim angles is imported into

ADAMS rotor model to obtain simulation results in the trimmed state. Trim calculation procedure of the ADAMS main rotor model is presented in Figure 2.49.

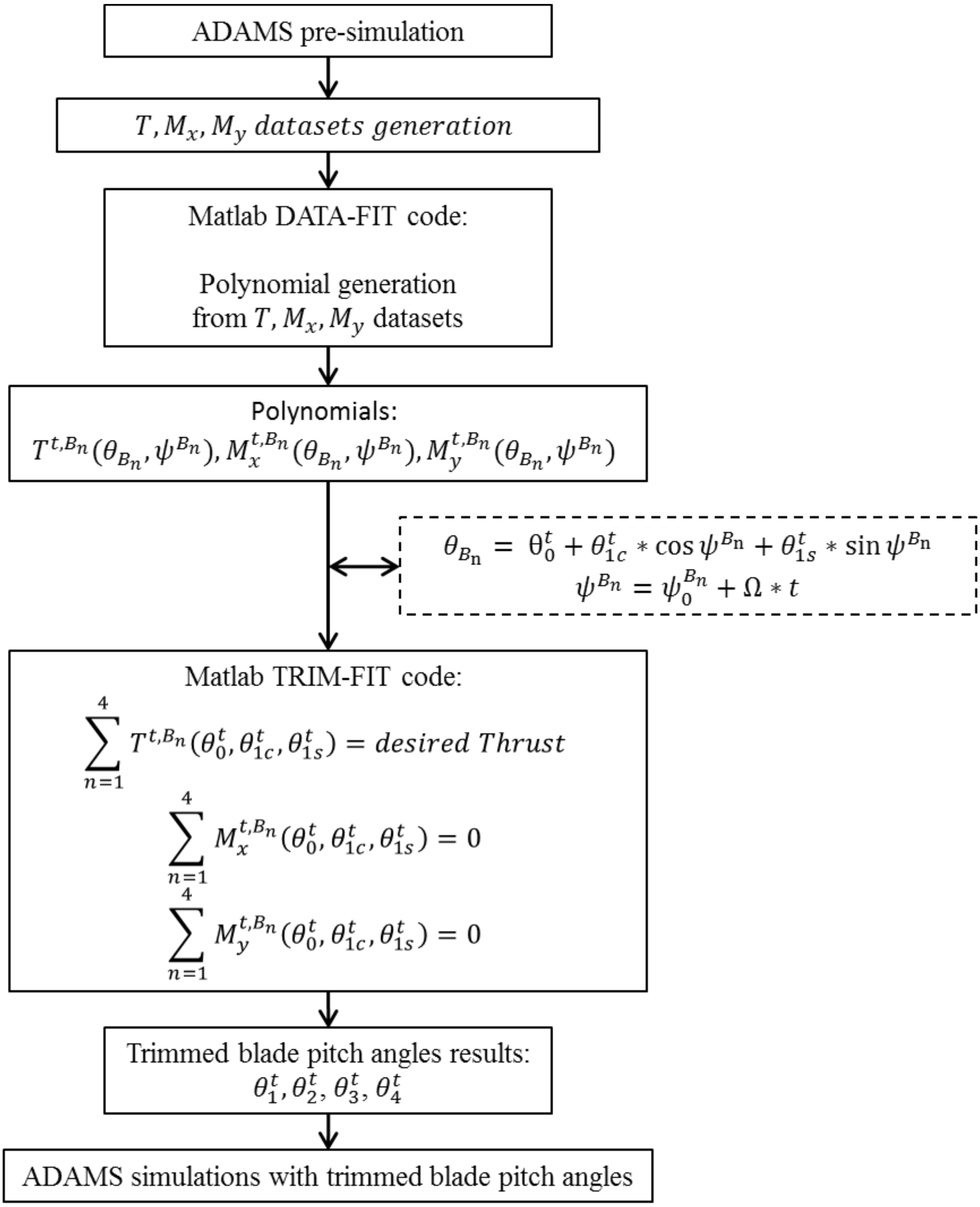

Figure 2.49 Flowchart of the trim calculations

2.7. Main Rotor Model in ADAMS

Typically, a helicopter main rotor has a large rotor radius (mostly around 5 – 6m) and it usually consists of two, three, or four blades, as presented in [23]. The rotor RPM is generally around 300. Rotor parameters are chosen arbitrary in view of the existent helicopter rotor. Parameters of the main rotor system (Figure 2.50) are summarized in Table *2.8* and preparation procedure of the ADAMS main rotor model is presented in Figure 2.51 as a block diagram.

Table 2.8 *Rotor parameters*

Rotor Type	Fully Articulated
Rotor Radius	4.75 m
Number of Blades	4
Chord	0.375m (constant)
Hinge offset	0.44 m
Blade effective region starting point	0.75 m
Torque offset	0 m
Pitch-Flap Coupling	0 deg
Airfoil	NACA 0012
Blade Mass	11.84 kg
Rotor Rotational Speed	1440 deg/s (240 RPM)
Damper	Stiffness Coefficient: 1000 N/mm Damping Coefficient: 5 Ns/mm

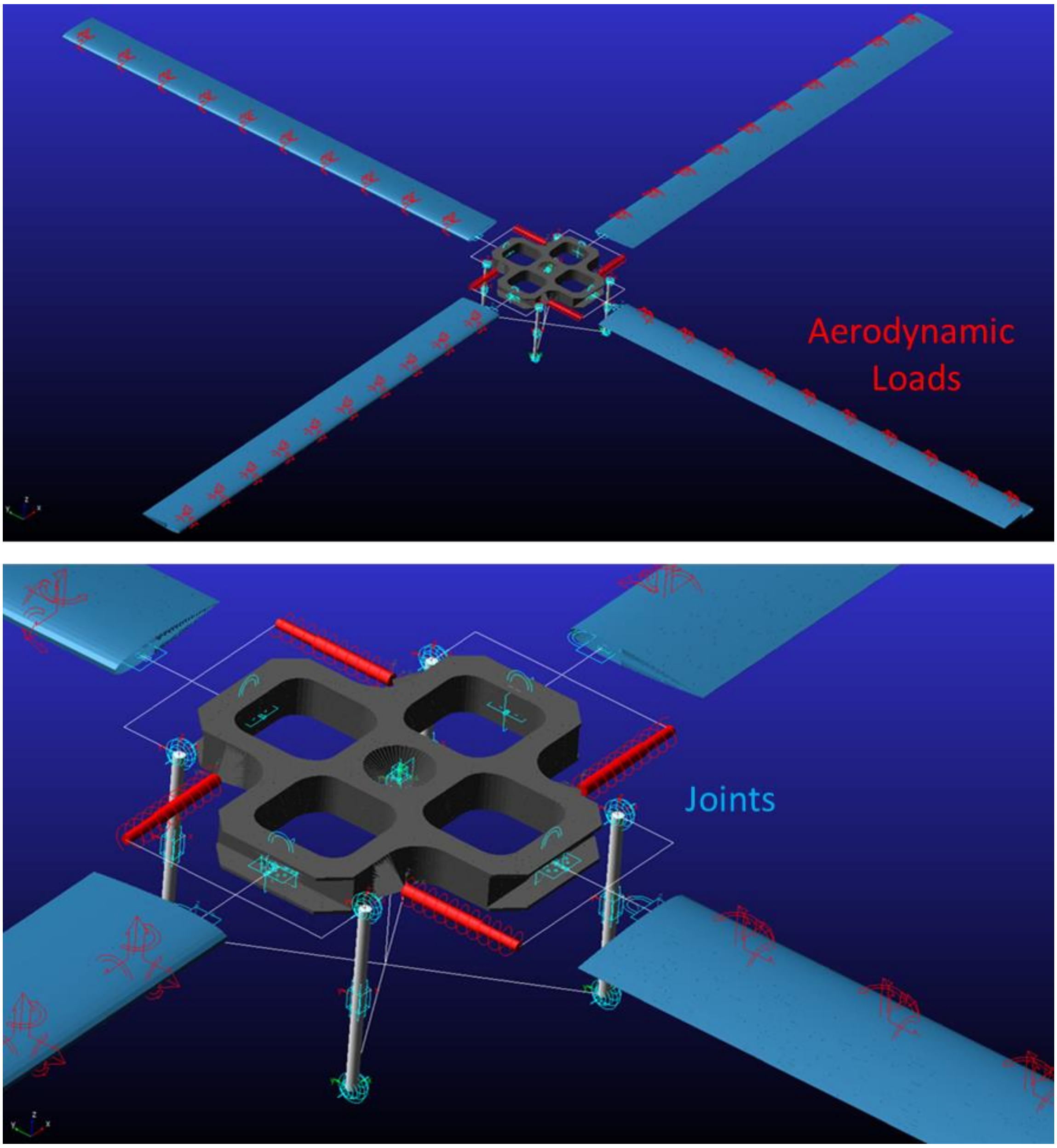

Figure 2.50 Main rotor multibody dynamics model in ADAMS

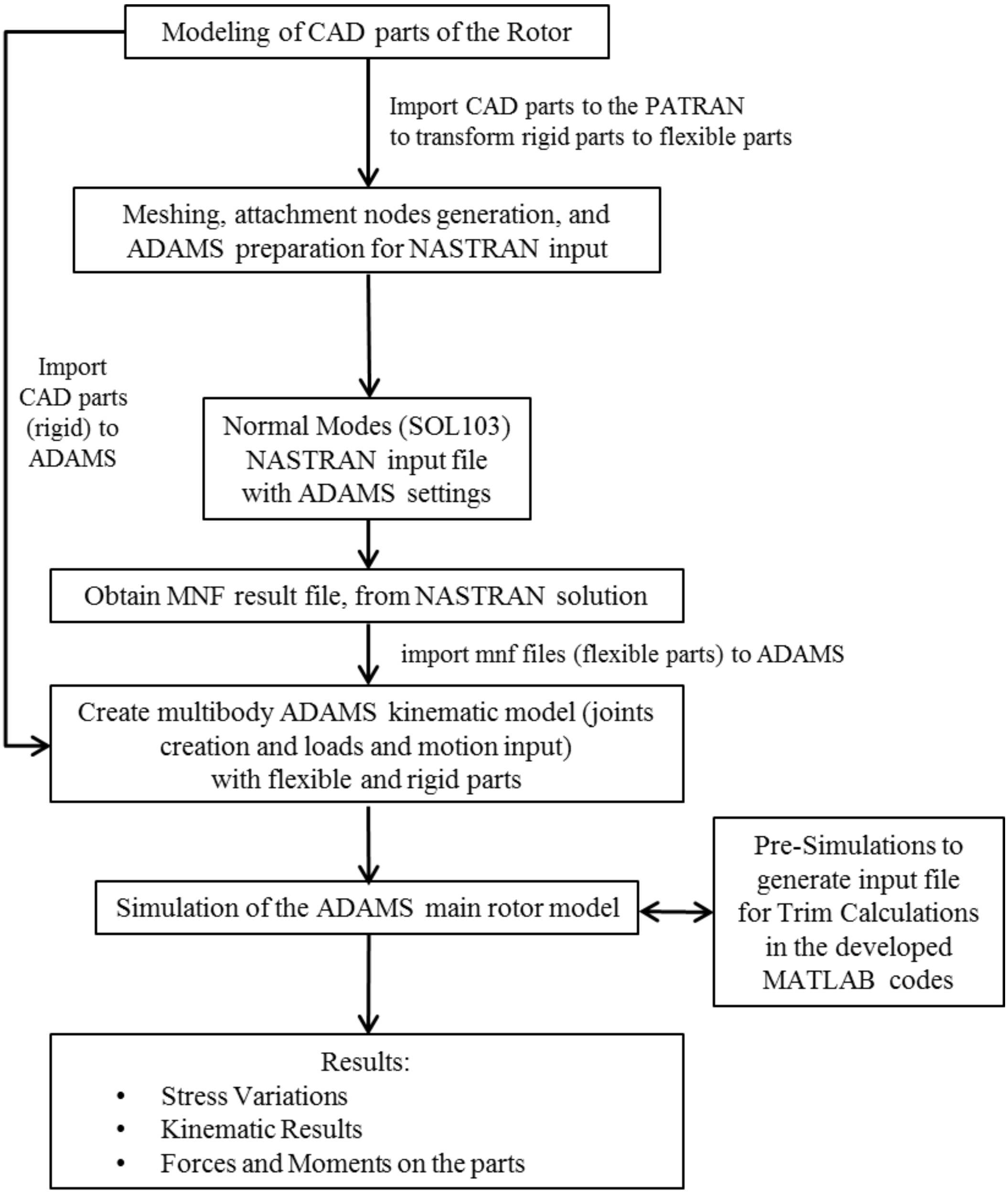

Figure 2.51 Block diagram of the multibody simulation process of the helicopter rotor

CHAPTER 3

NONLINEAR MODELLING OF THE FLEXIBLE ROTOR BLADE

3.1. Stiffening Effect under High Axial Force

The rotation of the beam like structures leads to a geometric stiffening effect, which is also known as the centrifugal stiffening in the literature. In the helicopter rotor case, stiffening effect cannot be neglected when the flexible helicopter main rotor blades are modeled since they are operated under high rotational velocity which leads to high centrifugal forces. However, in ADAMS, the stiffening effect cannot be included into the flexible body directly since ADAMS/Flex solver cannot handle nonlinearities. On the other hand, since helicopter main rotors are operated under constant rotational velocity, they are subjected to constant centrifugal force. Hence, when flexible main rotor blades are modeled, stiffening effect can be included.

In order to include the stiffening nonlinear effects of the preload on the flexible part, Nastran [14] provides restart analysis for SOL 106 (nonlinear statics solution sequence) into SOL 103 (normal modes solution sequence). A preload is an internal load and only works on the modal coordinates. It is considered as properties of the flexible structure due to the operational condition. For example, tip deflection and natural frequency of a rotating slender beam is different from the nonrotating condition due to stretching of the structure under the centrifugal force. Hence, in order to include this stretching effect, centrifugal force needs to be added to the structure as a preload.

Restart analysis is done in two steps. First, nonlinear static (SOL 106) analysis is performed under the desired load (preload), which is the centrifugal force for a long slender rotating structure like the helicopter rotor blade and the boundary condition for the generation of the nonlinear stiffness matrix. Second, normal modes analysis (SOL 103) analysis is done by using the stored nonlinear stiffness matrix. For the restart analysis in Nastran, some DMAP modifications need to be done in the Nastran input files (BDF); SOL 103 and SOL 106, presented in the APPENDIX.

In order to investigate the restart analysis results, a simple 3D rod is modeled in Patran for different preload cases and exported as the MNF file to use in ADAMS. The structure is modeled in a long and slender form to represent the helicopter rotor blade structure. It has constant square cross-section with 25x25 mm dimensions and 1000 mm in length, given in Figure 3.1. The structure consists of 900 six sided solid elements with 8 grid points (CHEXA) elements and 1618 nodes and it has homogeneous material with 200000 MPa Elastic Modulus and 0.3 Poisson ratio. It has clamped-free boundary condition. As for the preload, the structure is stretched by an axial force, which is applied at the free end. Boundary condition and stretching force application locations are given in Figure 3.2. Different rods are generated under the different stretching force and imported to ADAMS to compare their bending stiffness.

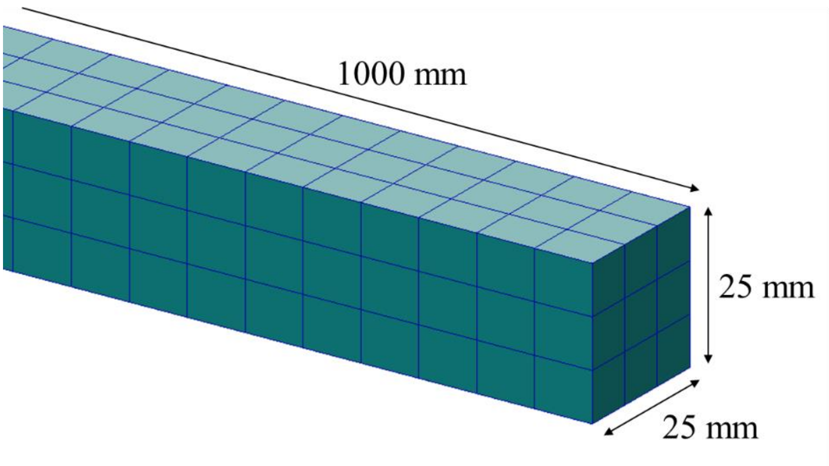

Figure 3.1 Dimensions of the simple structure

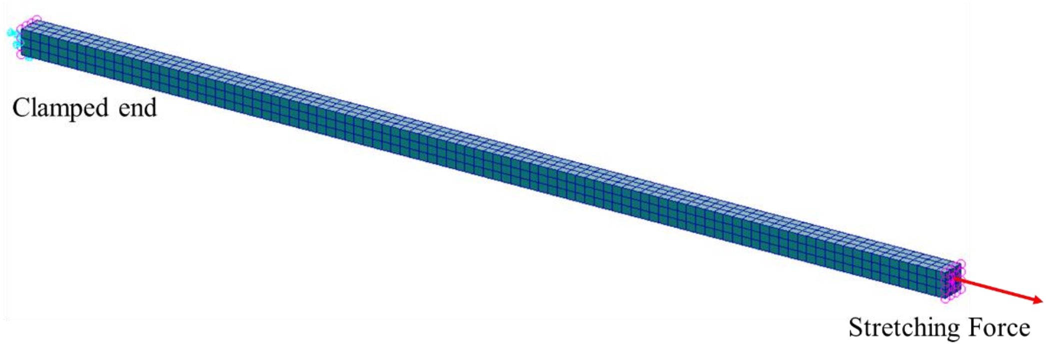

Figure 3.2 Boundary condition and force application of the rod in Patran

After the flexible structures are prepared in Patran for 0 (no preload), 50kN, 100kN, 1000kN stretching forces, they are imported to ADAMS and desired load and boundary conditions are applied individually. In ADAMS, load and boundary conditions are given in Figure 3.3. Structures are supported with the fixed joint at one end while a transverse force is applied at their free end and their tip deflections are compared.

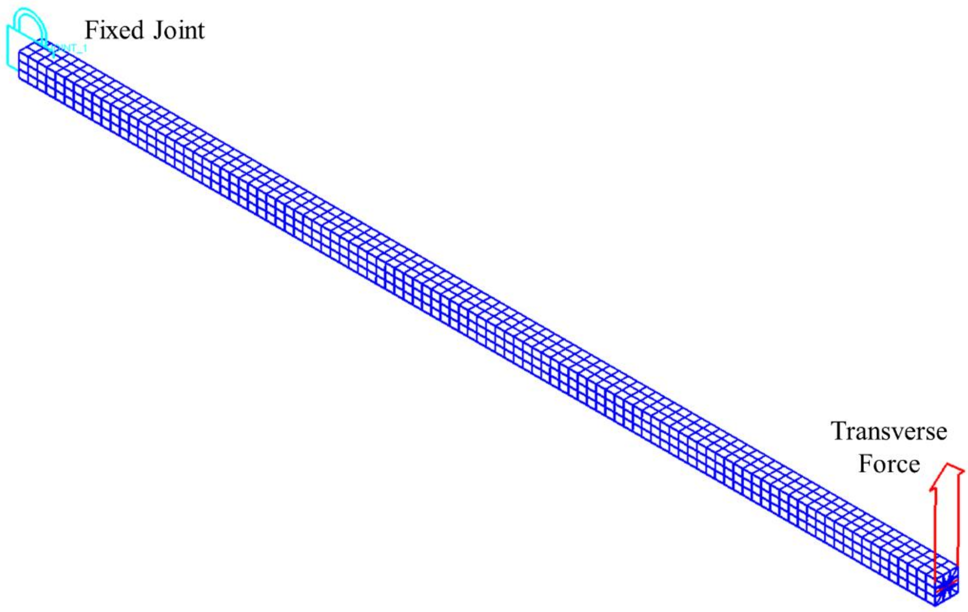

Figure 3.3 Loads and Boundary conditions in ADAMS

For different preload conditions, tip deflection variations are presented in Figure 3.4 and summarized in Table *3.1*. As it is expected, when the preload is increased, stiffness of the structure becomes higher.

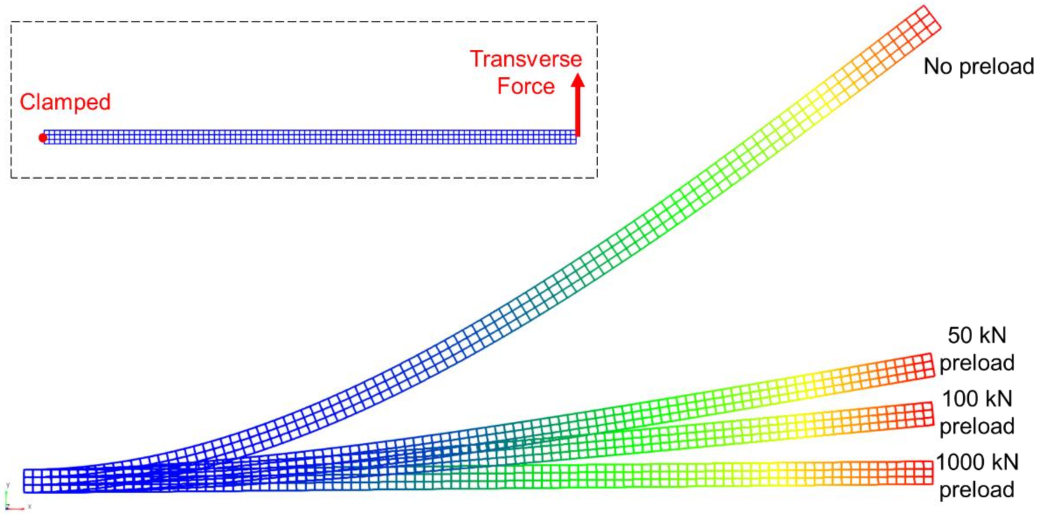

Figure 3.4 Deflection of the rods under different preload

Table 3.1 *Tip displacements of the rods under different preload*

Preload [kN]	Tip Displacement [mm] ADAMS	Tip Displacement [mm] ABAQUS NONLINEAR
0	510.5	417.1
50	128.1	126.6
100	74.34	74.15
1000	9.27	9.27

In addition to the tip displacement comparison, natural frequencies of the structures are also investigated. For different preload conditions, first bending natural frequency variations are summarized in Table *3.2*. As it is expected, when the preload is increased, natural frequencies of the rod becomes higher.

Table 3.2 *First Bending Frequencies of the rods under different preload*

Preload [kN]	Natural Frequency [Hz]
0	20.22
50	37.78
100	47.80
1000	121.97

3.2. Inclusion of the Large Deformation Effect in ADAMS Model

For small deformation problems, linear analysis can be done because differential equation of the deflection curve is simplified due to the very small deflection and deflection curve slope. However, for long and slender structures, this assumption cannot be applied directly due to the large relative rotation. Therefore, for the calculation of the large deformation, system of nonlinear equations needs to be solved. In order to solve nonlinear equations, iterative based solution methods are utilized by using nonlinear solvers in FE codes. However, in ADAMS, deformations are always linear and large deformation effect cannot be implemented directly. For this purpose, segmental shooting technique, which is presented by Faulkner, Lipsett, and Tam [24], is utilized. In this method, the structure is divided into a series of segments, hence small deflection assumption becomes valid for each segment relatively. As demonstrated in Figure 3.5, deflection equation can be linearized within each small segment. In Figure 3.5, $f(\xi)$, defined in a local coordinate, is a nonlinear function and it is linearized using piecewise linear functions L_i and L_{i+1}. Using the piecewise linear function, at ξ_i, ξ_{i+1}, and ξ_{i+2}, same results with the nonlinear function can be achieved.

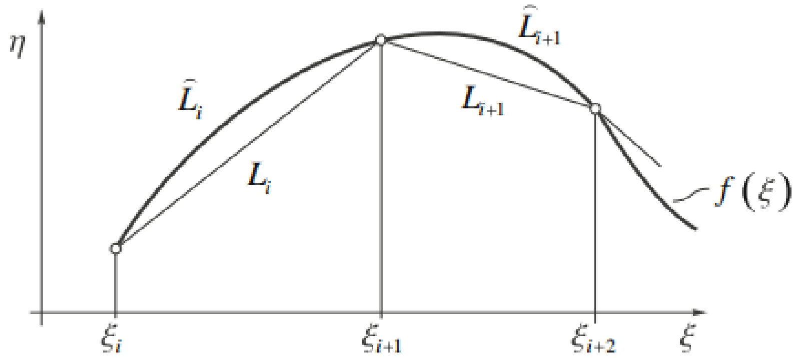

Figure 3.5 Linearization of the deflection equation [25]

In Figure 3.6, illustration of two consecutive segments j and $j+1$ is given in their local coordinate systems with the global axes relationship. As it can be seen from the figure, two segments are connected to each other at node i, which is end point of the first segment, as well as the starting point of the local coordinate system of the second segment. For the first segment, local coordinate system is known from the initial geometry and for the second segment, end point of the first segment is used to locate second segment's local coordinate system. This process is repeated for the other segments which form the structure. Hence, the local coordinate systems of each segment are found relative to global axes.

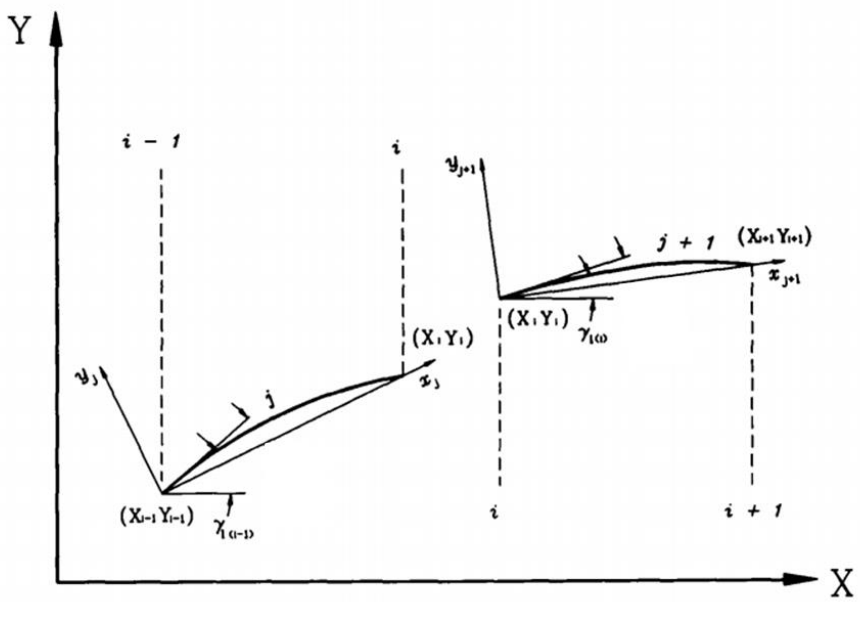

Figure 3.6 Illustration of the two consecutive segments [24]

Several studies have been done for solving nonlinear deformation problem with the discretization approach. Sitar, Kosel, and Brojan [25] presented a simple method for determining large deflection states of arbitrarily curved elastic beams. In this study, arbitrarily curved structure, presented in Figure 3.7, is modeled by a finite set of initially straight flexible segments, which are connected each other with rigid connection.

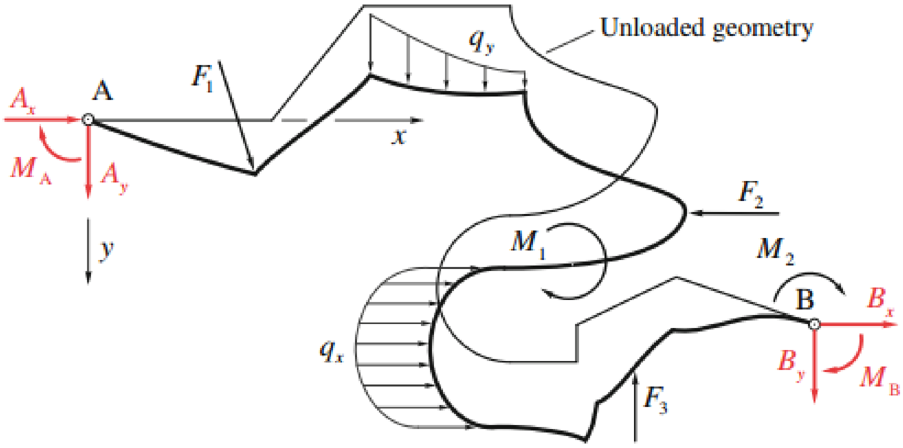

Figure 3.7 Deflected and non-deflected state of the curved beam [25]

Since the helicopter main rotor blades are long and slender structures and undergo large deformations, small deformation assumptions become invalid. Hence, when the nonlinear deformation effects are not modeled in ADAMS, unrealistic deformation results are obtained. Therefore, in the main rotor simulation model, discretization method needs to be implemented into the ADAMS model, when the flexible blades are modeled.

For this purpose, two simple rod structures are utilized for the validation and investigation of the discretization method in ADAMS. One rod is created as a single continuous 1000 mm long part and the second rod is created by bringing together 10 smaller subparts in ADAMS with rigid connection. Rod structures are prepared by using Patran/Nastran with same, uniform material properties and exported to ADAMS as flexible parts for analysis. Discrete flexible rod consists of 10 smaller segments, each being 100 mm long. They are arranged end to end and connected to each other with fixed joint by using the corresponding nodes to form a 1000 mm long rod. On the other hand, single rod consists of one part which is 1000 mm long. Both single continuous rod and the discrete rod dimensions are presented in Figure 3.8.

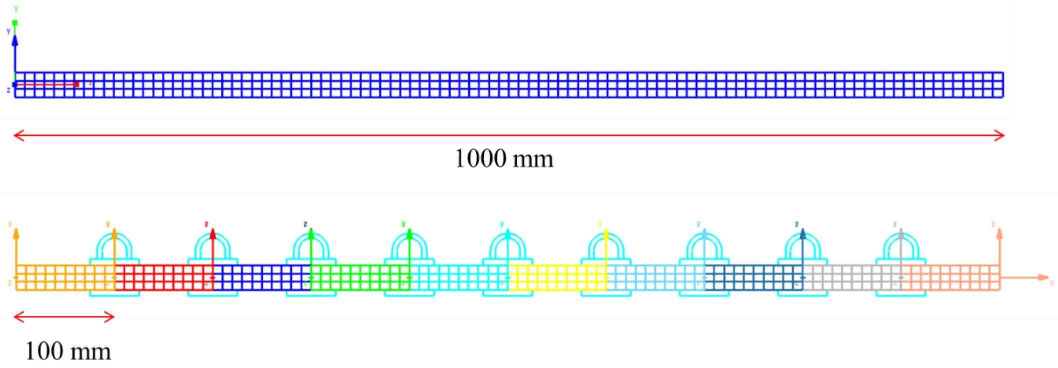

Figure 3.8 Single continuous and discrete rod structures

In ADAMS analysis of the rod structures, they are subjected to concentrated transverse force at the free end while the left end is clamped to simulate the cantilever beam problem (clamped-free boundary condition). Loads and BCs are presented in Figure 3.9. When flexible parts are generated as mnf files in Patran/Nastran, applied boundary condition must be the same as in ADAMS analysis. Hence, for the single rod structure, clamped-free boundary condition is also applied in Patran/Nastran. However, for discrete flexible rod case, only first segment (left end) is fixed to the ground and other segments are connected to the previous segment as mentioned in segmental shooting technique. Therefore, first rod segment is prepared under clamped-free boundary condition, while other rod segments are prepared under free-free boundary condition in Patran/Nastran.

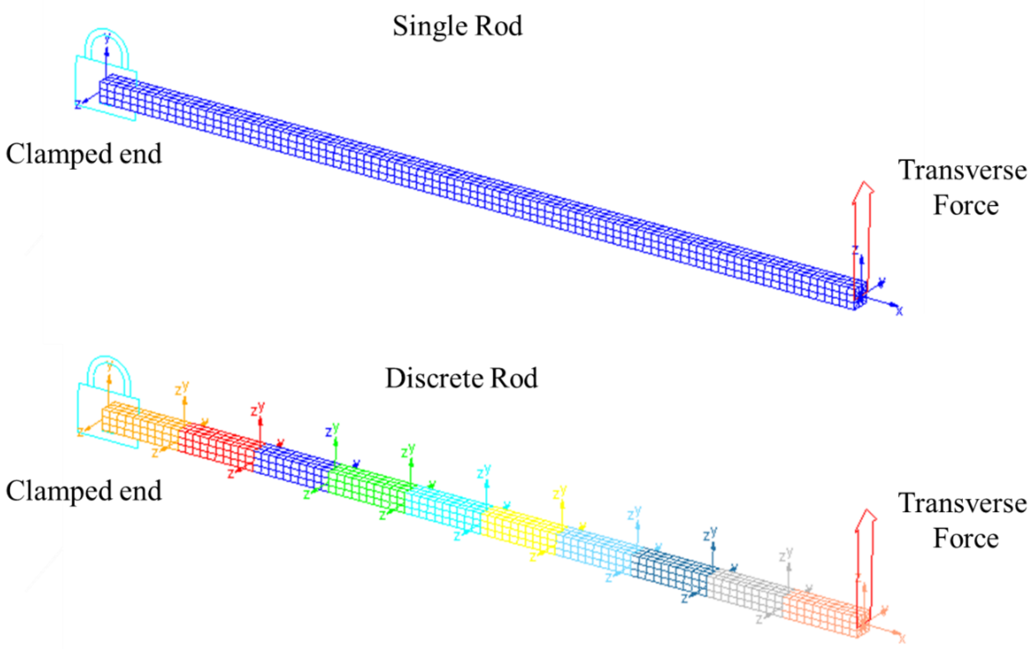

Figure 3.9 Load and boundary conditions applied to continuous and discrete beams

In ADAMS simulation, applied forces are gradually increased and obtained tip deflections are compared. In Figure 3.10, applied forces versus tip deflections of each beam are presented. As it can be seen from the plots, single continuous beam deformation is always linear while the applied force is increasing as it is expected. On the other hand, for the discrete flexible cases, nonlinear deformation response can be achieved in ADAMS.

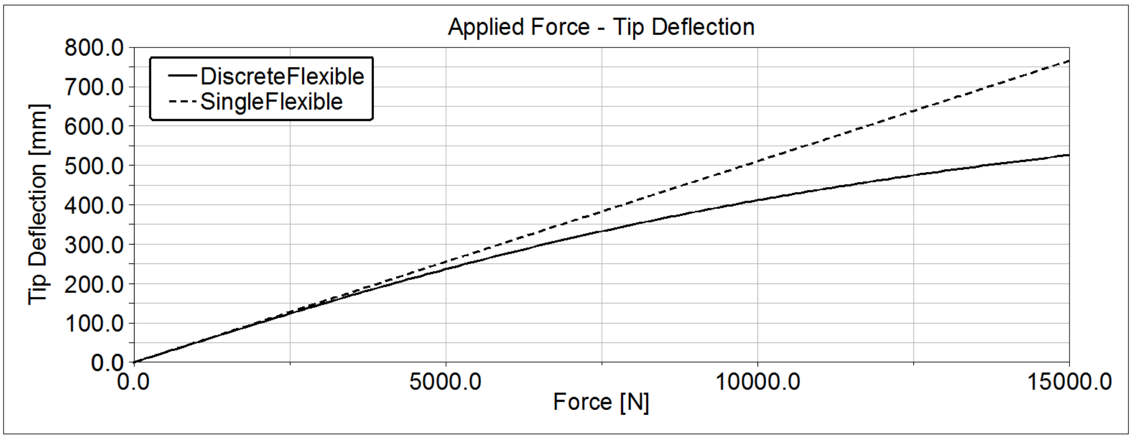

Figure 3.10 Tip deflections of single and discrete rods

Deformed plots for different forces are presented in Figure 3.11 and applied force versus corresponding tip displacement results are summarized in Table *3.3*. As it can be seen from the deformation plots, with the single flexible beam ADAMS cannot capture the geometric nonlinearity.

Table 3.3 *Tip displacement results from ADAMS for single and discrete beams under different forces*

Force [N]	Tip Displacement [mm] Single Flexible	Tip Displacement [mm] Discrete Flexible
100	5.1	5.0
500	25.5	25.1
1000	51.1	50.1
2500	127.6	123.7
5000	255.2	236.5
10000	510.5	411.4
15000	765.7	526.0

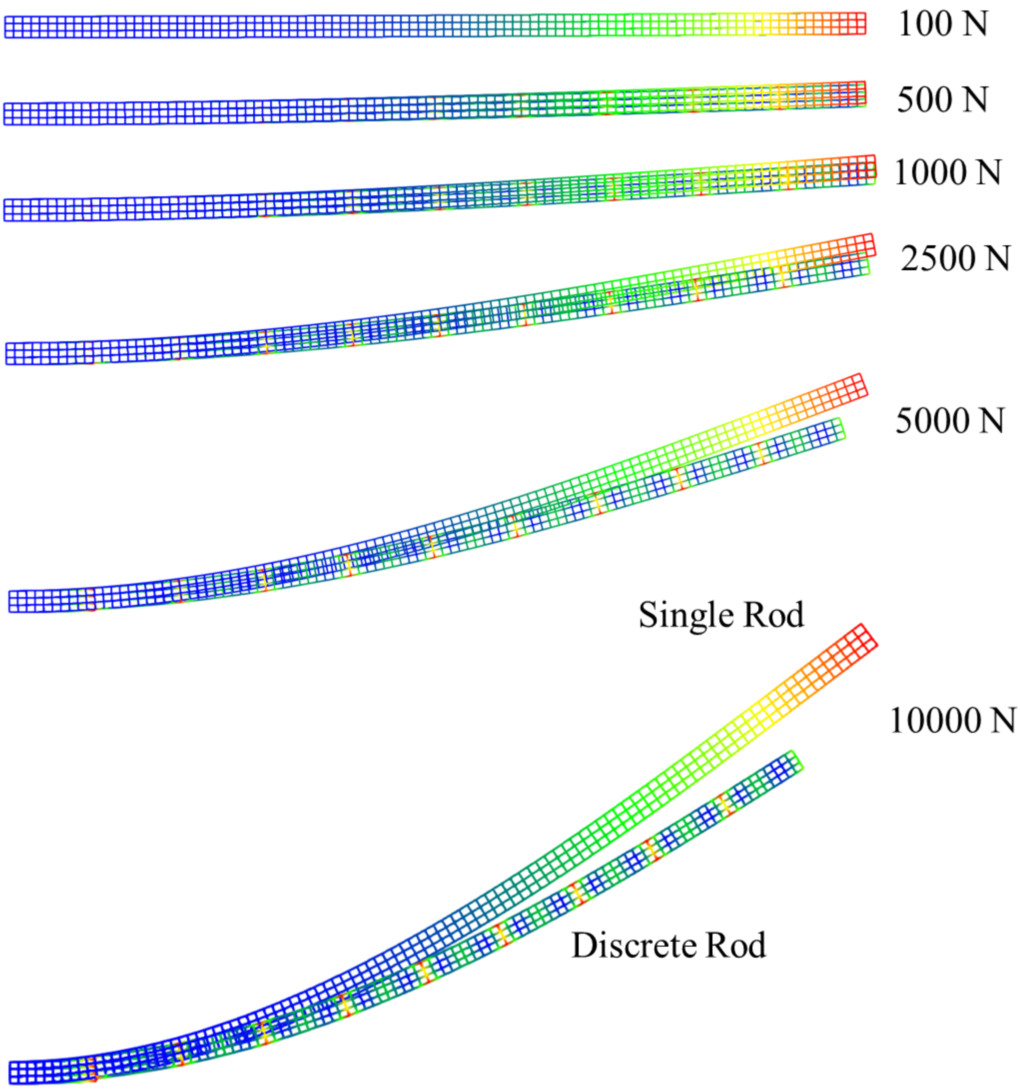

Figure 3.11 Displacement plots under different loads

For further validation of ADAMS implementation of the discrete flexible method, Abaqus [26] is used as a different FEA software. In Abaqus, the same rod is modeled as a single part and bending analysis is repeated under the same load and boundary conditions by using the Abaqus NONLINEAR SOLVER. Abaqus results are then compared with the ADAMS discrete flexible rod results. In Table *3.4*, tip displacements obtained by Abaqus Nonlinear and by the discrete flexible model and by single flexible model are presented. It is seen discrete flexible beam results obtained by ADAMS are in good agreement with the Abaqus results.

Table 3.4 *Tip displacement results of ADAMS discrete flexible and Abaqus nonlinear*

Applied Force [N]	**Tip Displacement [mm] Single Flexible ADAMS**	**Tip Displacement [mm] Discrete Flexible ADAMS**	**Tip Displacement [mm] ABAQUS NONLINEAR**
100	5.1	5.0	5.1
500	25.5	25.1	25.4
1000	51.1	50.1	50.7
2500	127.6	123.7	125.0
5000	255.2	236.5	239.2
10000	510.5	411.4	416.4
15000	765.7	526.0	534.0

Stress variations results of the discrete flexible structures are also compared with the stress variation results of the Abaqus Nonlinear under the 10000 N transverse tip force. Von Mises stress and normal-x stress variations are given in Figure 3.12 and Figure 3.13. Stress results show that discrete flexible model gives very close stress results compared to the stress results of Abaqus nonlinear.

These studies show that with the discrete flexible modelling approach, geometric nonlinearity can be captured in ADAMS analysis.

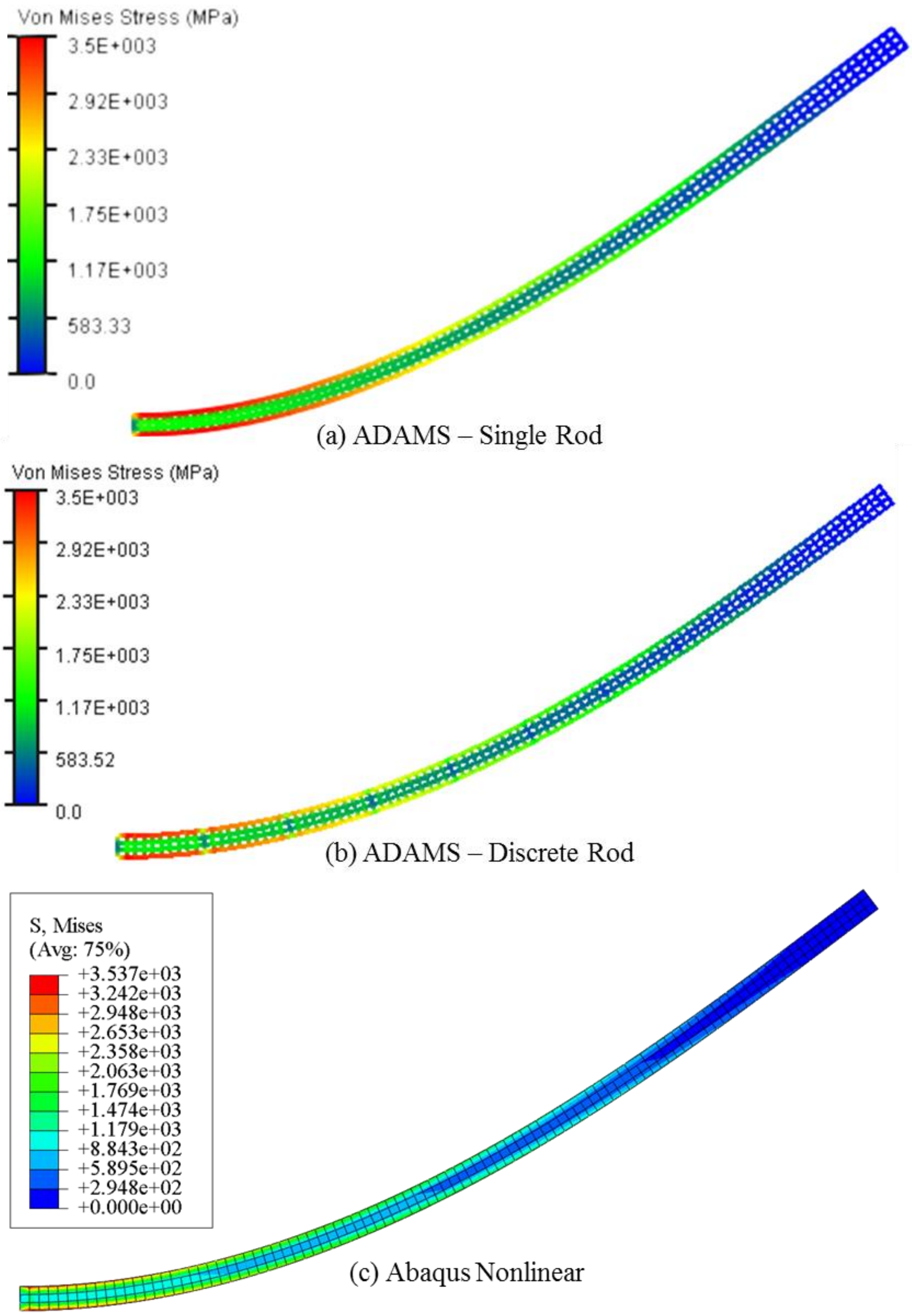

Figure 3.12 Von Mises stress variations of Abaqus Nonlinear and the flexible models in ADAMS

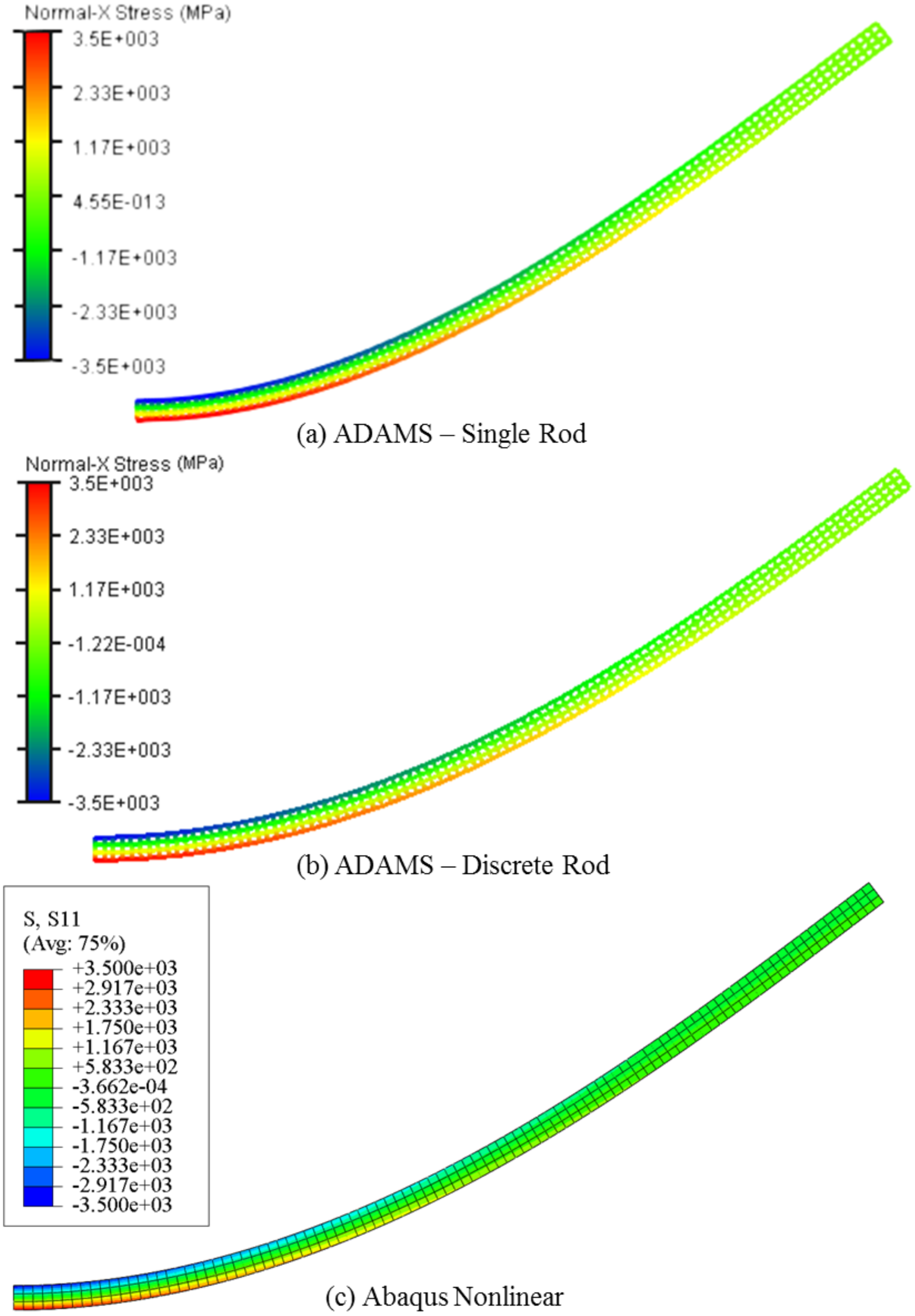

Figure 3.13 Normal-X stress variations of Abaqus Nonlinear and the flexible models in ADAMS

3.3. The Rotor Blade Nonlinearity

Since geometric nonlinearities have significant effect on the rotating long slender structures, these effects are implemented to the helicopter rotor blade model. For the implementation of the stiffening effect to the rotor blade, restart analysis procedure is utilized on the 3D FE model of the helicopter rotor blade. In the restart analysis, the blade is preloaded by axial tensile loading of 20750 N (centrifugal loading at 1440 deg/s). The change in the bending mode (Figure 3.14) natural frequency of the rotor blade due to the centrifugal stiffening is given in Table *3.5*.

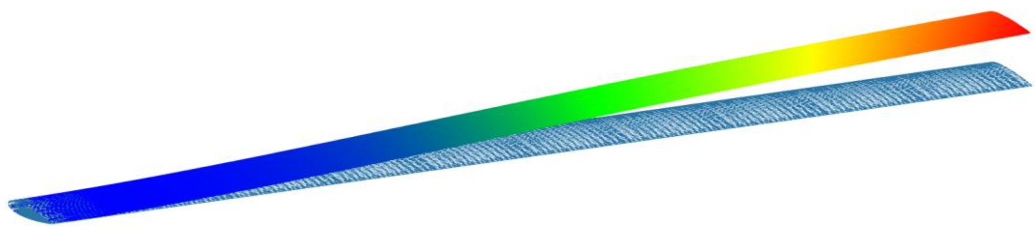

Figure 3.14 Bending mode of the rotor blade

Table 3.5 *Natural frequency of the rotor blade with and without centrifugal stiffening*

Blade Model	Natural Frequency [Hz]
without centrifugal stiffening	2.91
with centrifugal stiffening	6.94

On the other hand, for the large deformation geometric nonlinearity, discretization method is utilized for the 3D FE model of the rotor blade. For this purpose, as given in Figure 3.15, the rotor blade is divided into five segments and they are arranged end to end and connected to each other with fixed joint in ADAMS, given in Figure 3.16, to form the full rotor blade. For discrete flexible rotor blade case, only first segment is attached to the rotor hub and other segments are connected to the previous segment as mentioned in the segmental shooting technique. Therefore, mnf file for the first blade segment is prepared under clamped-free boundary condition, while mnf files of other blade segments are prepared under free-free boundary condition in Patran/Nastran.

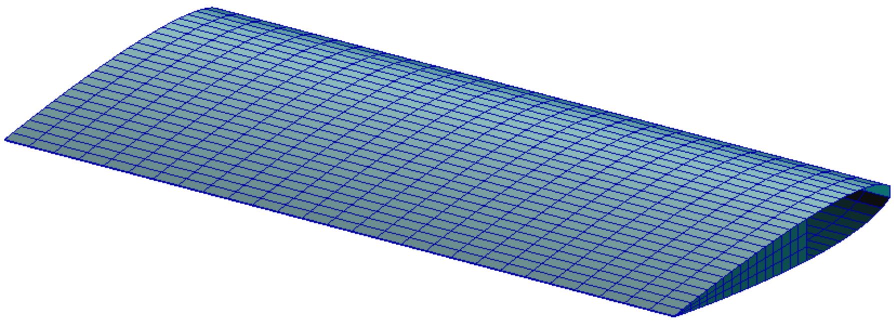

Figure 3.15 A rotor blade segment in Patran for the discretization method

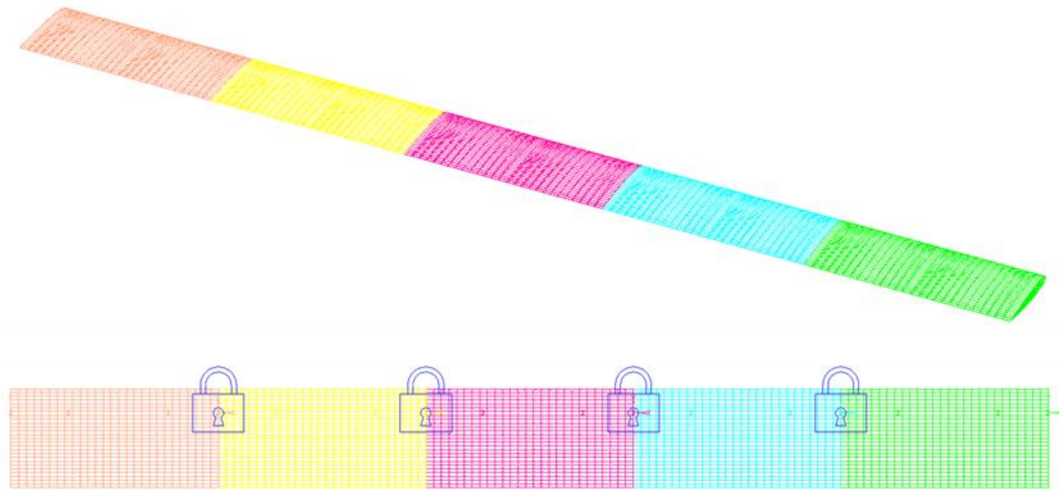

Figure 3.16 Formation of the full blade in ADAMS by discrete segments

In order to investigate the effects of geometric nonlinearities on the rotor blade, the main rotor model is simulated using rotor blade model with and without including geometric nonlinearities. For this purpose, three different rotor blades are prepared; nonlinearities are not included, only centrifugal stiffening included, and only large deformation included. Combination of the centrifugal stiffening and large deformation is not modeled; because combination of the centrifugal stiffening and large deformation cannot be used as a modeling approach in MSC ADAMS. When the discretization method is utilized, it is not possible to apply the centrifugal stiffening force to the segment prepared by using the free-free boundary condition; because in the modal approach used to generate the mnf file, because of the free-free boundary condition, when the preload due to the centrifugal force is applied to the segments, singularity arises. Hence, it has not been possible to apply the combination of the centrifugal stiffening and discrete flexible approach to model large deformation effect.

The main rotor model is simulated in hover flight condition by using the blade model with and without including geometric nonlinearities individually. As a result of the hover flight condition, von Mises stress variations of the blades in the spar are investigated, and these results are given in Figure 3.17 - Figure 3.19. It is seen that the blade without geometric nonlinearity gives significantly high von Mises stress results. Therefore, large deformation and stiffening nonlinear effects are taken into account during the further analysis of the helicopter rotor. Preparation procedure of the main rotor model in ADAMS with the implementation of blade geometric nonlinearity is presented in Figure 3.20 as a block diagram.

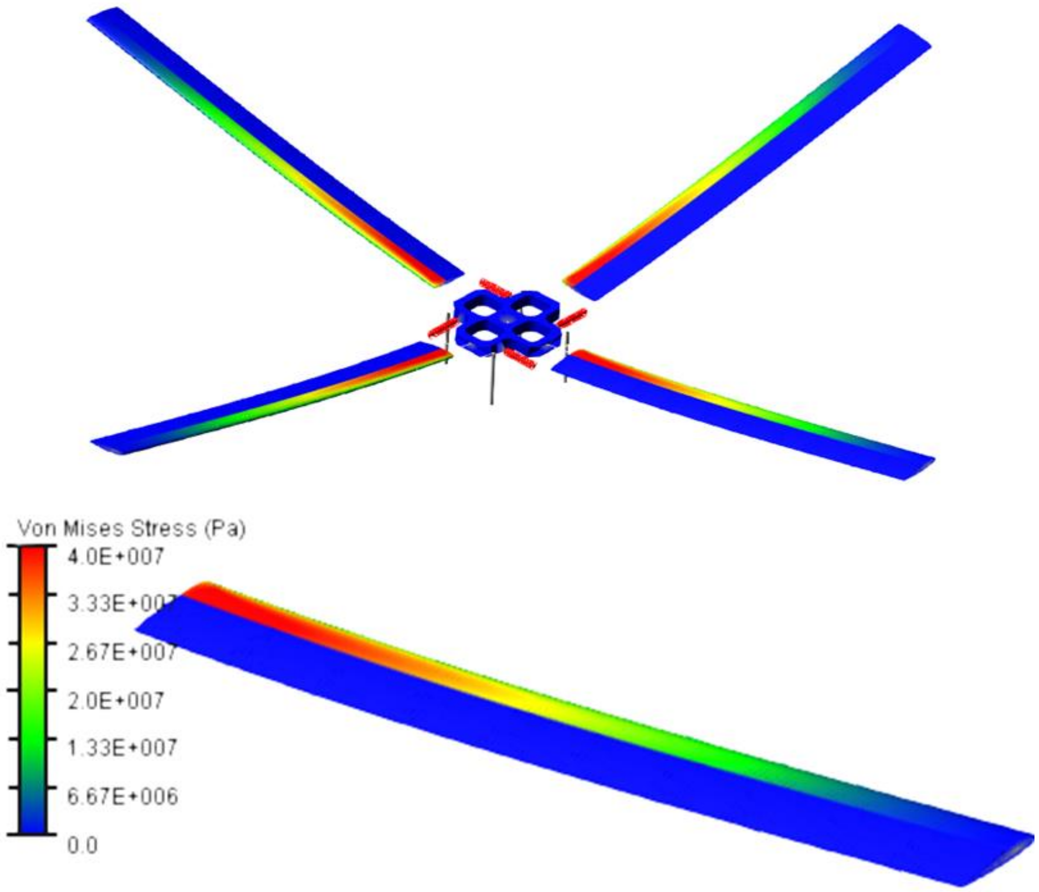

Figure 3.17 Von Mises stress result plot in the blade without geometric nonlinearity

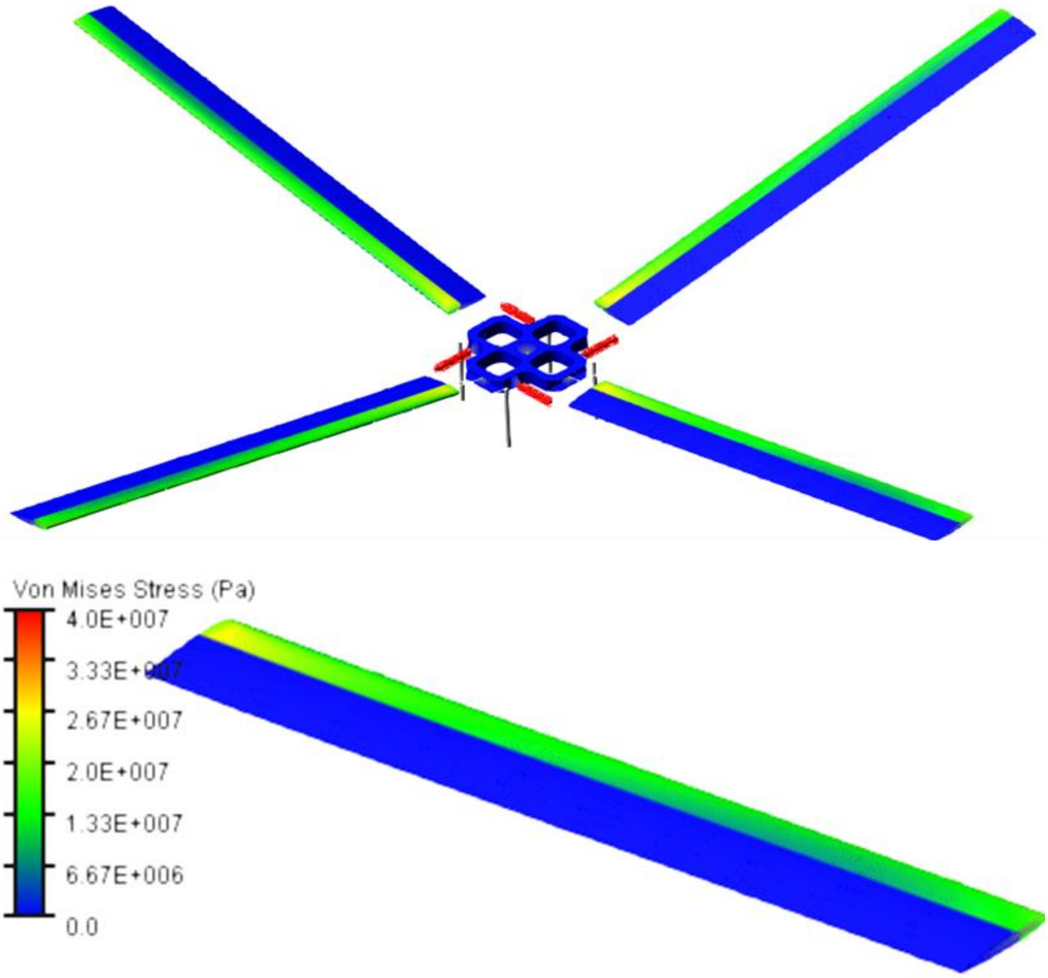

Figure 3.18 Von Mises stress result plot in the blade with centrifugal stiffening included

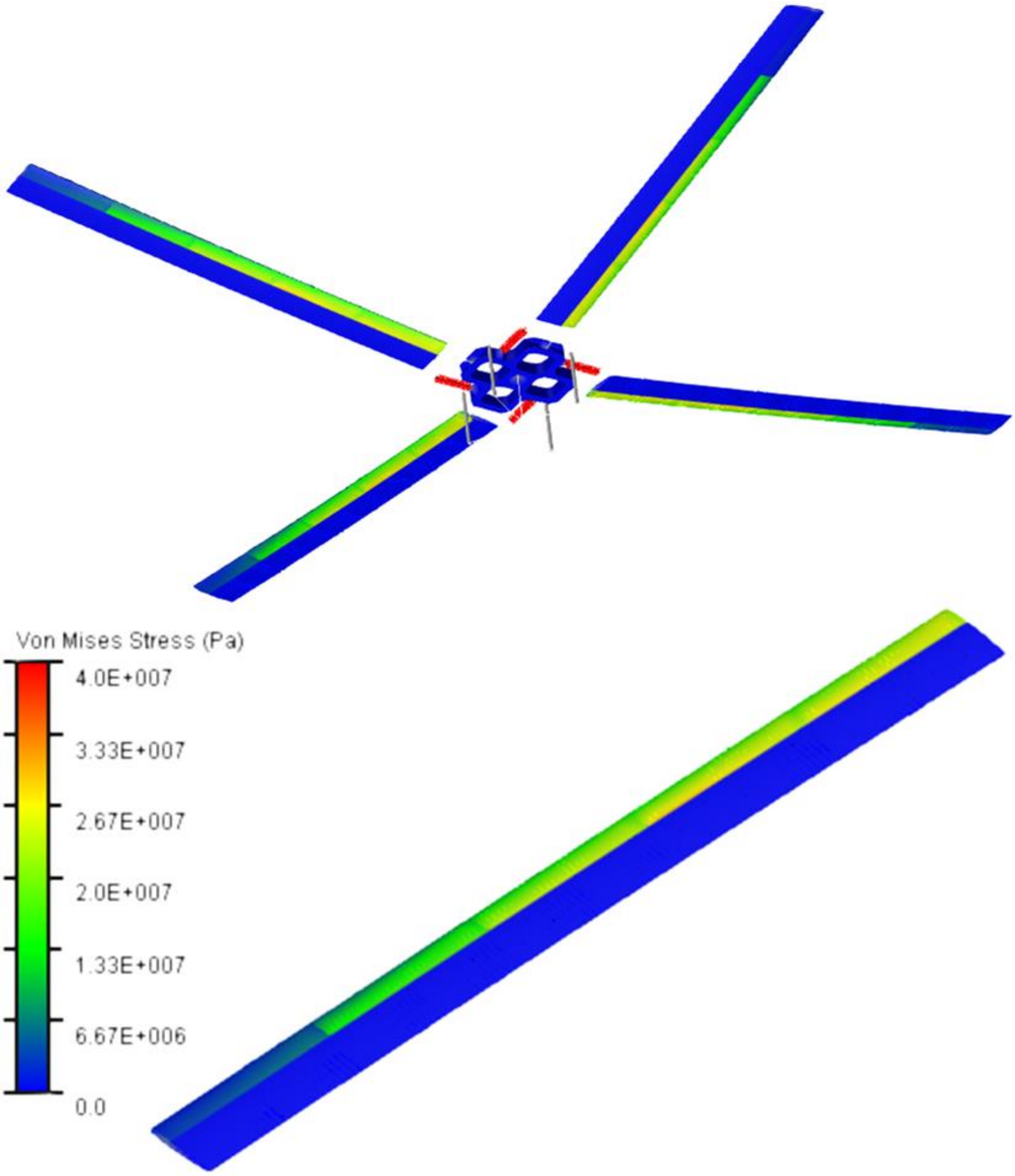

Figure 3.19 Von Mises stress result plot in the blade with large deformation effect included through discrete flexible modeling approach

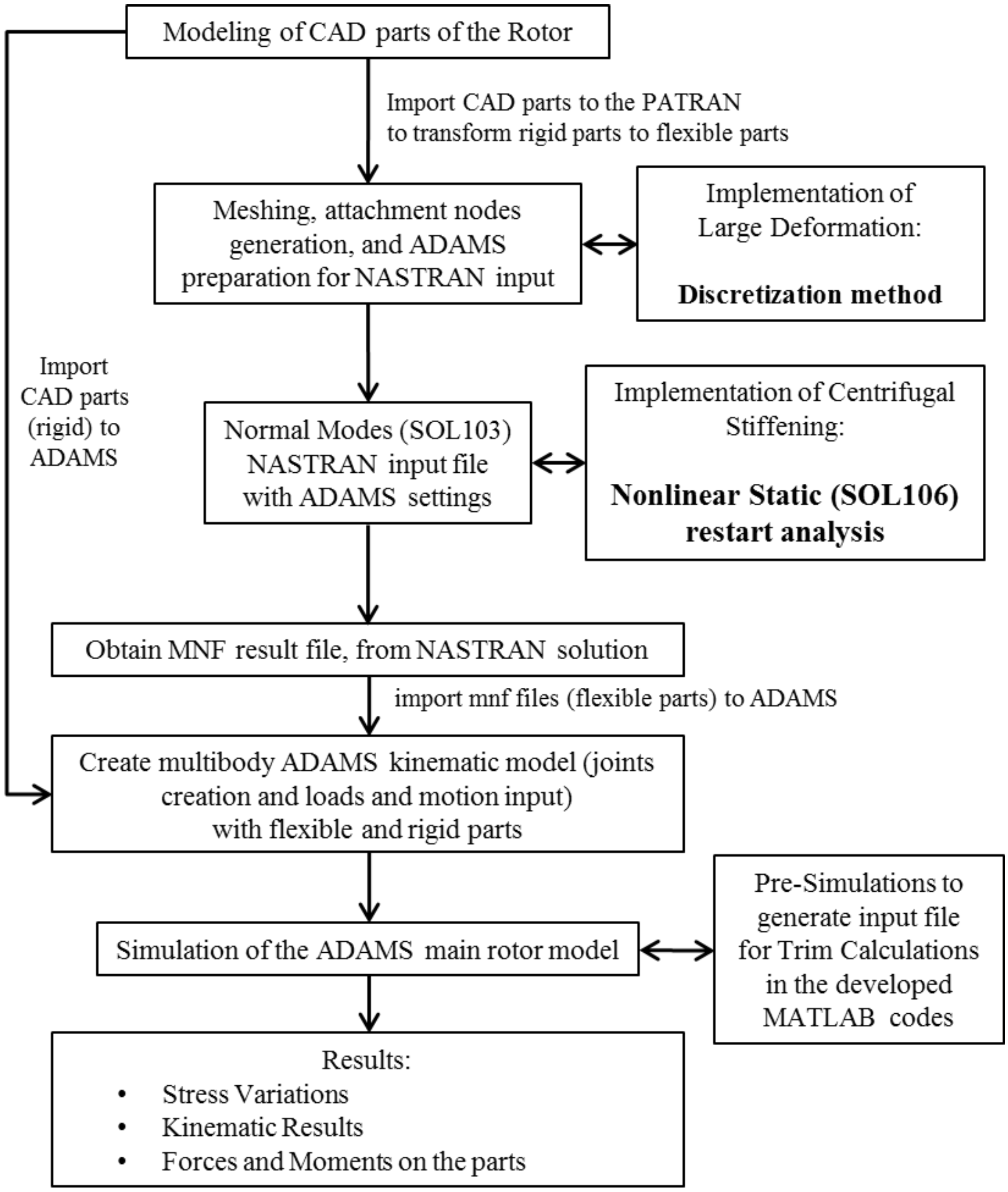

Figure 3.20 Block diagram of the multibody simulation process of the helicopter rotor with the geometric nonlinearity

CHAPTER 4

ANALYSIS OF THE MAIN ROTOR SYSTEM

4.1. Flight Conditions

In the literature, generally two main flight conditions are studied in detail for helicopter rotor dynamics calculations; namely hover and forward flight. Since hover and forward flight conditions are correctly simulated, other flight conditions can be easily simulated by using the same theory.

4.1.1. Hover

In the hover flight condition, helicopter has zero forward or vertical speed and so flow condition on the rotor disk is axially symmetric. In other words, rotor does not have any vertical or horizontal velocity component relative to air and the air flow on the blades only comes from the rotation of the rotor, which is a constant parameter for helicopter rotors. Hence, all main rotor blades operate under the same aerodynamic and dynamic conditions and the same blade angle variations exist for all of the rotor blades.

4.1.2. Forward flight

In the forward flight case, since the helicopter has forward velocity, air flow on the rotor blades are affected both from the forward velocity of the helicopter and the rotation of the rotor blades. As presented in Figure 4.1, velocity of the blade is decreased on the retreating side, whereas it is increased on the advancing side. This situation causes a periodical change in the blade velocity and asymmetry in the blade loads. In other words, increasing blade velocity on the advancing side causes to more lift generation and on the retreating side less lift generation.

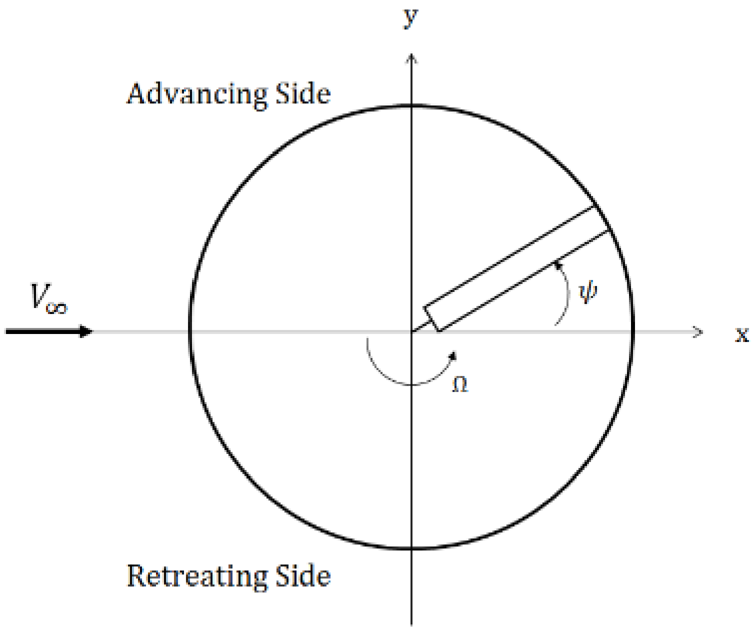

Figure 4.1 Advancing and retreating side of the rotor blade

As a result of lift asymmetry, blades tend to make relative up and down motion, called as the flapping motion. Furthermore, as a result of the flapping motion, additional inertial forces are introduced; namely Coriolis forces. Coriolis forces cause forward and backward motion of the blades, called as the lagging motion. In the literature, flap (β) and lag (ζ) motions are described by the Fourier series as given by Equations (34) and (35),

$$\beta(\psi) = \beta_0 + \beta_{1c} * \cos\psi + \beta_{1s} * \sin\psi + H.O.T. \tag{34}$$

$$\zeta(\psi) = \zeta_0 + \zeta_{1c} * \cos\psi + \zeta_{1s} * \sin\psi + H.O.T. \tag{35}$$

where ψ is the azimuth angle and $H.O.T.$ denotes the higher harmonics of the flap ($\beta_{2c} * \cos 2\psi + \beta_{2s} * \sin 2\psi + ..$) and lag ($\zeta_{2c} * \cos 2\psi + \zeta_{2s} * \sin 2\psi + ..$) motion. The rotor blade motions are usually described by using zeroth and first harmonics terms because the higher harmonics are relatively small.

When the flap motion is independent of the azimuth angle, all flap angles of the blades are equal β_0, which is called as the coning angle (Figure 4.2a). On the other hand, when the lag motion is independent of the azimuth angle, all lag angles of the blades are equal ζ_0, which is called as mean lag angle (Figure 4.2b).

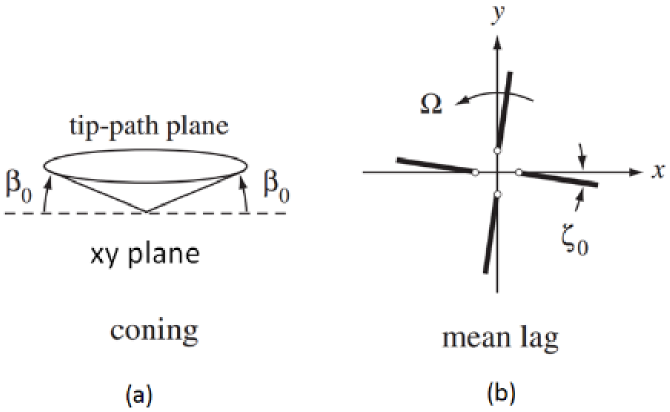

Figure 4.2 (a) Coning and (b) mean lag angle [1]

4.2. Verification of the Simulation Model

Since the helicopter main rotor simulation model consists of several disciplines; such as kinematics, aerodynamics, structural modeling, trim calculations, it should be verified in order to ensure that it gives reasonable results. Therefore, rotor simulation system is analyzed for the hover and the forward flight conditions under different cases and compared with theoretical results.

4.2.1. Theoretical Verification

For the theoretical verification of the main rotor simulation model, different scenarios are generated to compare them with the theory expectation. For instance, in the hover condition, since rotor blade loads and velocities are independent of the azimuth angle, axial symmetry is expected among the rotor blade angles. Furthermore, from flap and lag equations (Eqns. (34) and (35)), when the blade angle is independent of the azimuth position, flap and lag angle of the all blades must be a constant value as $\beta = \beta_0$ (coning) and $\zeta = \zeta_0$ (mean lag).

For the verification of the ADAMS main rotor model, for the hover condition following analyses are performed:

- Rotor rotational speed = 1440 deg/s, collective pitch angle = 5^o, forward velocity = 0
- Rotor rotational speed = 1440 deg/s, collective pitch angle = 10^o, forward velocity = 0

In Figure 4.3 and Figure 4.4, for two different pitch angle conditions with zero forward velocity and constant rotational velocity, blade angles results are presented. As it can be seen from both results, typical hover condition can be observed such that flap and lag angles are constant at different azimuth positions and blades describe the coning and the mean lag motion as a feature of the hover condition. The existence of the lag motion is due to the drag force on the blade. Moreover, as the collective pitch angle of the blades is increased from 5^o to 10^o, flap and lag angles of the blades become higher due to the increase in aerodynamic loads. As a result of the hover condition analysis, it is concluded that main rotor simulation model gives reasonable results for this condition.

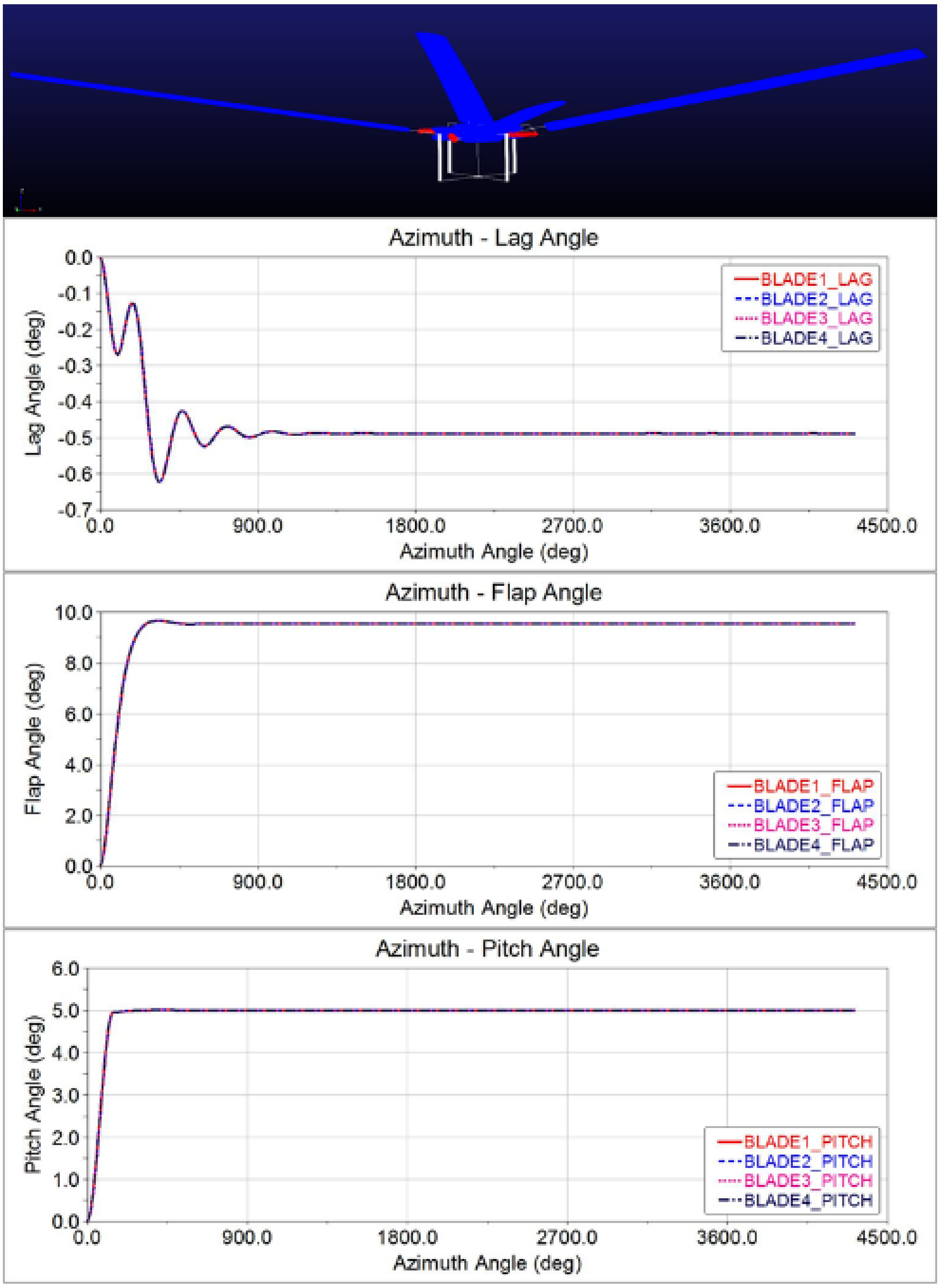

Figure 4.3 Blade angle variations for the hover condition at 5º pitch angle

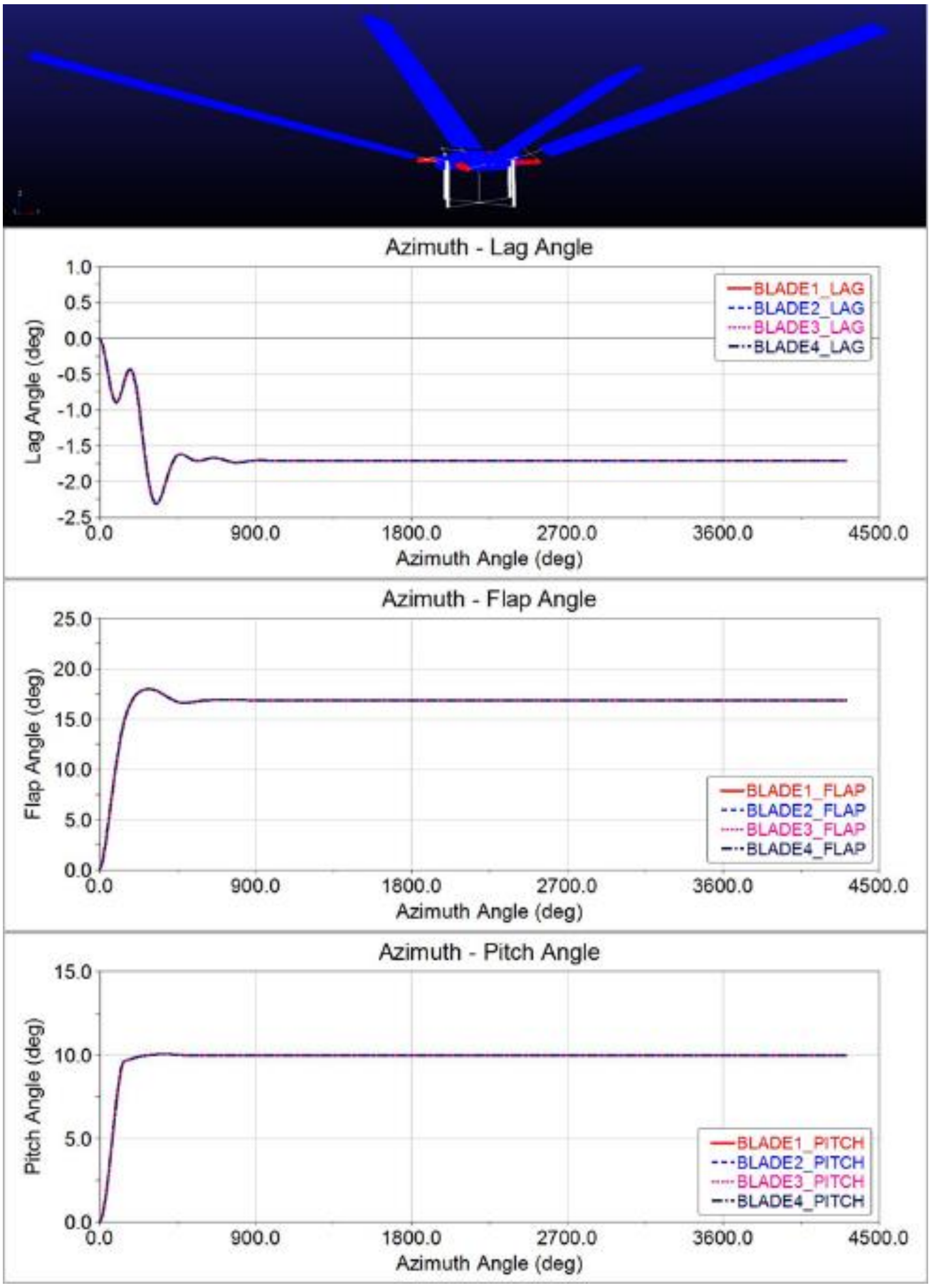

Figure 4.4 Blade angle variations for the hover condition at 10° pitch angle

In addition to the hover condition, forward flight results also need to be investigated for verification. In a forward flight, since the combined rotational velocity and the forward velocity affect the aerodynamic loads, asymmetries must be observed in the blade angles, in other words, blade motions and loads must depend on the azimuthal position.

For the verification of the ADAMS main rotor model, for the forward flight condition, following analyses are performed:

- Rotor rotational speed = 1440deg/s, collective pitch angle = 5^o, forward velocity = 10m/s
- Rotor rotational speed = 1440deg/s, collective pitch angle = 5^o, forward velocity = 30m/s

In order to simulate the forward flight condition, forward velocity is applied to the main rotor simulation model in ADAMS. It is seen that as a result of the resultant air velocity variation with the blade azimuth angle, each blade has different flap and lag angles which depend on the azimuth angle, and these angles change periodically with a period of 2π, as presented in Figure 4.5 and Figure 4.6.

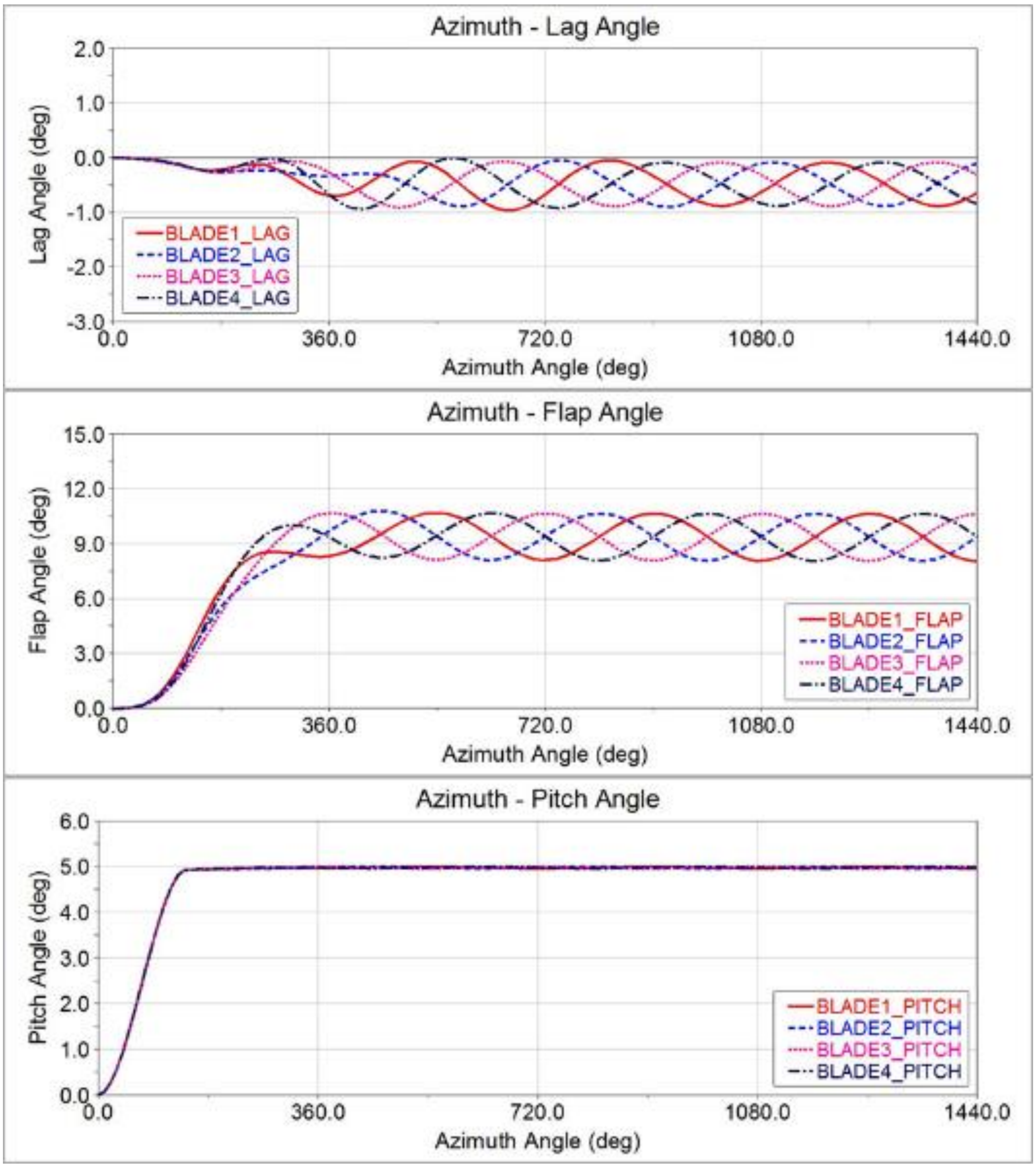

Figure 4.5 Blade angle variations for the forward flight at 10m/s

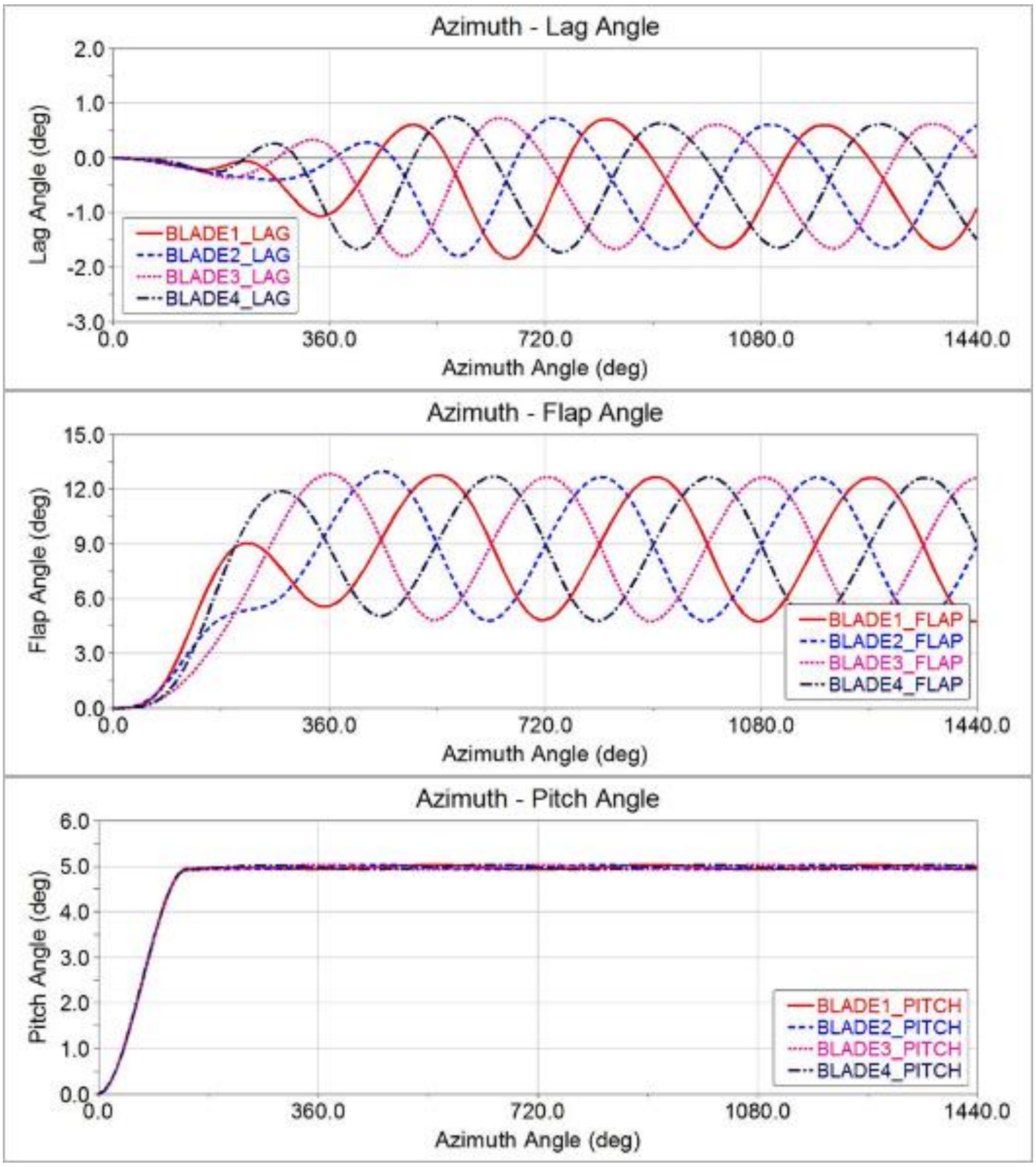

Figure 4.6 Blade angle variations for the forward flight at 30m/s

Moreover, in order to investigate effect of the different forward flight velocities, in the ADAMS main rotor model, two different forward velocities are applied as 10m/s and 30m/s. When the forward velocity is increased, resultant air velocity difference is higher and as a result of this blade flap and lag motion magnitudes must be higher. As presented in Figure 4.5 for the 10m/s forward velocity; blade lag motion is between -

1^o and 0^o, and the blade flap motion is between about 7.5^o and 10.5^o. On the other hand, as presented in Figure 4.6 for the 30m/s forward velocity; blade lag motion is between -2^o and 0.75^o, and the blade flap motion is between 5^o and 12.5^o. Based on the forward flight condition analyses, it can be concluded that the main rotor simulation model also gives reasonable results for this condition.

4.2.2. Trim Model Verification

For the verification of the developed trim model, a sample forward flight case is generated. Since the trim targets are the rotor hub moments and the rotor thrust, these values are presented with and without the trimmed state of the rotor. In Figure 4.7, coordinate system of the rotor model is presented such that the rotor thrust is in the z direction and the rotor hub moments are in the x and y directions respectively. In this analysis, isolated main rotor trim is performed for the 20 m/s forward velocity and trim targets are 14000N hub thrust and zero hub moments. In order to understand that the trim calculations are feasible, trimmed and non-trimmed results are presented. The rotor thrust values are given in Figure 4.8 for the trimmed and non-trimmed simulation conditions. It is seen that oscillatory thrust values are observed for the non-trimmed simulation whereas for the trimmed simulation, constant 13750N thrust value can be maintained. In addition, there is a small difference between the target and the trimmed thrust value, which comes from use of the polynomial fit functions. Similarly, for the hub moments (Figure 4.9 and Figure 4.10), trimmed simulation moment results oscillate around zero, while the non-trimmed simulation results do not oscillate around zero.

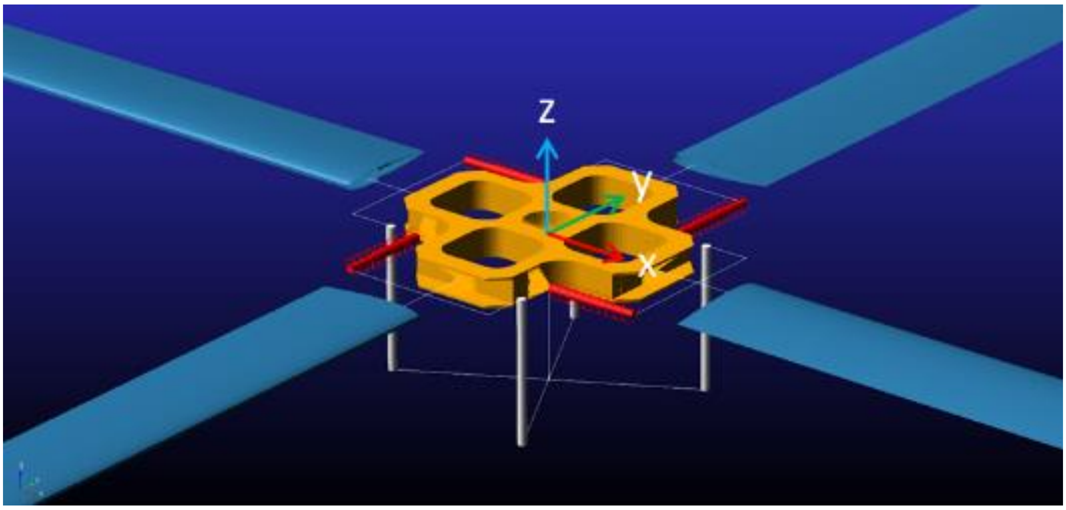

Figure 4.7 Rotor coordinates in the ADAMS Model

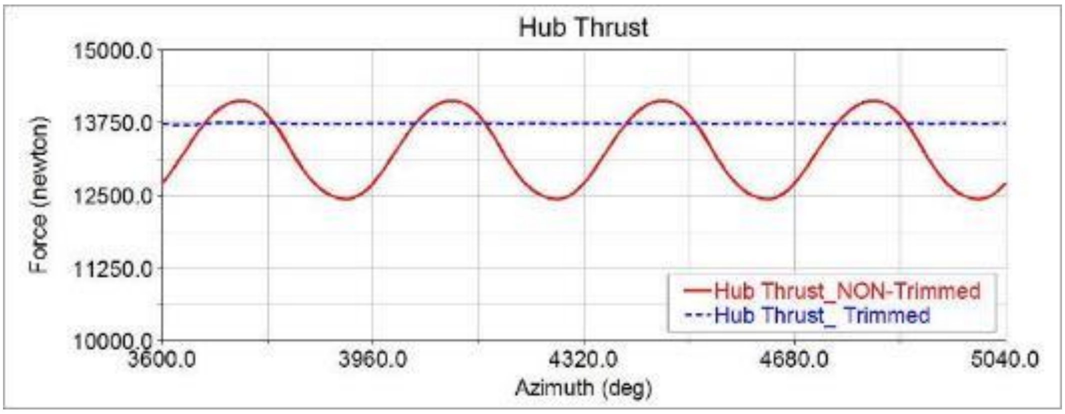

Figure 4.8 Rotor thrust for the trimmed and the non-trimmed conditions

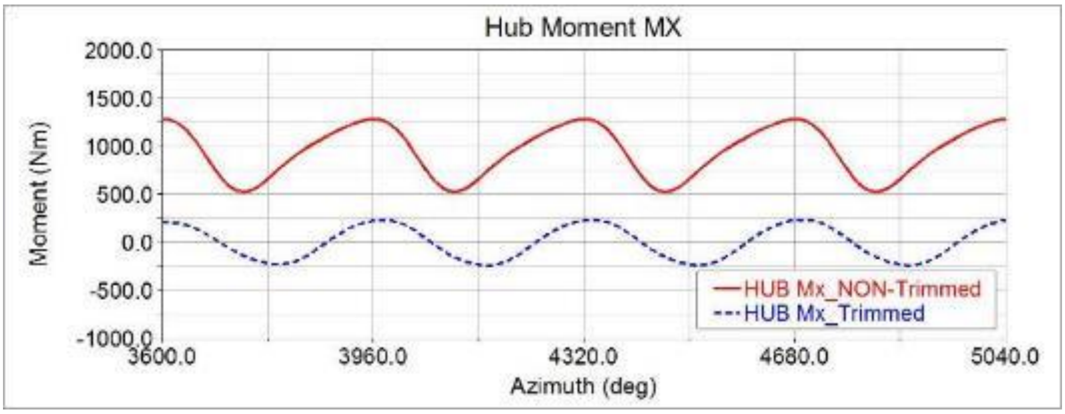

Figure 4.9 Rotor hub x-moment results for the trimmed and the non-trimmed conditions

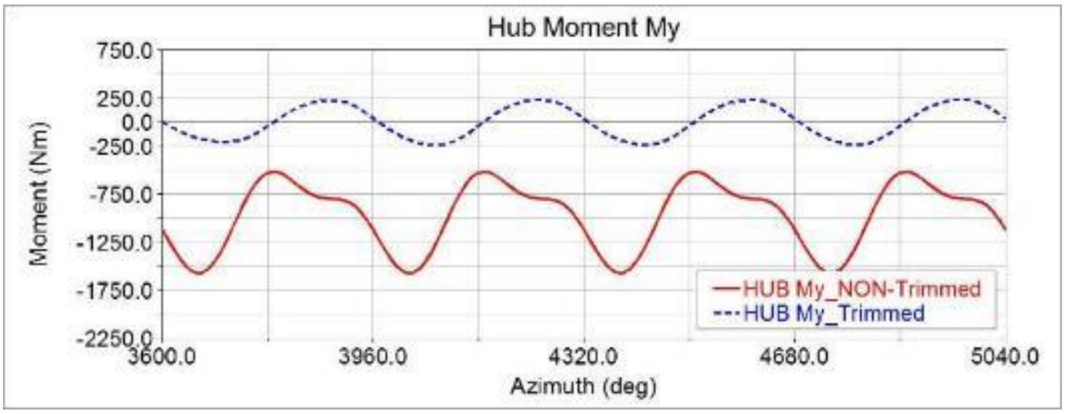

Figure 4.10 Rotor hub y-moment results for the trimmed and the non-trimmed conditions

4.3. Structural Analysis of the Main Rotor Model

Structural analysis of the flexible parts can also be performed by using the ADAMS main rotor simulation model. For this purpose, first of all, hover and forward flight conditions are simulated under different cases to determine the most critical flight case for both strength and durability of the structure. In addition to this, by using the stress results, critical locations on the rotor hub and the rotor blade can be determined for design improvements or limitations.

In order to generate different flight conditions, forward flight velocity and the generated rotor thrust are utilized as flight variables for the hover and the forward flight conditions. By using the developed trim code, it is possible to find the blade angles to produce the required thrust value.

Simulation of the main rotor model is performed for four revolutions of the rotor and the results are investigated after two full revolutions have been completed since the results are periodic and converged after the second revolution. For the forward flight analysis for forward velocity of 20m/s and thrust of 10kN, von Mises stress variation in the root of the blade spar leading edge region, shown in Figure 4.11, is given in Figure 4.12. The presented result shows that stress plot is periodic after 720^o azimuth angle position and repeats itself for every full revolution.

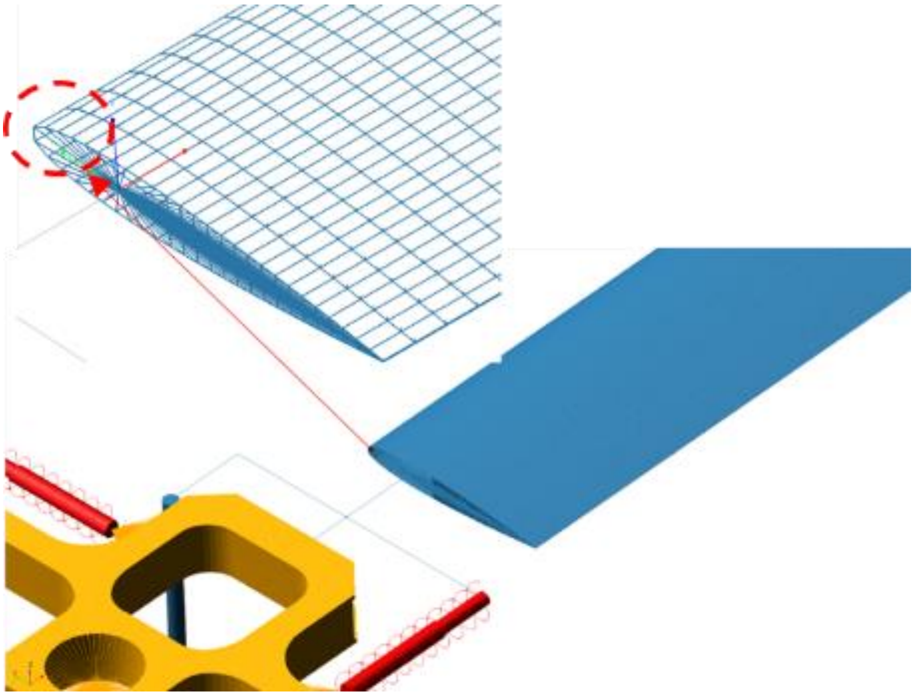

Figure 4.11 Von Mises stress result plot location in the rotor blade spar

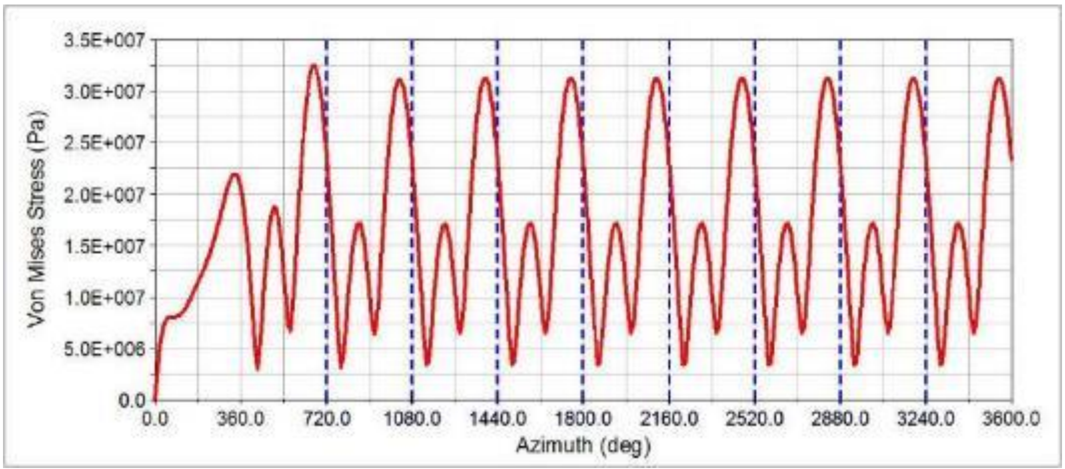

Figure 4.12 Von Mises stress result (in the root of the blade spar leading edge region) for a sample forward flight case

Since the geometric nonlinearity is implemented to the rotor blade separately, the simulation of the rotor system in ADAMS is also done separately by using the blade with the centrifugal stiffening effect included and large deformation effect included and the corresponding structural analysis results are presented.

The reference system used for the blade structure is given in Figure 4.13, where x-direction is towards the blade tip from the blade root, y-direction is towards the leading edge, and z-direction is towards the upper surface satisfying the right-hand rule.

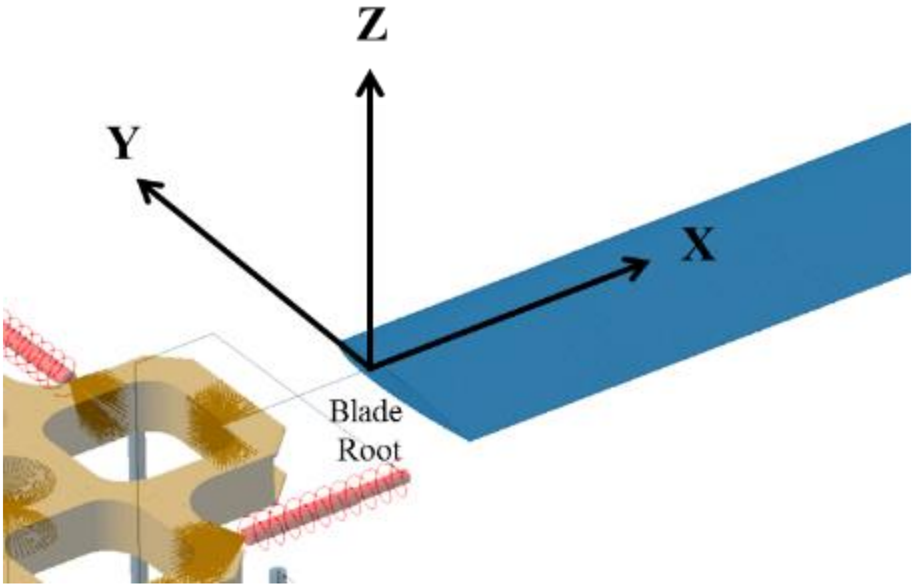

Figure 4.13 Reference coordinate system of the blade structure

4.3.1. Analysis with the Centrifugal Stiffening Effect Included

In this section, the simulation of the rotor system in ADAMS is performed by using the centrifugal stiffening effect included blade and the corresponding structural analysis results are presented.

4.3.1.1. Analysis of the Hover Condition

In the hover condition, rotor is simulated for the 10kN and the 15kN thrust cases and corresponding normal-x stress variation results in the blades and von Mises stress variation results in the hub are presented. From the stress variation results, critical locations are identified and for these locations stress results for the full revolution are plotted. The critical location is selected considering where the highest stress concentration is observed.

In Figure 4.14 and Figure 4.15, normal-x stress distribution and the critical locations in the blades are given for the 10kN and 15kN thrust cases, respectively. The critical location in the blade is determined in the spar component at root region. Furthermore, in Figure 4.16 normal-x stress variations at the critical location of the blade for the 10kN and 15kN thrust hover conditions are presented for four revolutions of the blade.

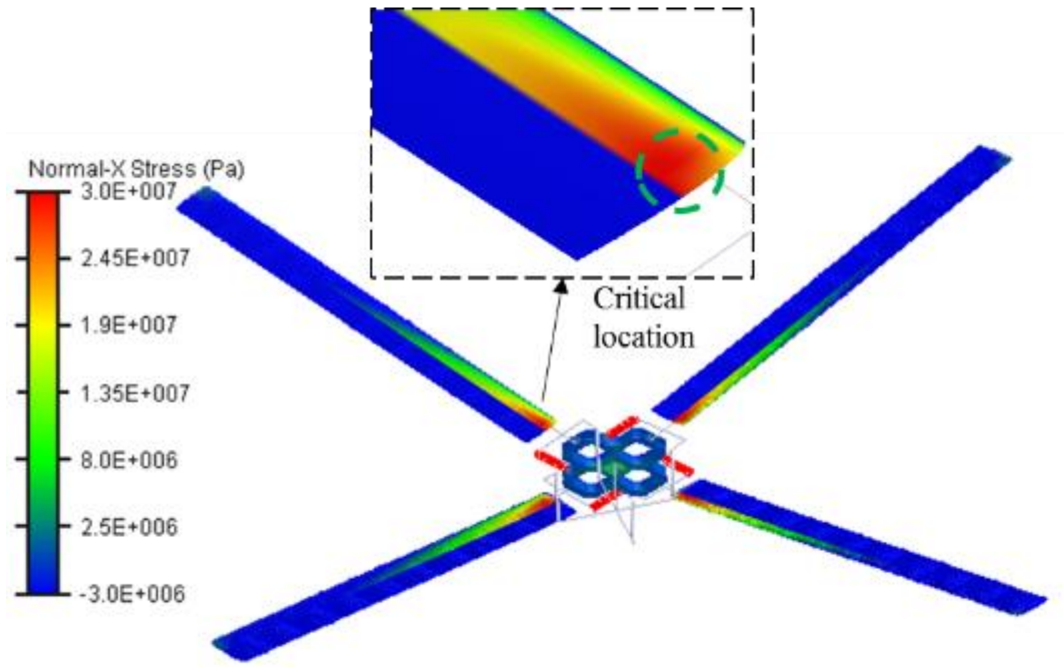

Figure 4.14 Normal-x stress result plot in the blade spar for 10kN thrust hover condition

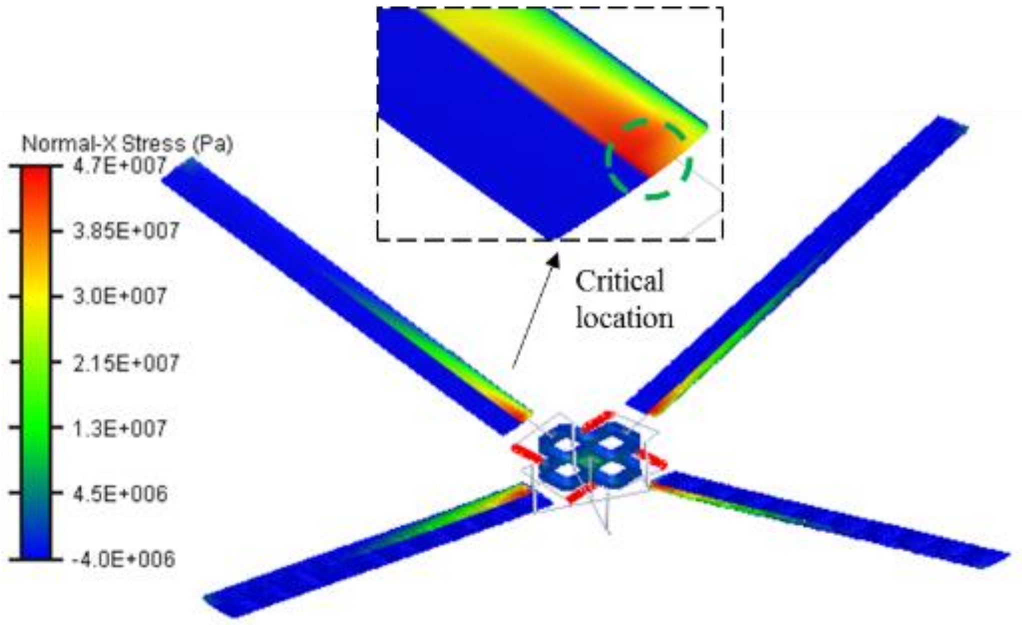

Figure 4.15 Normal-x stress result plot in the blade for 15kN thrust hover condition

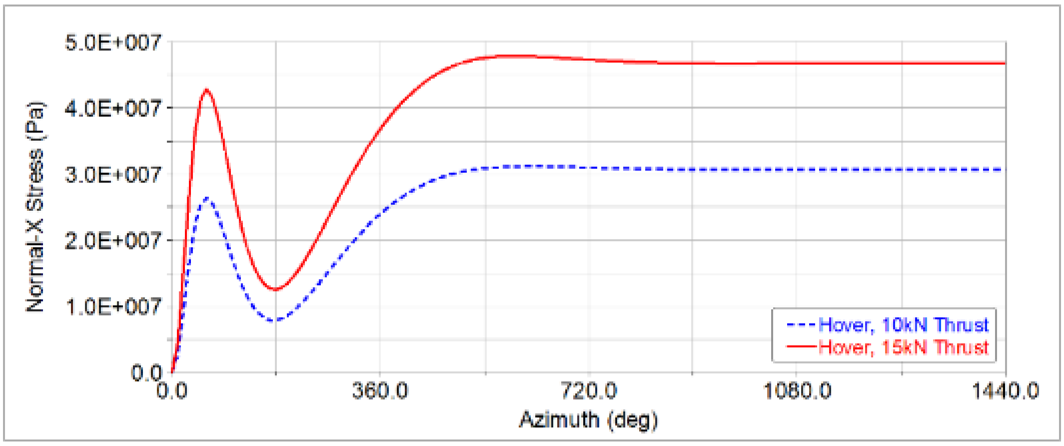

Figure 4.16 Normal-x stress variation in the critical location of the blade for the 10kN and 15kN thrust hover conditions

In Figure 4.17 and Figure 4.18, von Mises stress distributions and the critical locations in the hub are given for the 10kN and the 15kN thrust cases, respectively. Furthermore, in Figure 4.19 von Mises stress variation in the critical location of the hub for the 10kN and 15kN thrust hover condition is presented respectively.

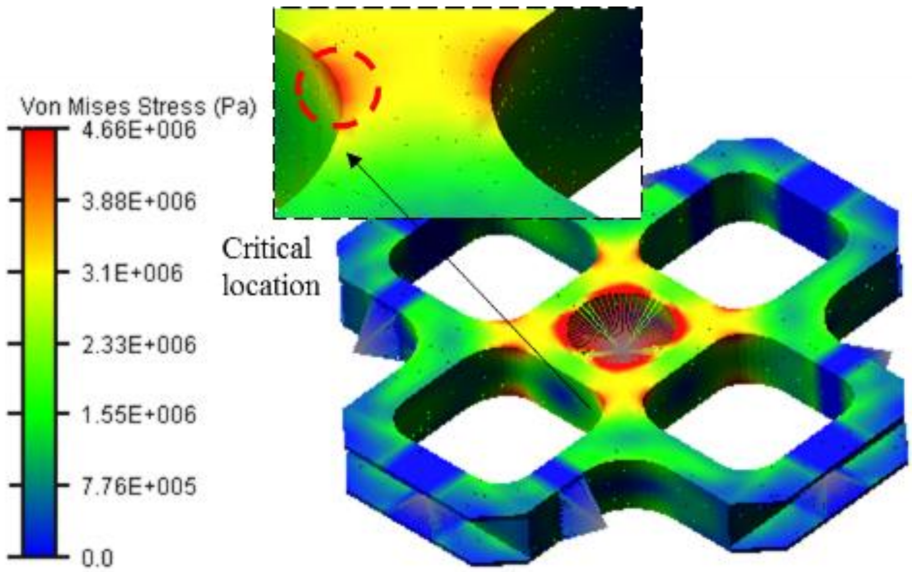

Figure 4.17 Von Mises stress result plot in the hub for the 10kN thrust hover condition

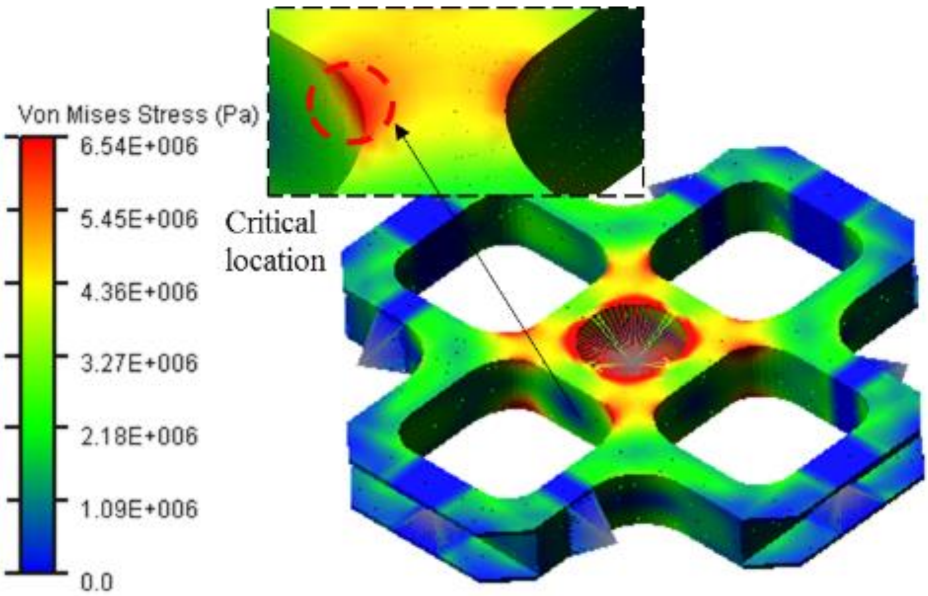

Figure 4.18 Von Mises stress result plot in the hub for the 15kN thrust hover condition

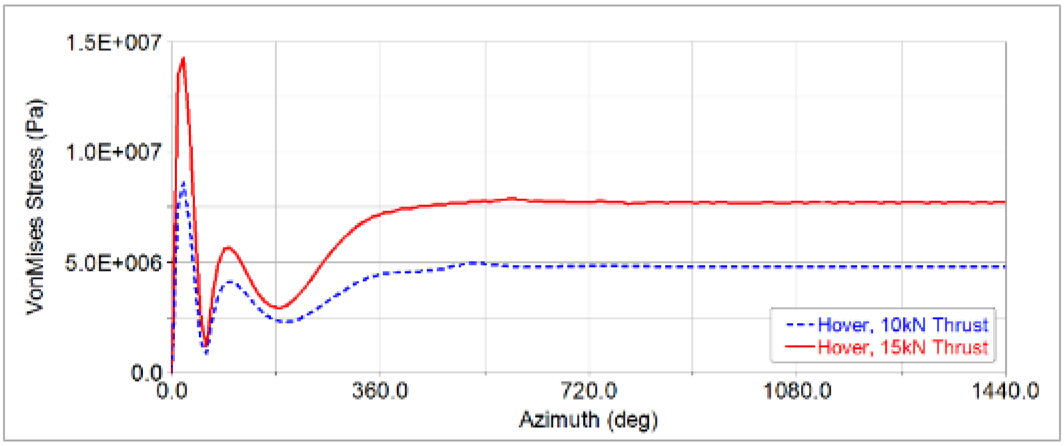

Figure 4.19 Von Mises stress variation in the critical location of the hub for the 10kN and 15kN thrust hover conditions

It is seen that for both rotor blades and hub, stress variations are constant at different azimuth positions and the stress value increases by the same ratio as the increase in the thrust value.

4.3.1.2. Analysis of the Forward Flight Condition

In the forward flight condition, rotor is simulated for the combination of 10kN and 15kN thrust with 10m/s and 30m/s forward flight velocity. Analysis cases are listed below.

- Forward Velocity = 10m/s, Thrust =10kN
- Forward Velocity = 10m/s, Thrust =15kN
- Forward Velocity = 30m/s, Thrust =10kN
- Forward Velocity = 30m/s, Thrust =15kN

After the simulation of the main rotor for the specified forward flight cases, the corresponding normal-x stress variations in the blades (Figure 4.20, Figure 4.21, Figure 4.22, and Figure 4.23) and von Mises stress variations in the hub (Figure 4.25, Figure 4.26, Figure 4.27, and Figure 4.28) are presented when the maximum stresses are observed at different azimuths. In addition to this, from the stress variation results, critical locations are specified and their full revolution stress results are plotted for the blade in Figure 4.24 and for the hub in Figure 4.29.

It is seen that as a result of the forward flight condition, stress variation in the critical location of both the blade and hub increases significantly and periodic stress variation is observed compared to the hover condition results. Moreover, results show that change in the thrust value affects the mean stress of the parts while the forward velocity affects the stresses periodically. Such a periodic variation of stress is the primary source of the fatigue failure in the long run.

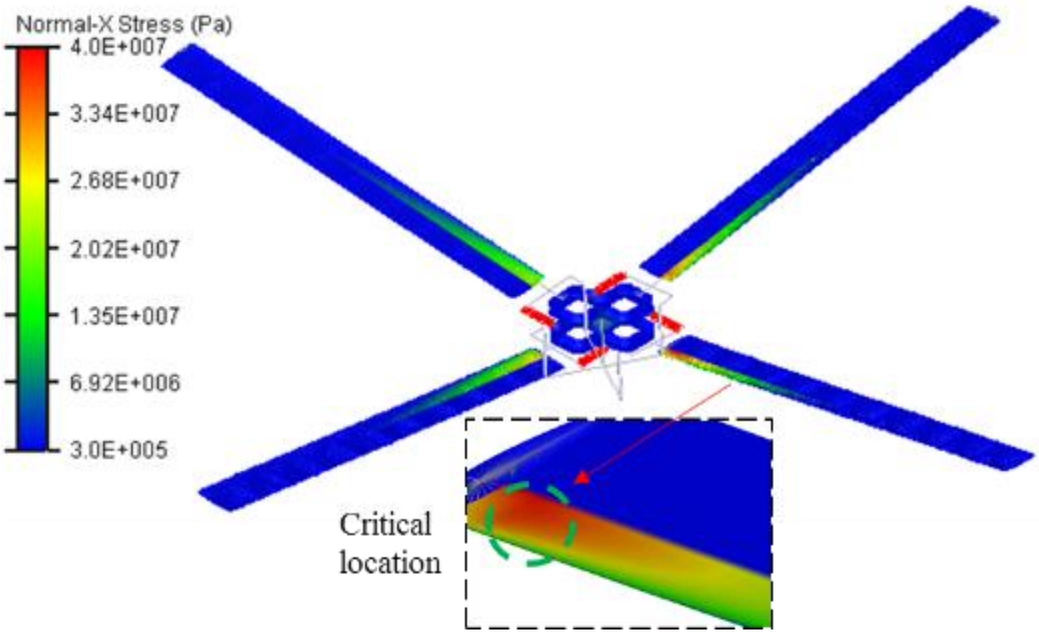

Figure 4.20 Normal-x stress result plot in the blade spar for 10kN thrust with 10m/s forward flight condition at azimuth = 810°

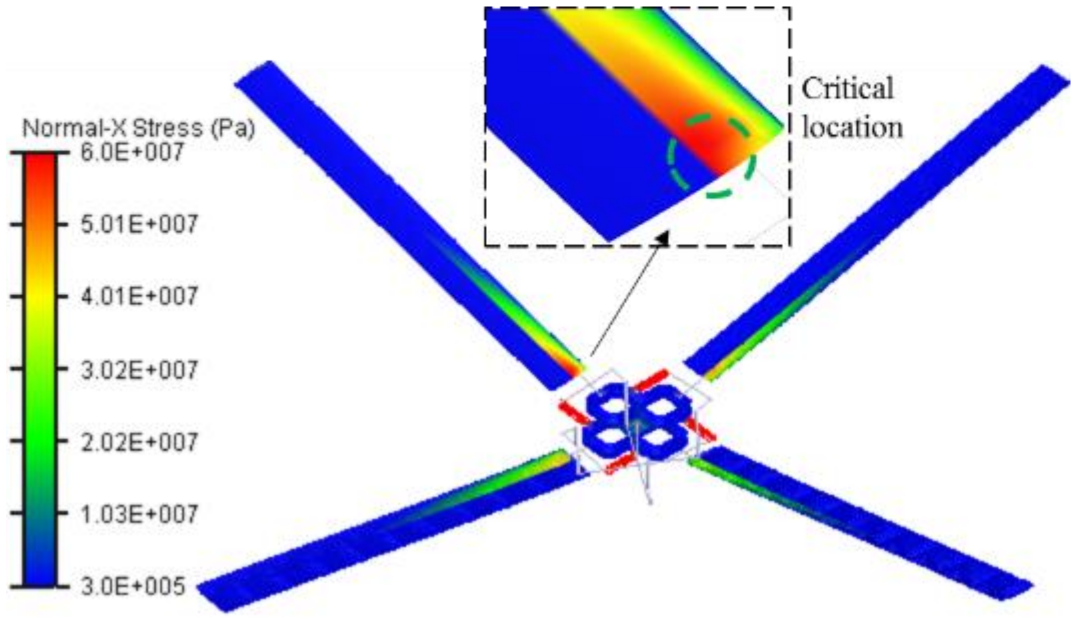

Figure 4.21 Normal-x stress result plot in the blade spar for the 15kN thrust with 10m/s forward flight condition at azimuth = 810^{o}

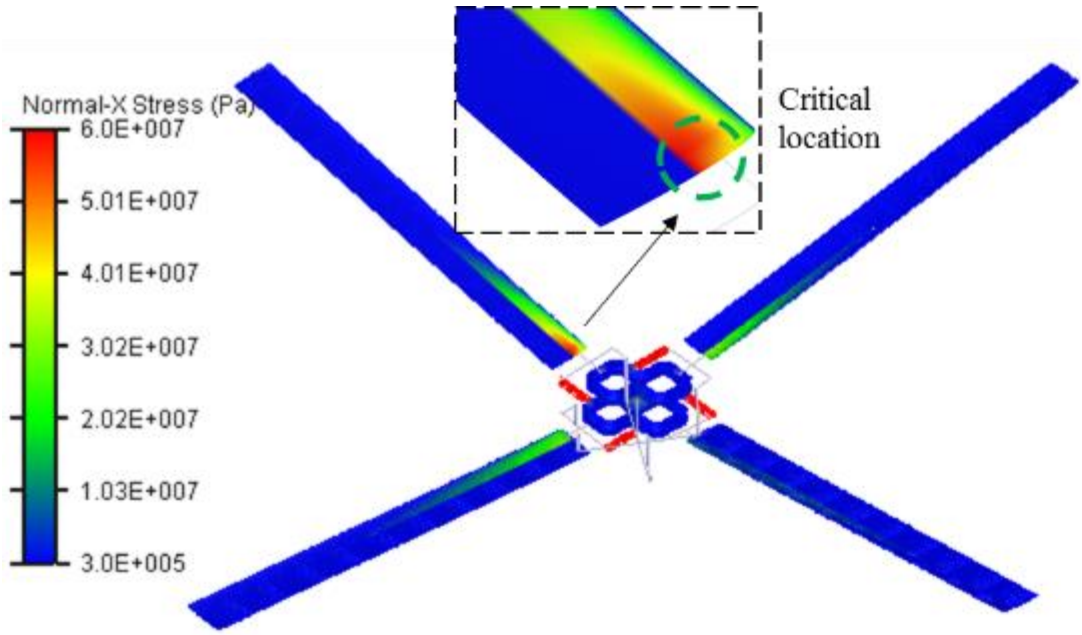

Figure 4.22 Normal-x stress result plot in the blade spar for the 10kN thrust with 30m/s forward flight condition at azimuth = 810^{o}

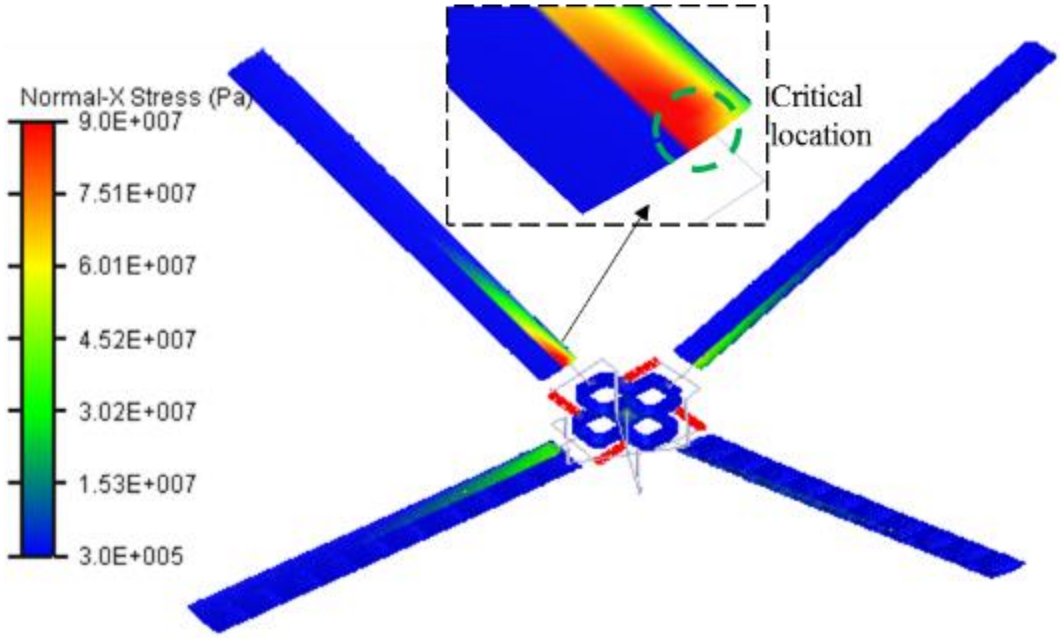

Figure 4.23 Normal-x stress result plot in the blade spar for the 15kN thrust with 30m/s forward flight condition at azimuth = 810°

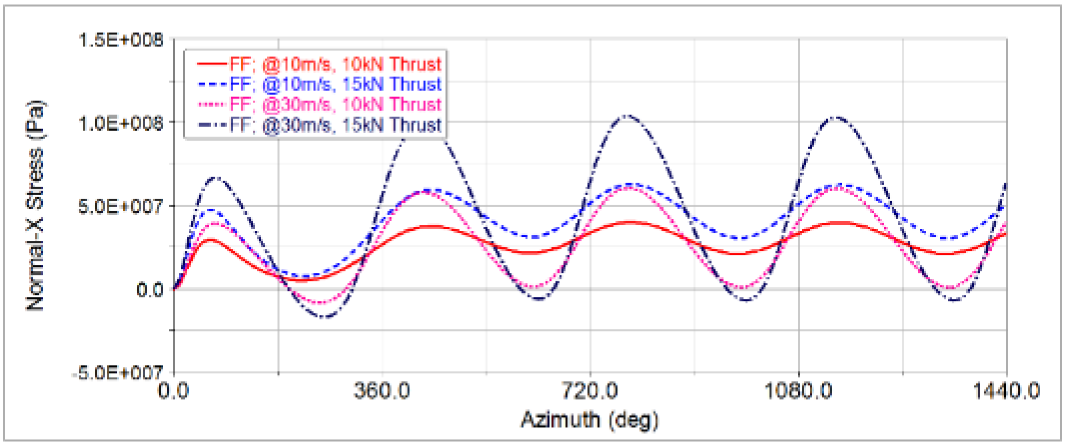

Figure 4.24 Normal-x stress variations in the critical location of the blade for the 10kN and 15kN thrust with 10m/s and 30m/s forward flight condition

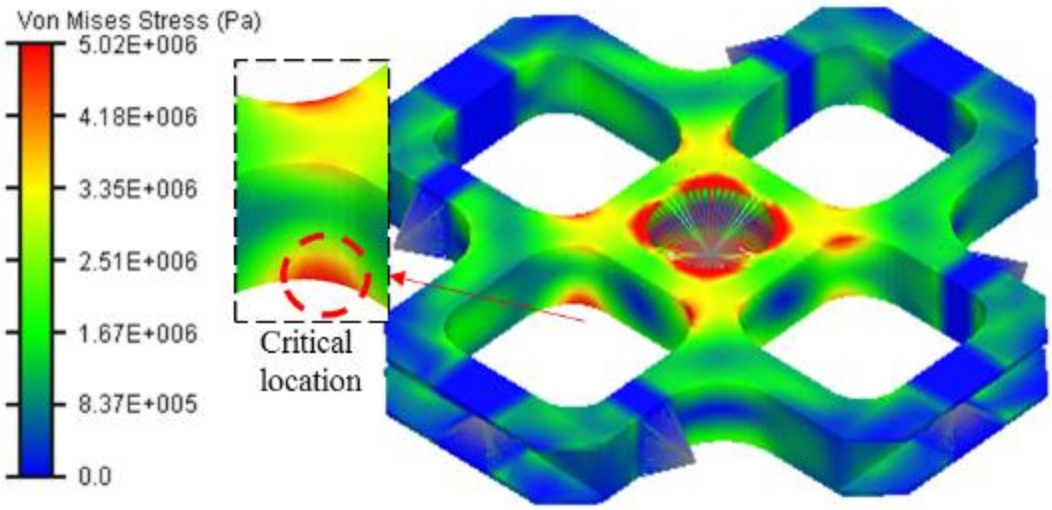

Figure 4.25 Von Mises stress result plot in the hub for the 10kN thrust with 10m/s forward flight condition at azimuth=810º

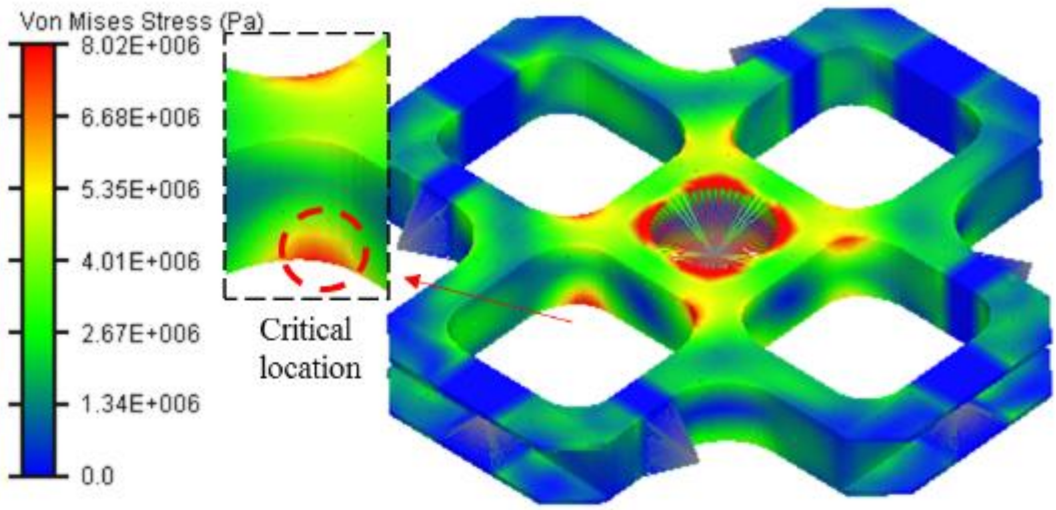

Figure 4.26 Von Mises stress result plot in the hub for the 15kN thrust with 10m/s forward flight condition at azimuth=810º

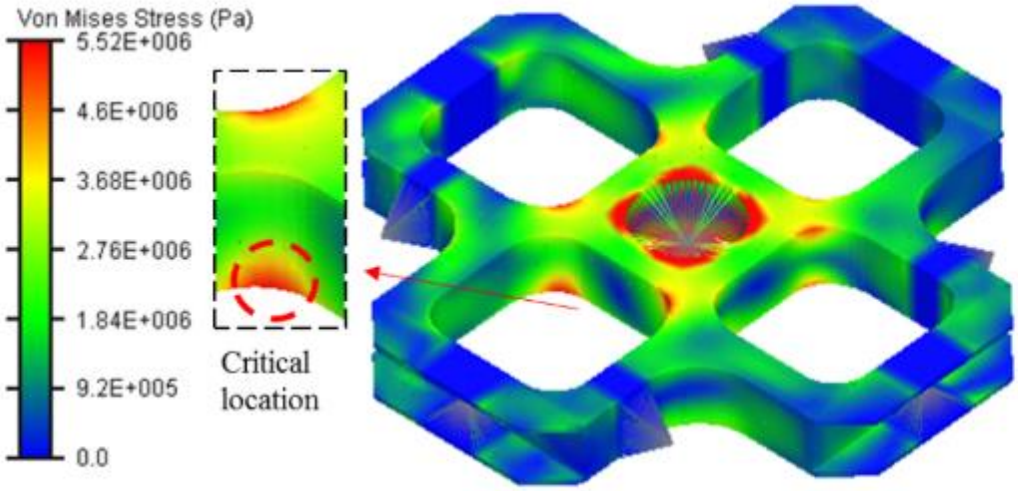

Figure 4.27 Von Mises stress result plot in the hub for the 10kN thrust with 30m/s forward flight condition at azimuth=810°

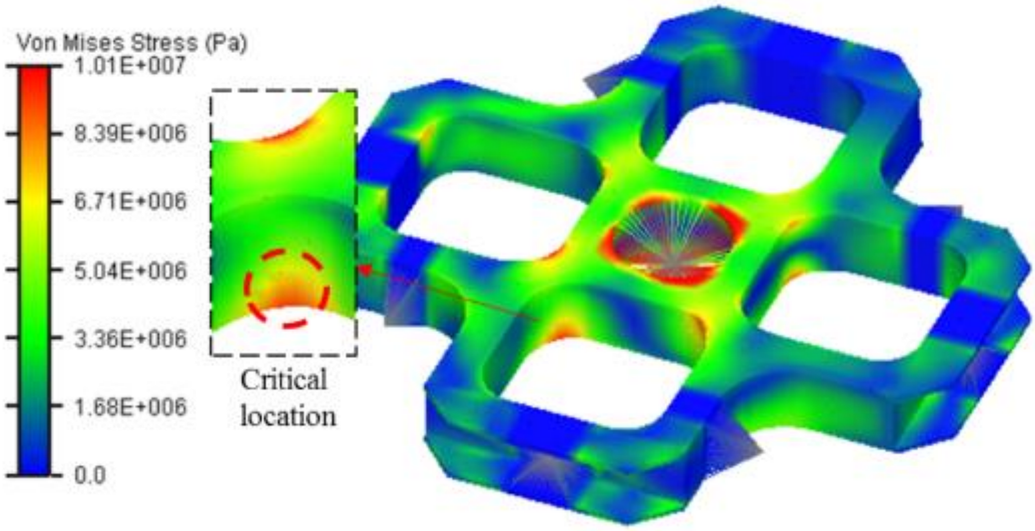

Figure 4.28 Von Mises stress result plot in the hub for the 15kN thrust with 30m/s forward flight condition at azimuth=820°

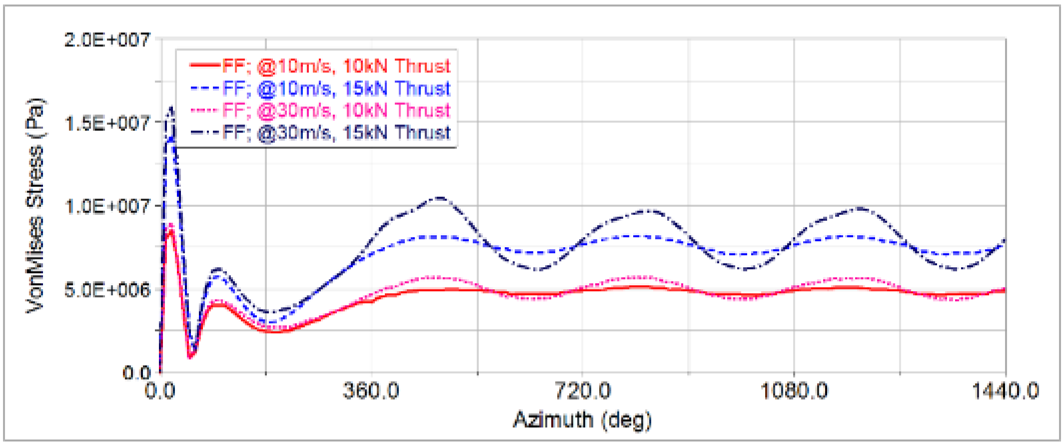

Figure 4.29 Von Mises stress variations in the critical location of the hub for the 10kN and 15kN thrust with 10m/s and 30m/s forward flight condition

4.3.2. Analysis with Large Deformation Effect Included

In this section, the simulation of the rotor system in ADAMS is performed by using the large deformation effect included blade and the corresponding structural analysis results are presented.

4.3.2.1. Analysis of the Hover Condition

In the hover condition, rotor is simulated for the 10kN and the 15kN thrust cases and corresponding normal-x stress variation results in the blades and von Mises stress variation results in the hub are presented. From the stress variation results, critical locations are identified and for these locations stress results for the full revolution are plotted. The critical location is selected considering where the highest stress concentration is observed.

In Figure 4.30 and Figure 4.31, normal-x stress distribution and the critical locations in the blades are given for 10kN and 15kN thrust cases, respectively. The critical location in the blade is determined in the spar component and circled. Furthermore, in Figure 4.32 normal-x stress variations at the critical location of the blade for the 10kN and 15kN thrust hover conditions are presented for four revolution of the blade. It is seen that location where the maximum stress is observed in root region of the blade spar but it is not apparent relative to centrifugal stiffened blade case.

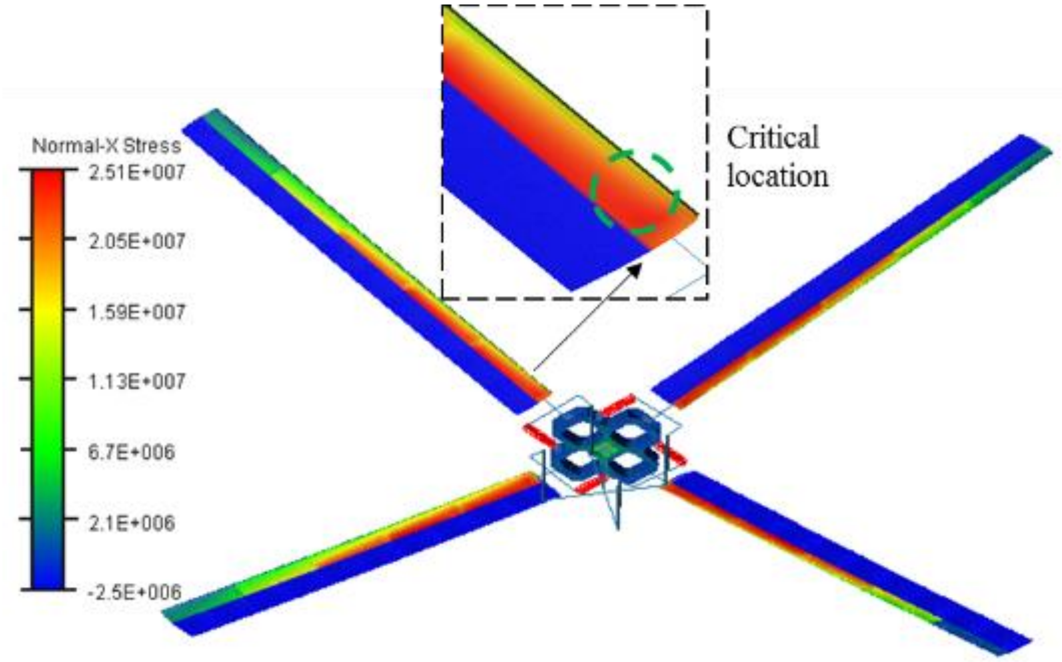

Figure 4.30 Normal-x stress result plot in the blade spar for 10kN thrust hover condition

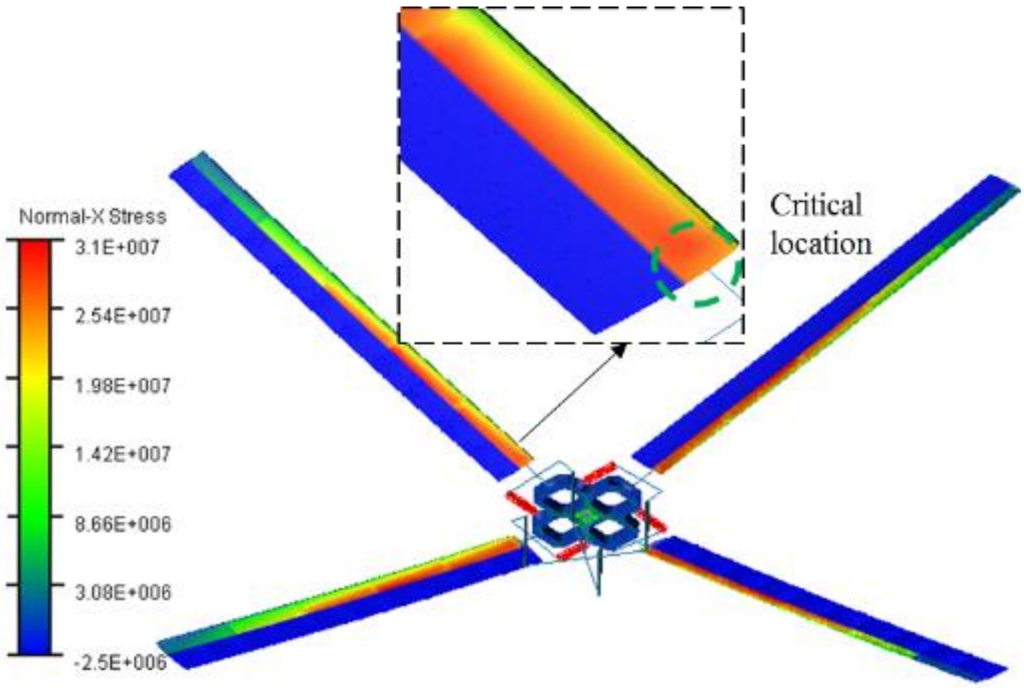

Figure 4.31 Normal-x stress result plot in the blade for 15kN thrust hover condition

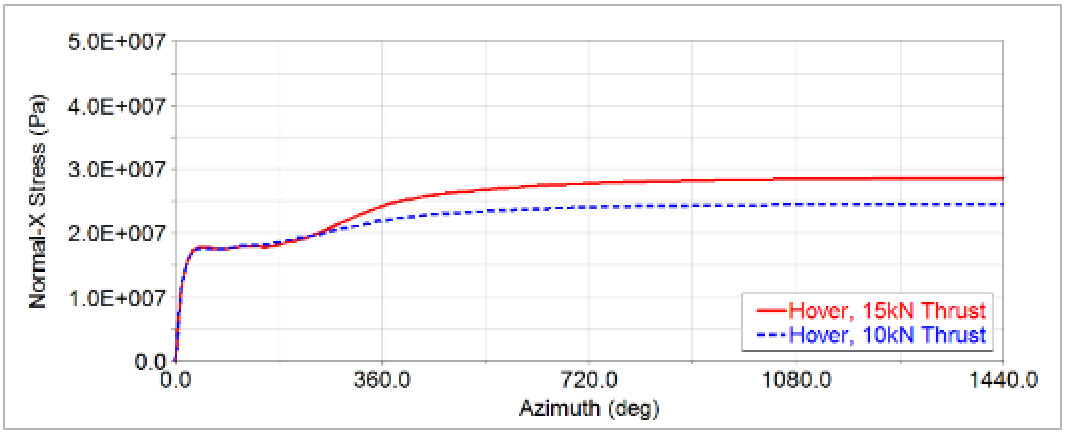

Figure 4.32 Normal-x stress variation in the critical location of the blade for the 10kN and 15kN thrust hover conditions

In Figure 4.33 and Figure 4.34, von Mises stress distributions and the critical locations in the hub are given for the 10kN and the 15kN thrust cases, respectively. Furthermore, in Figure 4.35 von Mises stress variation in the critical location of the hub for the 10kN and 15kN thrust hover condition is presented respectively.

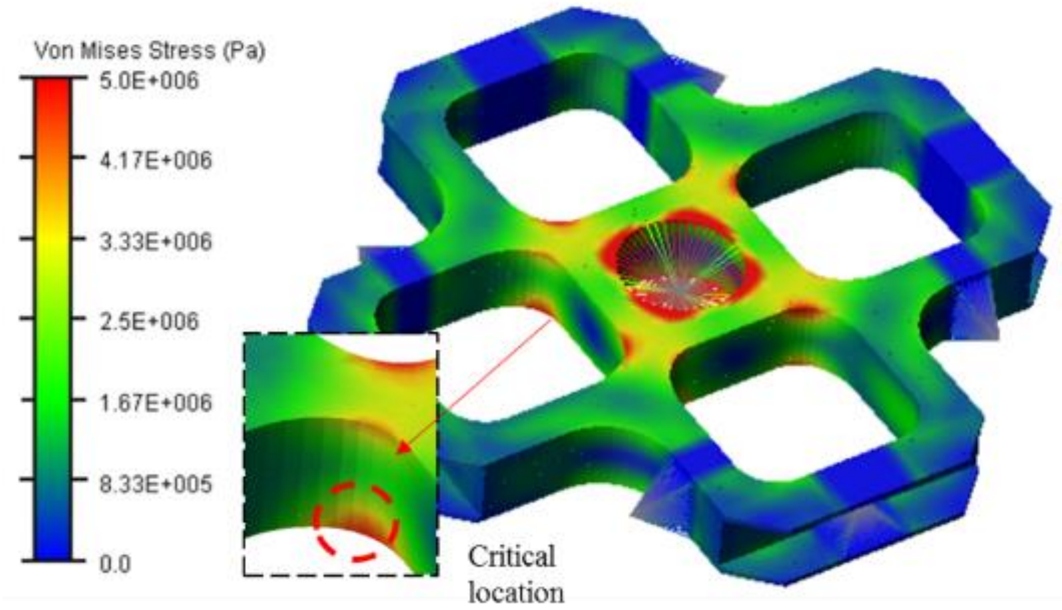

Figure 4.33 Von Mises stress result plot in the hub for the 10kN thrust hover condition

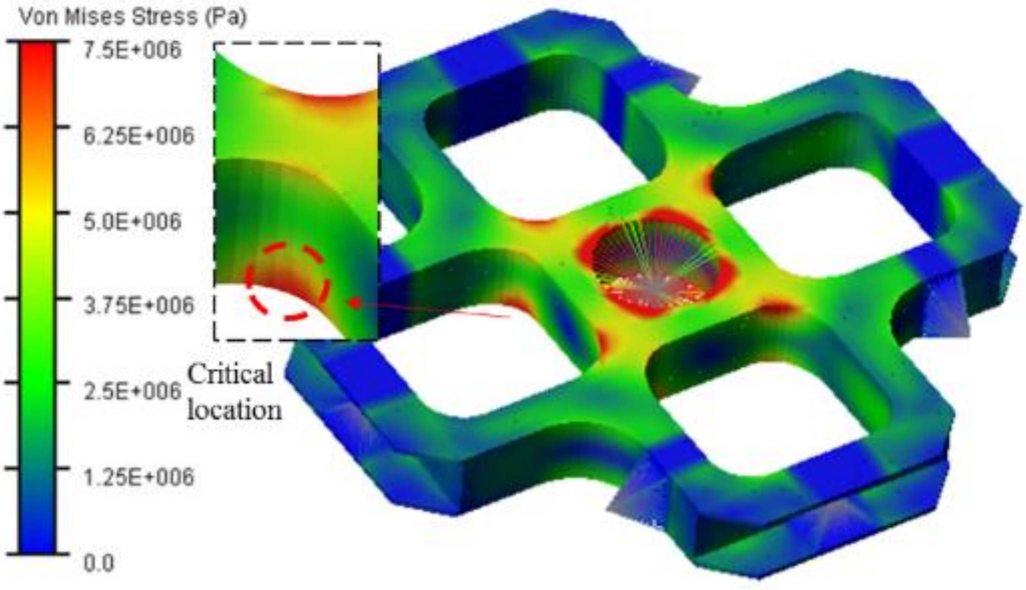

Figure 4.34 Von Mises stress result plot in the hub for the 15kN thrust hover condition

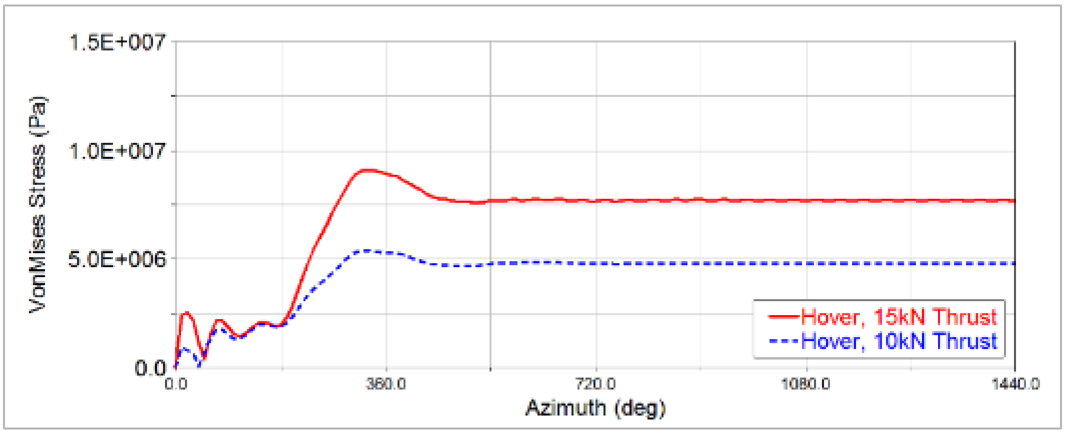

Figure 4.35 Von Mises stress variation in the critical location of the hub for the 10kN and 15kN thrust hover conditions

It is seen that for both rotor blades and the hub, stress variations are constant at different azimuth positions and the stress value increases by the same ratio as the increase in the thrust value.

4.3.2.2. Analysis of the Forward Flight Condition

In the forward flight condition, rotor is simulated for the combination of 10kN and 15kN thrust with 10m/s and 30m/s forward flight velocity. Analysis cases are listed below.

- Forward Velocity = 10m/s, Thrust =10kN
- Forward Velocity = 10m/s, Thrust =15kN
- Forward Velocity = 30m/s, Thrust =10kN
- Forward Velocity = 30m/s, Thrust =15kN

After the simulation of the main rotor for the specified forward flight cases, the corresponding normal-x stress variations in the blades (Figure 4.36, Figure 4.37, Figure 4.22, and Figure 4.39) and von Mises stress variations in the hub (Figure 4.41, Figure 4.42, Figure 4.43, and Figure 4.44) are presented when the maximum stresses are observed at different azimuths. In addition to this, from the stress variation results, critical locations are specified and their full revolution stress results are plotted for the blade in Figure 4.40 and for the hub in Figure 4.45.

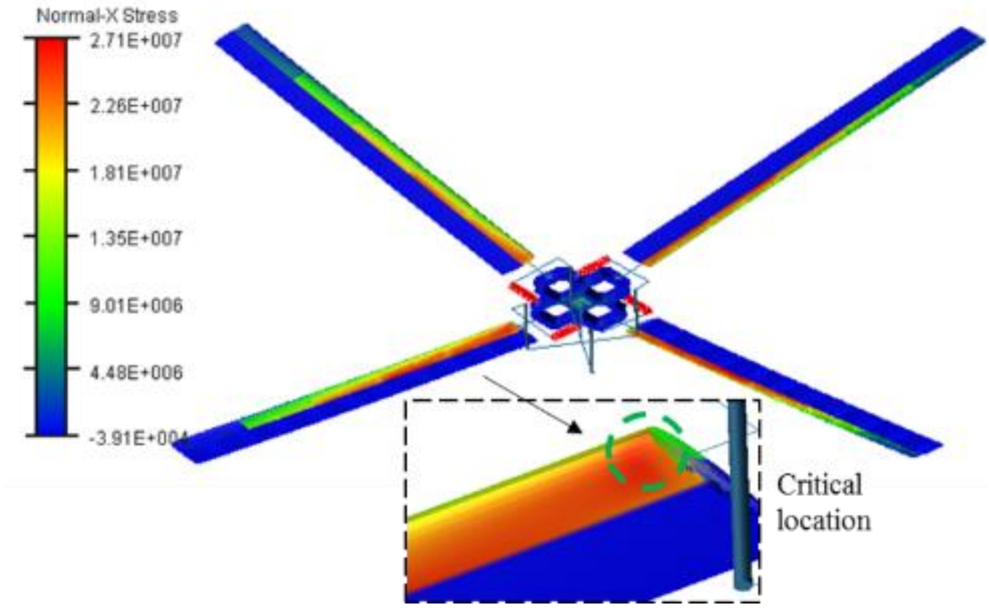

Figure 4.36 Normal-x stress result plot in the blade spar for 10kN thrust with 10m/s forward flight condition at azimuth = 1080º

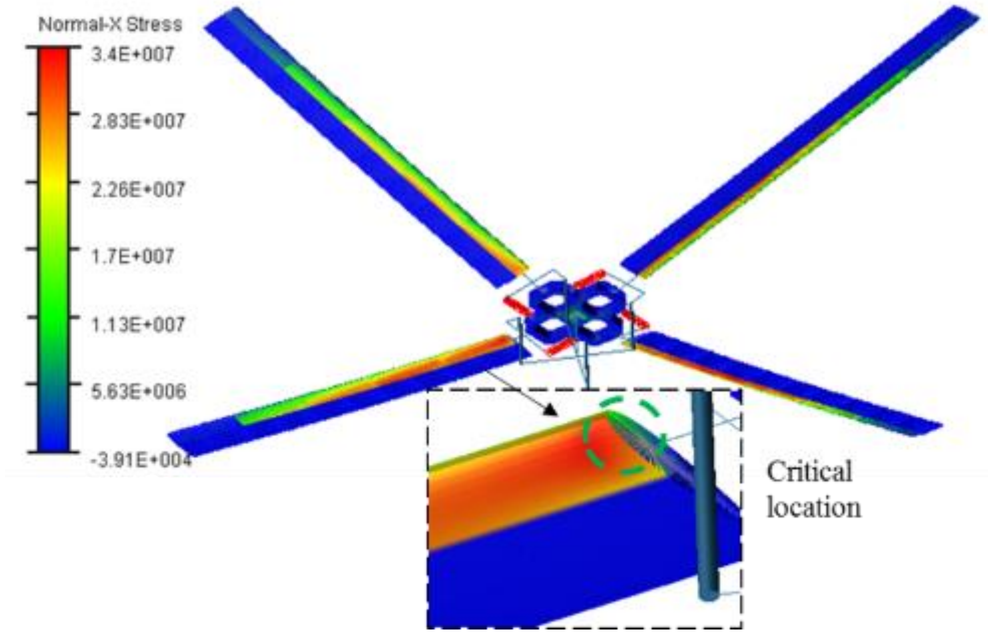

Figure 4.37 Normal-x stress result plot in the blade spar for the 15kN thrust with 10m/s forward flight condition at azimuth = 1080°

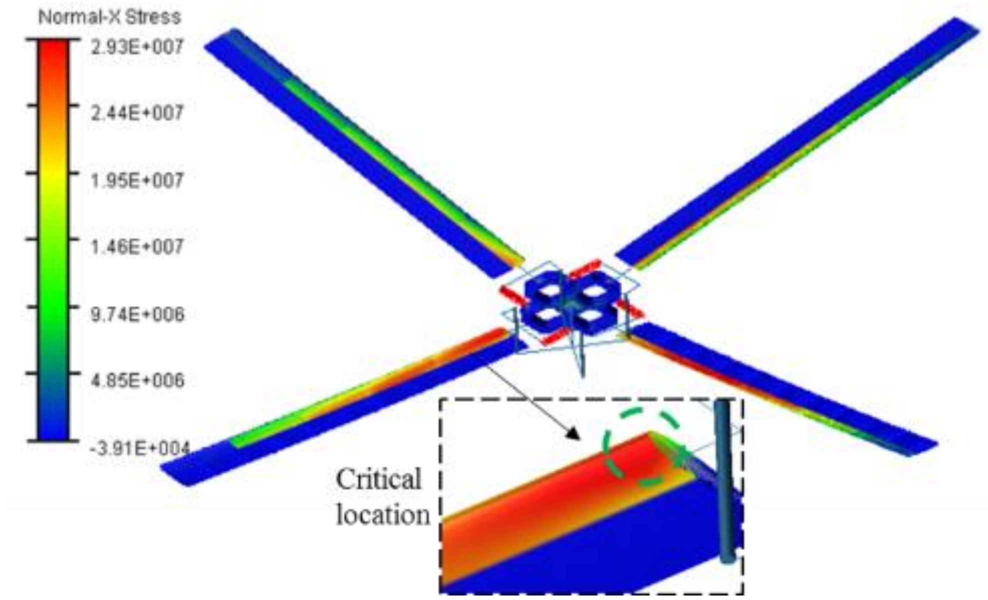

Figure 4.38 Normal-x stress result plot in the blade spar for the 10kN thrust with 30m/s forward flight condition at azimuth = 1080°

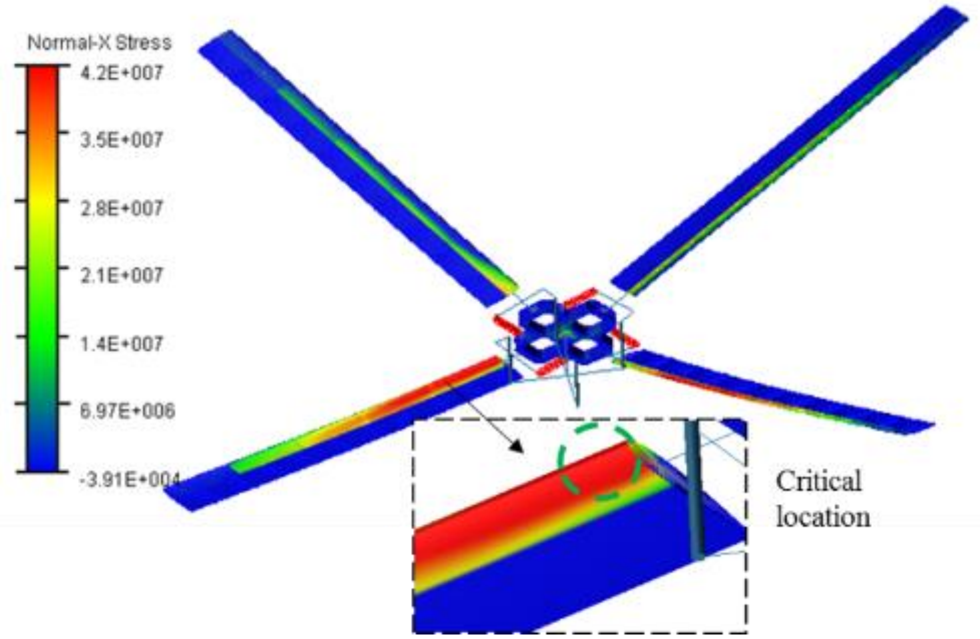

Figure 4.39 Normal-x stress result plot in the blade spar for the 15kN thrust with 30m/s forward flight condition at azimuth = 1080°

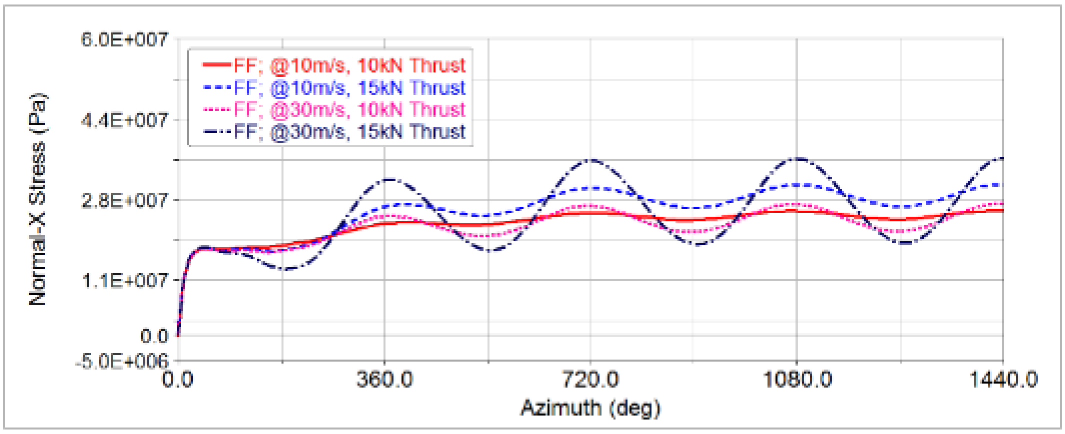

Figure 4.40 Normal-x stress variations in the critical location of the blade for the 10kN and 15kN thrust with 10m/s and 30m/s forward flight condition

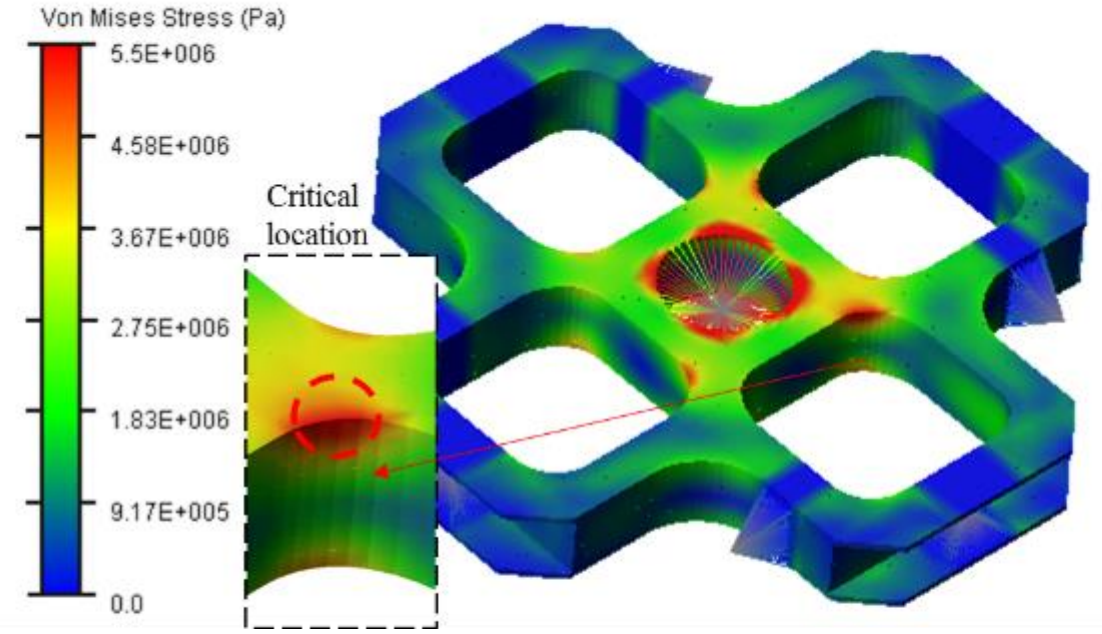

Figure 4.41 Von Mises stress result plot in the hub for the 10kN thrust with 10m/s forward flight condition at azimuth=770º

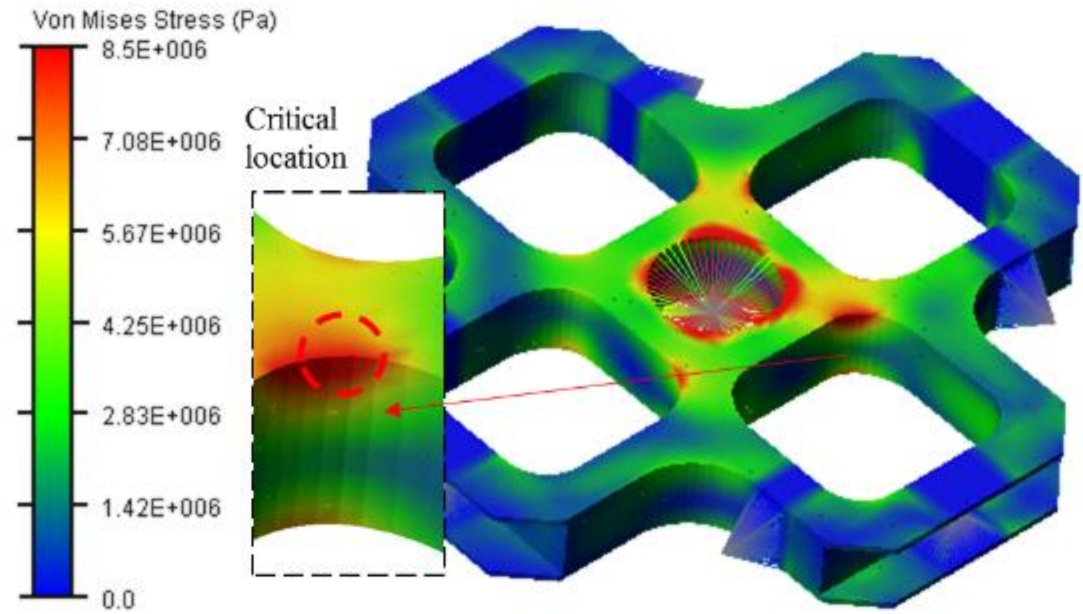

Figure 4.42 Von Mises stress result plot in the hub for the 15kN thrust with 10m/s forward flight condition at azimuth=770º

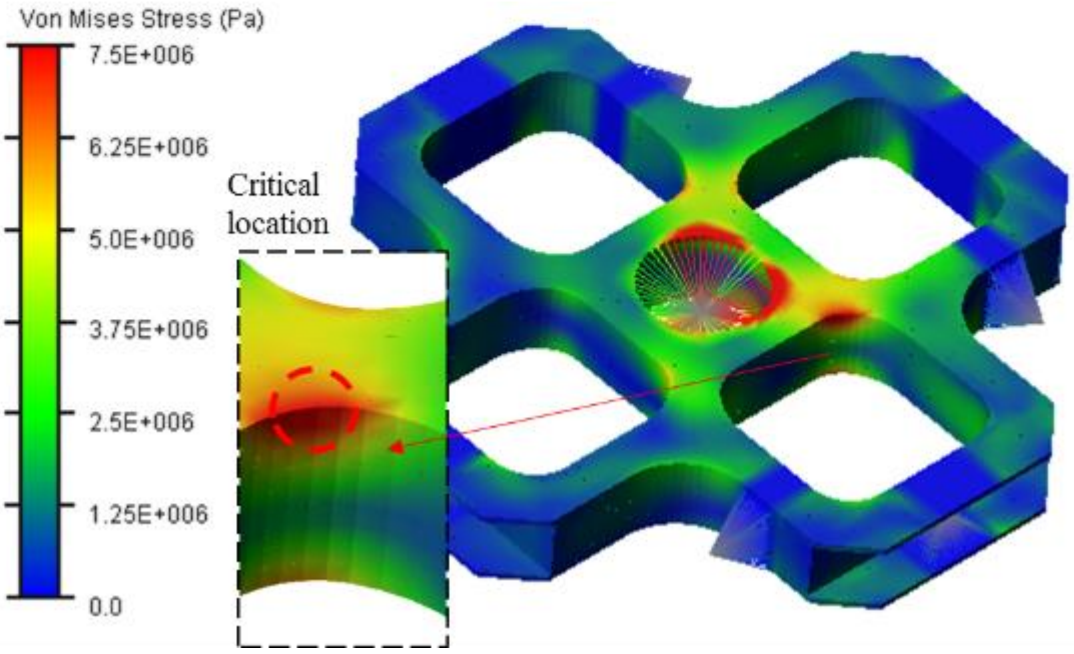

Figure 4.43 Von Mises stress result plot in the hub for the 10kN thrust with 30m/s forward flight condition at azimuth=770º

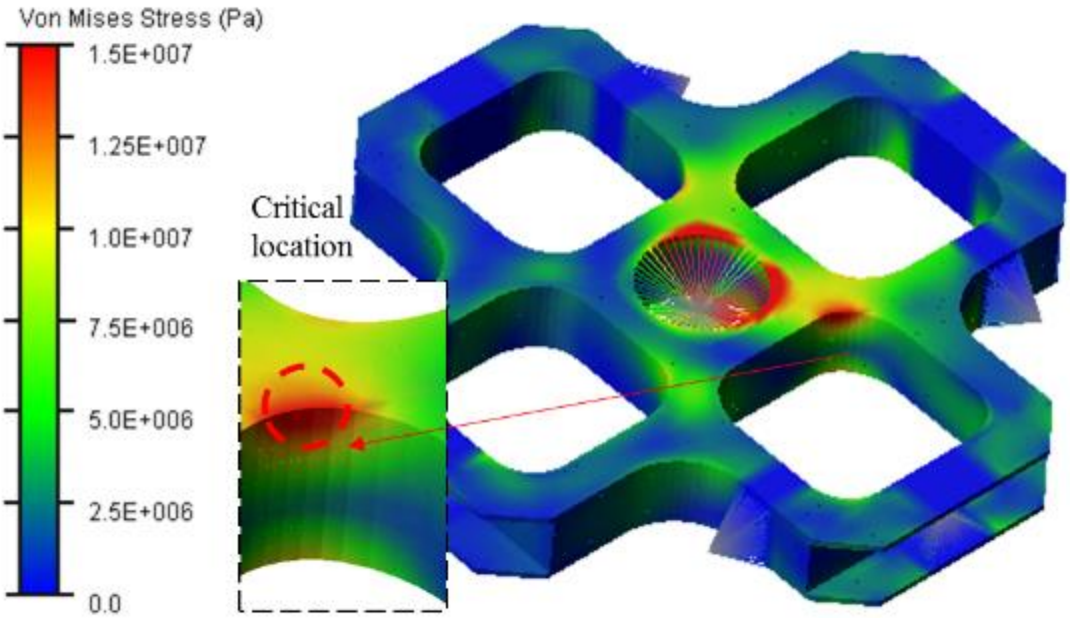

Figure 4.44 Von Mises stress result plot in the hub for the 15kN thrust with 30m/s forward flight condition at azimuth=770º

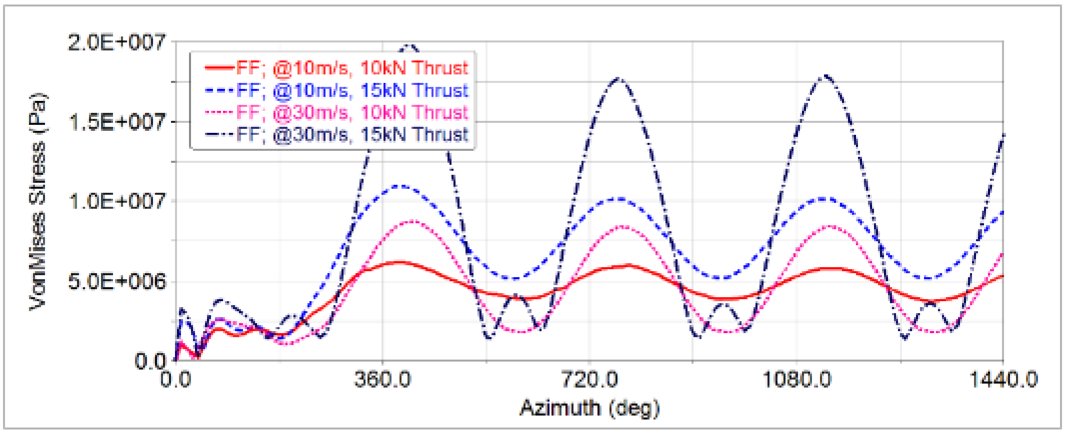

Figure 4.45 Von Mises stress variations in the critical location of the hub for the 10kN and 15kN thrust with 10m/s and 30m/s forward flight conditions

4.4. Effect of Design Parameter Modification on rotor simulation results

4.4.1. Damper Modifications

In this section, as an example of the effect of design modification, effect of different lag damper stiffness coefficient is investigated for the forward flight case of 30m/s forward velocity and 15kN thrust. In this section only the centrifugal stiffening effect is included in the rotor simulations. For this purpose, while the damping coefficients are kept constant, dampers with 500 N/mm 1000 N/mm, and 1500 N/mm stiffness values are implemented in the rotor model established in ADAMS. Dampers have significant effects on the dynamic characteristic of a rotor by directly affecting the lagging motion of the helicopter rotor blade. It can be seen in Figure 4.46 that higher damper stiffness coefficient causes a decrease in the lag angle and the lower lag angle accounts for a more stable rotor; because change in the center of gravity location of the blade becomes smaller. In addition to this, due to the smaller lag angle, required space for blade motion becomes smaller.

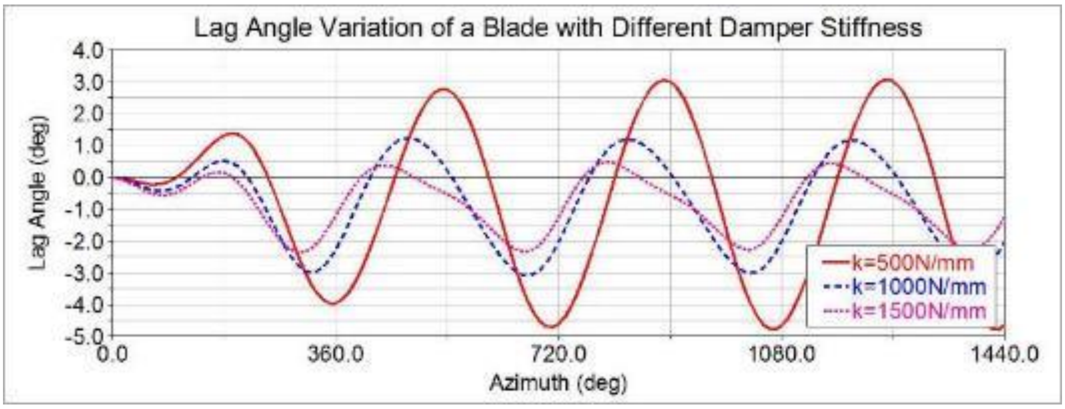

Figure 4.46 Lag angle variations of the blades for the 500N/mm, 1000N/mm, and 1500N/mm lag damper stiffness

On the other hand, in Figure 4.47, the critical locations in the hub and the blade are shown for the stress plots. The change in the damper stiffness coefficient does not have significant effect on the rotor hub and the rotor blade stresses, presented in Figure 4.48 and Figure 4.49; because damper produces more or less the same force with lower damper stroke due to the higher stiffness.

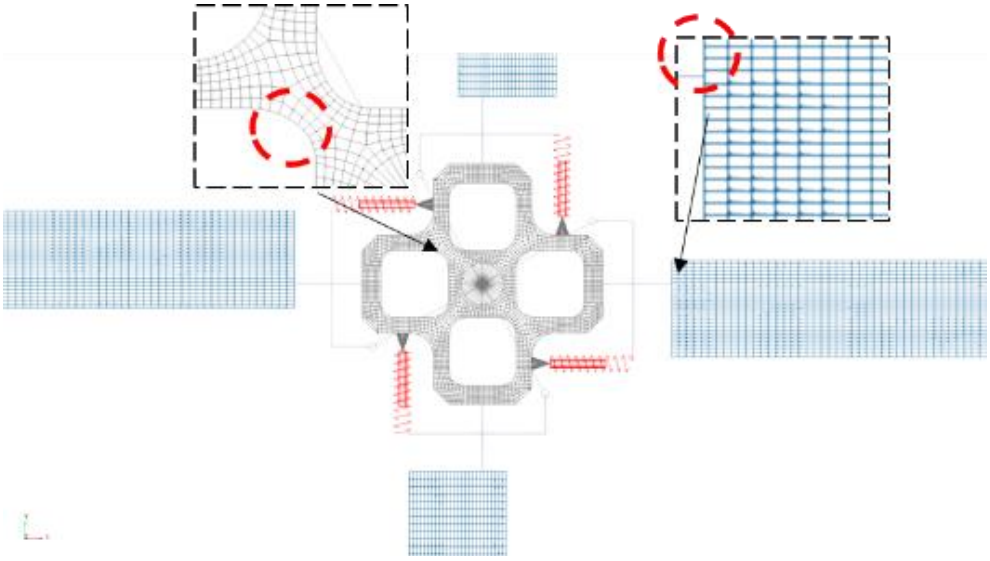

Figure 4.47 Rotor hub and the rotor blade critical locations

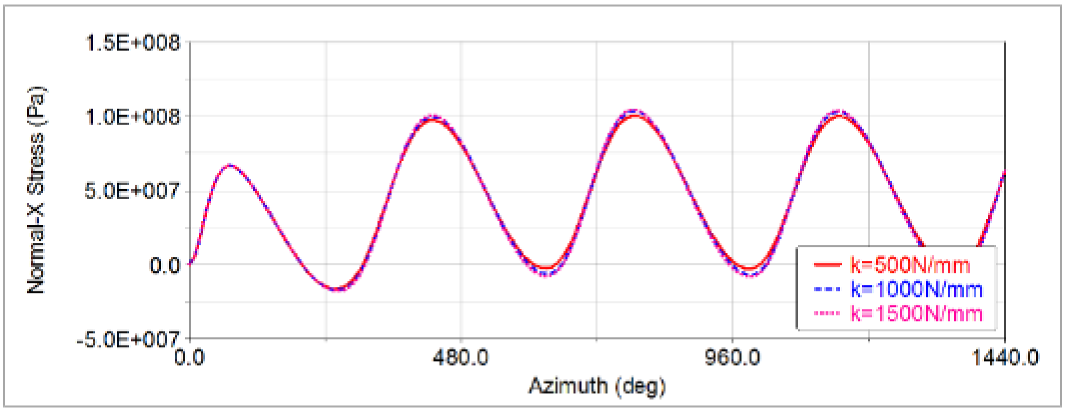

Figure 4.48 Normal-x stress variations of the critical location in the blade for 500N/mm, 1000N/mm, and 1500N/mm lag damper stiffness for 15kN thrust with 30m/s forward flight condition

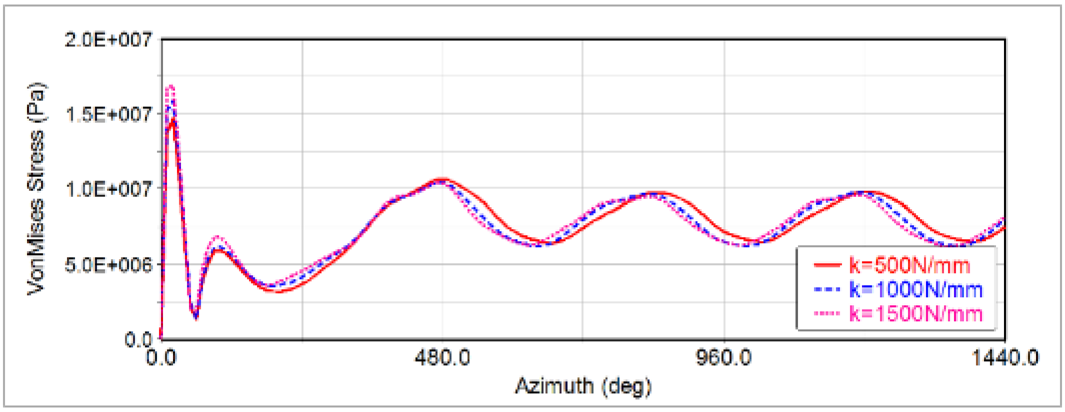

Figure 4.49 Von Mises stress variations of the critical location in the hub for 500N/mm, 1000N/mm, and 1500N/mm lag damper stiffness for 15kN thrust with 30m/s forward flight condition

4.4.2. Pitch-Flap coupling (δ_3 angle)

Pitch-Flap coupling, also known as the $\boldsymbol{\delta_3}$ angle is a kinematic relation between the pitch and the flap angles. In this coupling mechanism, the rotor blade pitch angle is affected from the blade flapping motion. It is introduced by changing the flap hinge rotation direction or the pitch link – pitch horn connection point location for hingeless type rotors, as demonstrated in Figure 4.50. When $\boldsymbol{\delta_3}$ angle is positive, an increase of the flap angle causes a decrease of the blade pitch angle and hence the angle of attack of the blade. Basically, pitch-flap coupling works as an aerodynamic spring for the helicopter blade in flap motion. For the calculation of the effects of positive $\boldsymbol{\delta_3}$ angle on the blade pitch angle, simple geometric relation, shown in Figure 4.51, can be used as:

$$\Delta\theta = -\beta \tan \delta_3 \qquad (36)$$

where $\Delta\theta$ is the change in the pitch angle of the blade due to pitch-flap coupling, β is the flap angle of the blade.

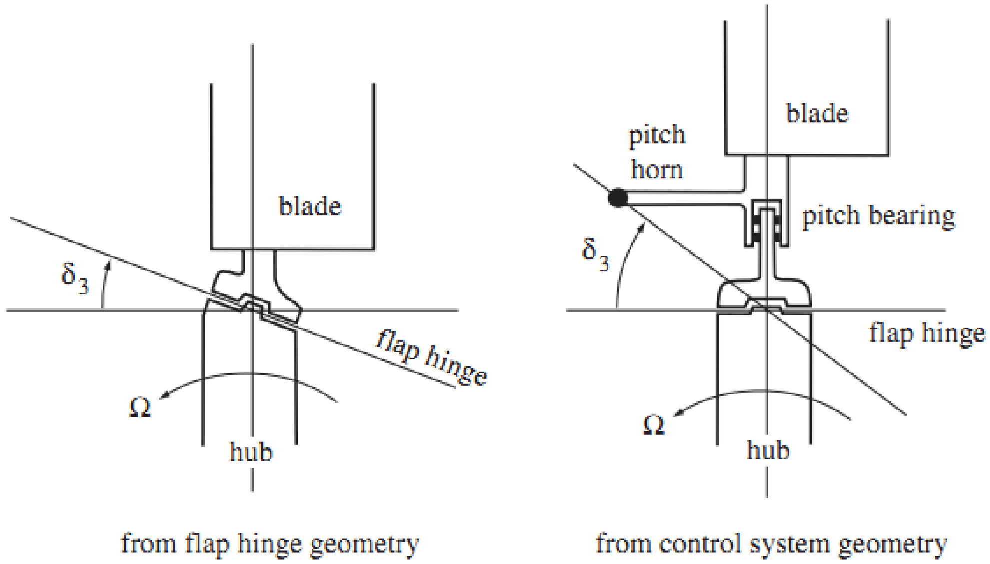

Figure 4.50 Pitch-flap coupling of a rotor [1]

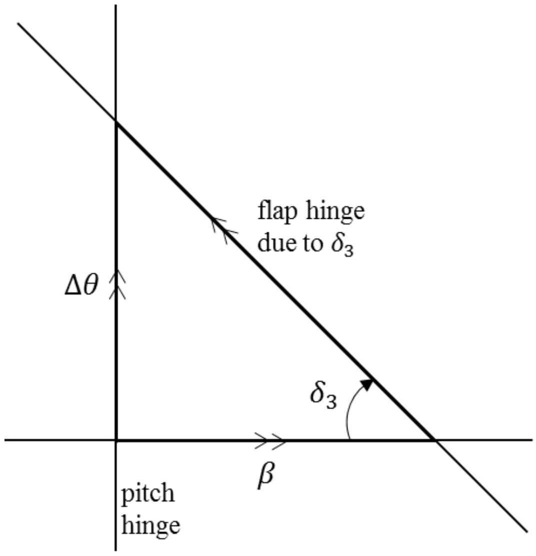

Figure 4.51 Geometric representation of the $\boldsymbol{\delta_3}$ angle

In the original main rotor simulation model, for the simplicity, zero δ_3 angle is chosen for the analyses, however in order to investigate effects of the δ_3 angle, main rotor model is simulated and compared by using different δ_3 angle.

For the forward flight at 30m/s velocity with 15kN thrust, 0deg, 15deg, 30deg δ_3 angle configurations of the rotor are analyzed. In order to investigate the effect of the δ_3 angle, produced thrust value and pitch, flap and lag angles of one of the blades are compared.

In Figure 4.52, produced thrust values are presented for different δ_3 angle configurations. It is seen that the target thrust values are achieved for the three configurations; but for the 30deg δ_3 angle case, thrust value variations are more stable than the other configurations. On the other hand, as shown in Figure 4.53, in order to to produce the target thrust value, required pitch angle of the blade needs to be increased with the increase in the δ_3 angle, as would be expected.

In Figure 4.54 and Figure 4.55, flap and lag angle variations of a blade are presented. As it can be seen from these figures, for higher δ_3 angle, blade undergoes smaller flap angle variation and hence smaller lag angle variation since the δ_3 angle behaves like an aerodynamic spring in the rotor system. This result shows that decrease in the flap and the lag angle account for a more stable rotor; because change in the center of gravity location of the blade becomes smaller.

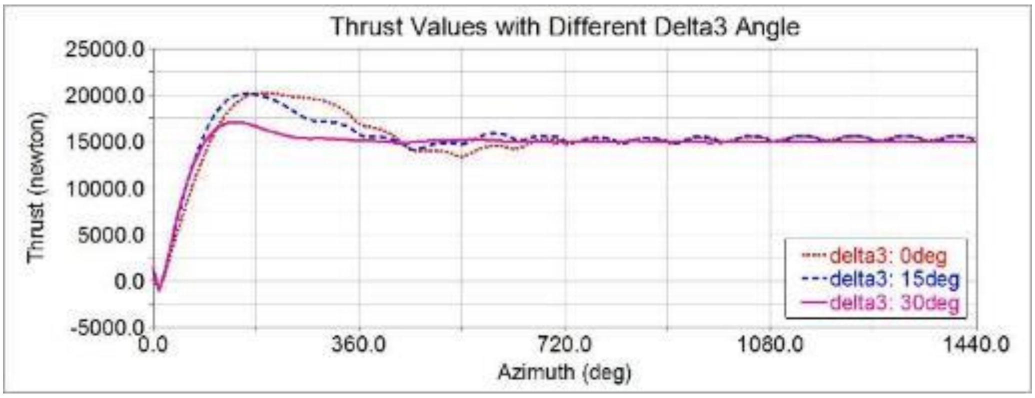

Figure 4.52 Thrust values of the rotor under different $\boldsymbol{\delta_3}$ angle configurations

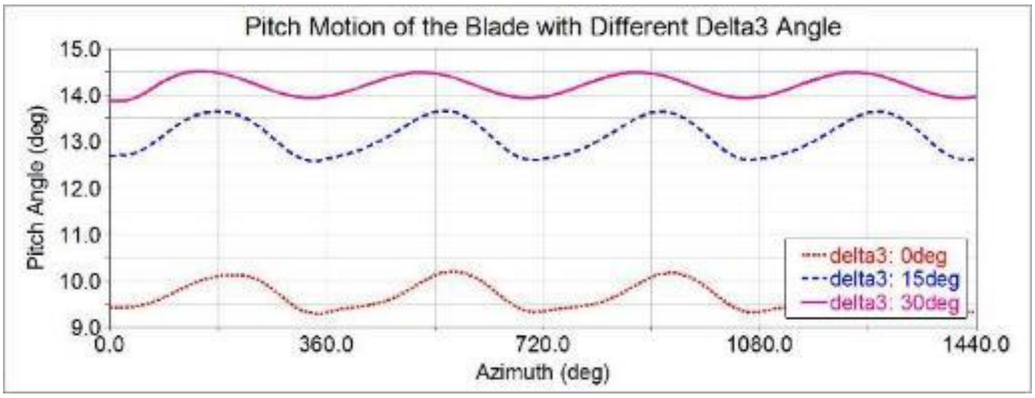

Figure 4.53 Pitch angle of a blade under different $\boldsymbol{\delta_3}$ angle configurations

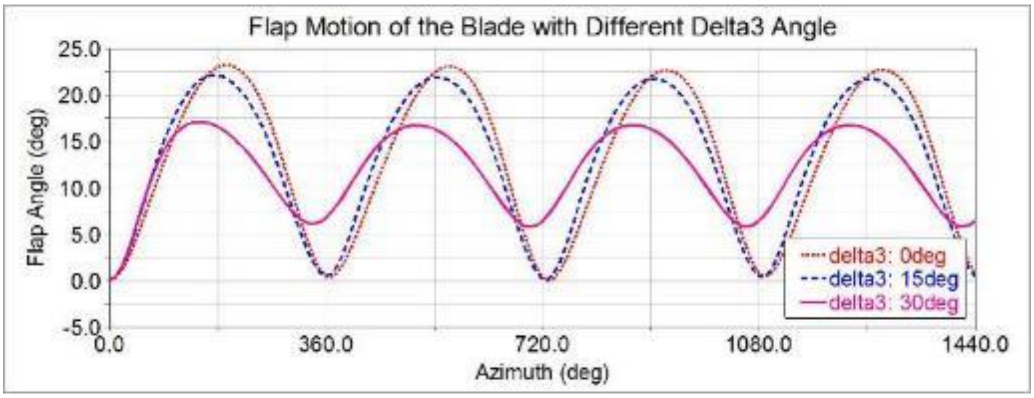

Figure 4.54 Flap angle of a blade under different $\boldsymbol{\delta_3}$ angle configurations

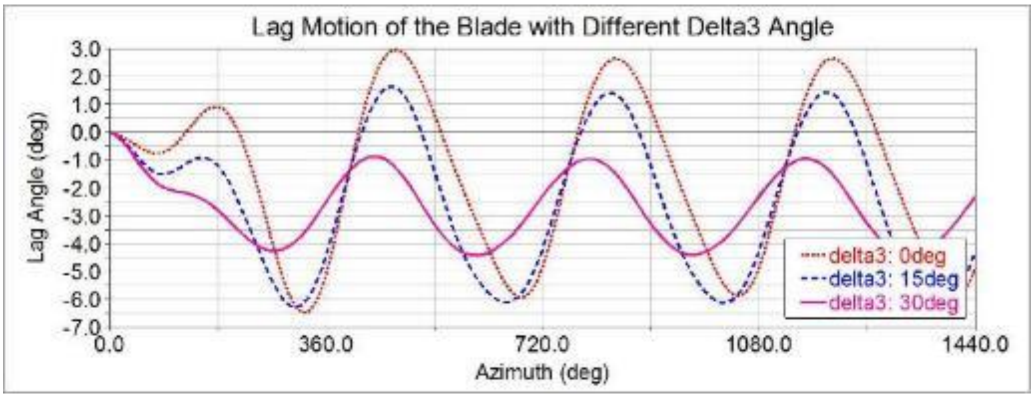

Figure 4.55 Lag angle of a blade under different $\boldsymbol{\delta_3}$ angle configurations

CHAPTER 5

CONCLUSION

In this study, multibody simulation of a helicopter main rotor system is presented by including structural flexibility. For this purpose, the helicopter rotor blade and rotor hub are modeled as flexible to use in multibody simulation of the helicopter rotor in MSC ADAMS. In addition, the simple aerodynamic load calculation method for the hover and the forward flight conditions is embedded in ADAMS without the use of any external aerodynamic load calculation tools.

The helicopter rotor is a complex mechanical system that consists of several sub structure with several joints. Helicopter rotor parts are connected to each other with different types of joints with different ways. In addition, various types of helicopter rotor configurations exist due to the connection method of the rotor parts. In this study, fully articulated rotor head type is utilized. The rotor system consists of the rotor hub, dampers, the rotor blades, pitch control levers, pitch links, and swash plate which are connected to each using kinematic joints to form a rotor mechanism in ADAMS.

In the present study, the lifting line theory is used for calculation of the aerodynamic forces and moments. The formulation of the lifting line theory is embedded into the ADAMS model for the calculation of these loads instantaneously in the ADAMS model. Hence, different flight scenarios can be simulated easily in the generated ADAMS model without a need for an external aerodynamic load calculation tool. In this study, it is not intended to integrate a detailed rotary wing aerodynamic solver to the established rotor system since this requires substantial amount of work and this is considered as future work of this study.

The trimming procedure has been applied to the multibody simulation model in order to obtain more realistic simulation results. Trimming a helicopter is generally classified into two types; full aircraft trim and isolated rotor trim. In this study, since the multibody model represents the isolated main rotor, isolated trim procedure is utilized for trim calculations. In the trim state, all force and moment vectors need to be in balance for desired flight condition. This state can be accomplished by optimizing the main rotor blades pitch angle settings individually to obtain balanced moments and forces. In the isolated trim calculations, one force and two moment; rotor thrust, rotor hub roll moment and rotor hub pitch moment, equilibrium condition is achieved. For this purpose, ADAMS multibody rotor model is utilized to determine the pitch angle settings for the trim condition.

Most of the multibody modeling and simulation tools for modeling helicopter rotors use beam models of the blade and the rigid rotor components. Stress recovery procedure in the blade and the rotor parts are then performed by means of cross-sectional analysis tools or finite element analysis tools which use the load information obtained in the multibody simulation of the rotor. In the present study, 3D finite element models of the blades and the hub have been implemented into ADAMS in order to achieve more realistic simulation of the helicopter rotor and obtain time dependent stress history result for the investigation of the effect of design modification on the stress history in the rotor hub and in the critical section of the blade. The flexibility of the parts and stress recovery is achieved by connecting ADAMS to Nastran using modal superposition principle. The finite element models are prepared in MSC.Patran and the MSC.Nastran/ADAMS integration is utilized to generate files of flexible parts to be used in ADAMS.

Since the rotor blades have significant effect in the dynamics of a rotor system, more detailed approach needs to be used for implementation of the blade flexibility. For this purpose, stiffening and large deformation geometric nonlinear effects are also taken into account during the modeling of the flexible rotor blades because of the presence of the high centrifugal force due to the rotation of the rotor and the long and slender structural form of the helicopter blade. In ADAMS, geometric nonlinearities cannot be included into the flexible body directly since ADAMS/Flex solver cannot handle nonlinearities. Hence, alternative methods need to be utilized for taking into account geometric nonlinearity implementation of the rotor blade.

In order to include the stiffening nonlinear effects of the centrifugal force on the rotor blade, Nastran[14] restart analysis method is utilized. In the restart analysis, first, nonlinear static analysis is performed under the centrifugal force for the generation of the nonlinear stiffness matrix and then normal modes analysis is done by using the stored nonlinear stiffness matrix. As a result of this, centrifugal stiffening nonlinear effect can be captured for the rotor blade in ADAMS.

For the inclusion of the large deformation effect in ADAMS, segmental shooting technique[24] is utilized. For this purpose, the rotor blade is divided into five segments and they are arranged end to end and connected to each other in ADAMS to form the full rotor blade. In this way, large deformation nonlinear effect can be implemented for the rotor blade in ADAMS.

Combination of the centrifugal stiffening and large deformation is not modeled; because combination of the centrifugal stiffening and large deformation cannot be used as a modeling approach in ADAMS. When the discretization method is utilized, it is not possible to apply the centrifugal stiffening force to the segment prepared by using the free-free boundary condition; because in the modal approach used to generate the mnf file, because of the free-free boundary condition, when the preload due to the centrifugal force is applied to the segments, singularity arises. Hence, it has not been possible to apply the combination of the centrifugal stiffening and discrete flexible approach to model large deformation effect.

Results presented for the hover show that for the hover condition at constant rotational velocity of the rotor, lag, flap and pitch angles of the blades remain constant and blades describe the coning and the mean lag motion as a feature of the hover condition. Besides, as the collective pitch angle of the blades is increased, flap and lag angles of the blades become higher due to the increase in aerodynamic loads, as expected.

For the forward flight condition, because of the change of the relative velocity with the azimuth angle, periodic variations of the lag, flap and the pitch angles are obtained in the simulations performed by ADAMS. In addition, it is observed that blade flap and lag motion magnitude is higher with increasing forward flight velocity. Periodic variation of the blade angles is the expected behavior in forward flight condition which shows that the established flexible rotor system is reliable.

Evaluation of the stresses in the flexible parts are done by using ADAMS main rotor simulation model with different hover and forward flight conditions. In addition, for the structural analysis, the simulation of the rotor system in ADAMS is done separately by using the blade, including centrifugal stiffening effect and large deformation effect. It is observed that for the large deformation effect included blade, location where the maximum stress is observed in root region of the blade spar but it is not apparent relative to centrifugal stiffened blade case.

It is seen that for both blades model and the hub, stress variations are constant at different azimuth positions and the stress value increases by the same ratio as the increase in the thrust value in the hover condition. For the forward flight condition, stress variation in the critical location of both the blade and hub increases significantly and periodic stress variation is observed compared to hover condition results. Moreover, results show that change in the thrust value affects the mean stress of the parts while the forward velocity affects the stresses periodically. Such a periodic variation of stress is the primary source of the fatigue failure in the long run. It is also shown that change in the damper stiffness coefficient does not have significant effect on the rotor hub and the rotor blade stresses.

The results presented for the presence of the pitch-flap coupling (δ_3 angle) show that blade undergoes smaller flap and lag angle variation. This result shows that decrease in the flap and the lag angle account for a more stable rotor; because change in the center of gravity location of the blade becomes smaller.

This study comprises the first phase for the establishment of a flexible helicopter rotor blade in MSC ADAMS. The results obtained showed that the flexible main rotor model established in MSC ADAMS provides the respective dynamic results in terms of the blade angles for the hover and the forward flight conditions reliably. Moreover, with the flexible rotor model, it is demonstrated that the stresses in the hub and the rotor blade can be determined inside MSC ADAMS for the different hover and the forward flight condition for further analyses. In addition, the large deformation and the stiffening nonlinear effects can be taken into account for the rotor blade in ADAMS. Design changes implemented during the course of the design process of the helicopter blade require the evaluation of the effect of the design change on the fatigue life of the rotor components. For this purpose, in the present study demonstration of the modification of the stiffness of the lag damper on the stresses at the critical locations for the blade and hub have been made for the forward flight case. It is shown that time history of the stress can be collected corresponding to a design change for further evaluation of the impact of the design change on the fatigue life of the rotor hub.

During the study, set up of a helicopter rotor model including structural flexibility, aerodynamic loading, trim calculations required extensive use of the features of MSC ADAMS; scripted simulations, simulation management, user-written subroutines, defining a runtime functions, and macros. In addition, for the implementation of the rotor blade geometric nonlinearities, advanced features of MSC Nastran are utilized; restart analysis and DMAP modifications. Moreover, for the trim calculations, Matlab features are also extensively used.

CHAPTER 6

FUTURE WORKS

For the future work of this study, geometric nonlinear response of the rotor blade could be improved by implementing the combination of the centrifugal stiffening and discrete flexible approach to model large deformation effect.

Aerodynamic load calculations could be improved by considering reverse flow, tip loss, and root cutout, inflow effect.

In addition to the hover and the forward flight, different flight condition such as start-up and shut-down ground cases could be investigated.

Moreover, by using time varying stress results, evaluation of the effect of design modifications on the fatigue life of the rotor hub and the rotor blade can be investigated via the fatigue damage equivalent load concept.

REFERENCES

[1] W. Johnson, *Rotorcraft Aeromechanics*. Cambridge: Cambridge University Press, 2013.

[2] A. R. S. R. S. Bramwell, G. Done, and D. Balmford, “Bramwell’s Helicopter Dynamics,” *Bramwell’s Helicopter Dyn.*, 2000.

[3] O. A. Bauchau, C. L. Bottasso, and Y. G. Nikishkov, “Modeling rotorcraft dynamics with finite element multibody procedures,” *Math. Comput. Model.*, vol. 33, no. 10–11, pp. 1113–1137, 2001.

[4] W. Johnson, “Technology Drivers in the Development of CAMRAD II,” pp. 1–17, 1994.

[5] T. Sun, J. Tan, and H. Wang, “Investigation of rotor control system loads,” *Chinese J. Aeronaut.*, vol. 26, no. 5, pp. 1114–1124, 2013.

[6] J. S. Park and S. N. Jung, “Comprehensive multibody dynamics analysis for rotor aeromechanics predictions in descending flight,” *Aeronaut. J.*, vol. 116, no. 1177, pp. 229–249, 2012.

[7] C. Monteggia and L. Alessandro, “DEVELOPMENT OF A METHOD TO ESTIMATE GUST LOADS ON A NON-ROTATING FLEXIBLE BLADE,” pp. 1–13.

[8] F. Bianchi and V. G. Agusta, “Helicopter Tail Rotor Analysis : Experience in Agusta With Adams.”

[9] P. Persson, P. Weinerfelt, and S. Aeronautics, “A coupled aero and structural dynamics model for computation of unsteady loads on the helicopter skeldar v200,” pp. 1–8.

[10] B. Vittorio, B. Francesco, and L. Marco, “Modeling Helicopter Rotor Dynamics with ADAMS.” .

[11] A. Abhishek, “Title of dissertation : ANALYSIS , VALIDATION , PREDICTION AND FUNDAMENTAL UNDERSTANDING OF ROTOR BLADE LOADS IN AN UNSTEADY MANEUVER Abhishek Abhishek , Doctor of Philosophy , 2010 Professor Inderjit Chopra Department of Aerospace Engineering,” University of Maryland, 2010.

[12] P. M. Shinoda, T. R. Norman, S. A. Jacklin, H. Yeo, A. P. F. Bernhard, and A. Haber, “Investigation of a Full-Scale Wide Chord Blade Rotor System in the NASA Ames 40- by 80-Foot Wind Tunnel,” *AHS 4th Decenn. Spec. Conf. Aeromechanics*, pp. 1–14, 2004.

[13] A. View, “Learning Basics Adams/View,” 2016.

[14] P. Line, “MSC.Nastran TM 2004,” *Optimization*, 2004.

[15] “Burkhard Domke.” [Online]. Available: https://www.b-domke.de/.

[16] M. Balaskó, G. Endrőczi, G. Tarnai, I. Veres, G. Molnár, and E. Sváb, “Non-Destructive Measurement Methods (Neutron-, X-ray Radiography, Vibration Diagnostics and Ultrasound) in the Inspection of Helicopter Rotor Blades,” no. April, 2005.

[17] “Composite Materials and Helicopter Rotor Blades.” [Online]. Available: http://classroom.materials.ac.uk/caseRoto.php.

[18] MSC-Nastran, *Patran 2012 User ' s Guide*. 2012.

[19] “ASM Aerospace Specification Metals Inc.” [Online]. Available: http://asm.matweb.com/search/SpecificMaterial.asp?bassnum=MA6061T6.

[20] A. Machinery, “Welcome to Adams / Machinery.”

[21] G. Leishman, *Principles of Helicopter Aerodynamics*. 2006.

[22] “Aerodynamic Coefficients.” [Online]. Available: http://airfoiltools.com/airfoil/naca4digit?MNaca4DigitForm%5Bcamber%5D=0&MNaca4.

[23] N. This and N. The, “Table A1- 1 . Legend for Figure A1-1 and Table A1-2 Figure A1-1 . Helicopter Dimensions,” pp. 141–160, 2004.

[24] M. G. Faulkner, A. W. Lipsett, and V. Tam, “On the use of a segmental shooting technique for multiple solutions of planar elastica problems,” *Comput. Methods Appl. Mech. Eng.*, vol. 110, no. 3–4, pp. 221–236, 1993.

[25] M. Sitar, F. Kosel, and M. Brojan, “A simple method for determining large deflection states of arbitrarily curved planar elastica,” *Arch. Appl. Mech.*, vol. 84, no. 2, pp. 263–275, 2014.

[26] C. A. E. User, “ABAQUS Users Manula,” pp. 1–12, 2004.

APPENDICES

A. Nastran Input File Modification for the Restart Analysis

SOL 106 – .bdf file modification

Replace the 19 with 7 to get restart DBALL file

```
$ Direct Text Input for Nastran System Cell Section
NASTRAN SYSTEM(316)=7
$ Replace the 19 in the above line with 7
$ to get a restart DBALL instead of what is
$currently written
$ Direct Text Input for File Management SectionQ
$ Direct Text Input for Executive Control
$ Nonlinear Static Analysis, Database
SOL 106
CEND
$ Direct Text Input for Global Case Control Data
TITLE = MSC.NASTRAN JOB CREATED ON
ECHO = NONE
SUBCASE 1
  SUBTITLE=Default
  NLPARM = 1
  METHOD = 1
  SPC = 2
  LOAD = 2
  DISPLACEMENT(SORT1,REAL)=ALL
  SPCFORCES(SORT1,REAL)=ALL
  STRESS(SORT1,REAL,VONMISES,BILIN)=ALL
$ Direct Text Input for this Subcase
BEGIN BULK
$ Direct Text Input for Bulk Data
PARAM   POST    0
PARAM   AUTOSPC NO
PARAM   LGDISP  1
PARAM   PRTMAXIM YES
NLPARM  1    10        AUTO   5    25        NO
PARAM   NMLOOP  1
EIGRL   1              10     0              MASS
$ Elements and Element Properties for region : block_prop
PSOLID  1    1    0
$ Pset: "block_prop" will be imported as: "psolid.1"
HEXA    1    1    1    2    103   102   405   406
```

When the normal modes are selected in the subcase parameters, they will automatically appear in the input file.

```
        507     506

                 ...

GRID     2001          1000.    0.      0.
$ Loads for Load Case : Default
SPCADD   2       1
LOAD     2      1.      1.       1
$ Displacement Constraints of Load Set : FIX
SPC1     1       123456  2000
SPOINT   2002    THRU    2011
$ Nodal Forces of Load Set : FORCE
FORCE    1       2001    0      100000. 1.       0.      0.
$ Referenced Coordinate Frames
ENDDATA a88214e7
```

This need to be added manually;

(The SPOINT Bulk Data entries are used to define the component modes.)

SOL 103 – .bdf file modification

SOL106 analysis creates .MASTER file to use in restart analysis. Created file name and restart analysis command need to be entered.

$ Direct Text Input for Nastran System Cell Section
$ Normal Modes Analysis, Database
ASSIGN MASTER='*(SOL106 analysis name)*.MASTER'
RESTART VERSION=1 KEEP
SOL 103
CEND
$ Direct Text Input for Global Case Control Data
TITLE = MSC.Nastran job created on
ECHO = NONE
$ Using Nastran default values for RESVEC
GPSTRAIN=ALL
GPSTRESS=ALL
SET 1=2
ADAMSMNF
FLEXBODY=YES,FLEXONLY=YES,OUTGSTRN=YES,OUTGSTRS=YES,PSE
TID=1
SUBCASE 1
$ Subcase name : Default
   SUBTITLE=Default
   METHOD = 1
   SPC = 2
   VECTOR(SORT1,REAL)=ALL
   SPCFORCES(SORT1,REAL)=ALL
OUTPUT(POST)
$ Elements (and connectors) for group : default_group
SET 2 = 1 THRU 899,900
BEGIN BULK
$
PARAM,NMLOOP,10
$
$ Direct Text Input for Bulk Data
PARAM   POST   0
PARAM   PRTMAXIM YES
DTI   UNITS   1   MGG   N   MM   S
EIGRL   1   10   0   MASS
$ Elements and Element Properties for region : block_prop
PSOLID   1   1   0
$ Pset: "block_prop" will be imported as: "psolid.1"
CHEXA   1   1   1   2   103   102   405   406
         507   506

From the SOL106 .f06 file, converged loop id need to be determined and entered this line.
'THE SOLUTION FOR LOOPID= 10 IS SAVED FOR RESTART'

```
                    ...
GRID     2001          1000.    0.      0.
$ Loads for Load Case : Default
SPCADD   2       1
$ Displacement Constraints of Load Set : fixx
SPC1     1       123456  2000
SPOINT   2002    THRU    2011
QSET1            2002    THRU    2011
$ Referenced Coordinate Frames
ENDDATA 45f41616
```